Aalto-yliopisto
Aalto-universitetet
Aalto University

Master's Programme in Water and Environmental Engineering

Nitrous oxide emissions at three Finnish wastewater treatment plants

Mechanisms behind nitrous oxide emissions and potential of process modelling in emission quantification

---

Milla Sieranen

Master's Thesis
2023

Author Milla Sieranen

Title of thesis Nitrous oxide emissions at three Finnish wastewater treatment plants – Mechanisms behind nitrous oxide emissions and potential of process modelling in emission quantification

Programme Master's Programme in Water and Environmental Engineering

Major Water and Environmental Engineering

Thesis supervisor Prof. Anna Mikola

Thesis advisor(s) D.Sc. (Tech.) Henri Haimi and D.Sc. (Tech.) Timo Larsson

Date 24.4.2023 **Number of pages** 117 **Language** English

Abstract

Nitrous oxide (N_2O) emissions contribute typically over 50% to the carbon footprint of a wastewater treatment plant (WWTP). The N_2O production occurs in biological nitrogen removal during nitrification and denitrification as a part of the metabolism of nitrogen-converting microorganisms. High variability in the emissions has been detected between treatment plants, resulting in inaccurate emission estimations with fixed emission factors.

In this thesis, the N_2O emissions were measured at WWTPs in Akaa, Mäntsälä (Kirkonkylä WWTP) and Tampere (Viinikanlahti WWTP) to determine plant-specific emission factors. At each plant, 1–2 to measurement campaigns of 4–19 days were conducted. The N_2O emissions were measured from the off-gas released from the aerobic compartments of the biological treatment units with a gas-collecting hood and a gas analyzer.

The emission factors relative to the total influent nitrogen load were 0.04% and 1.8% at Kirkonkylä WWTP in June–July 2022 and January 2023, respectively. At Viinikanlahti WWTP, the emission factors were 0.4% in September 2022 and 0.08% in November 2022. An emission factor of 0.2% was measured at Akaa WWTP in December 2022. The variability in the emissions was significant both between the plants and between two measurement campaigns conducted at the same plant. Moreover, the spatial and temporal variation was distinctive. Moderate to strong linear correlation was found between N_2O and inflow, pH, dissolved oxygen, and dissolved nitrite. N_2O was found to be produced mainly during nitrification, while significant contribution from denitrification was not detected.

A process model of the wastewater treatment process at Viinikanlahti WWTP was built with SUMO process modelling software to study the potential of process modelling in N_2O emission quantification. The results after relatively little calibration revealed that the model simulated similar off-gas N_2O concentrations to the aerobic compartments and did not detect the spatial variation that was measured at Viinikanlahti WWTP. However, the model was accurate in predicting the diurnal variability in N_2O.

Keywords nitrous oxide, wastewater treatment, emission factor, continuous off-gas measurement, process modelling

Tekijä Milla Sieranen

Työn nimi Typpioksiduulipäästöt kolmella suomalaisella jätevedenpuhdistamolla – Typpioksiduulipäästöjen muodostuminen ja prosessimallinnuksen potentiaali päästötason määrittämisessä

Koulutusohjelma Vesi- ja ympäristötekniikan maisteriohjelma

Pääaine Vesi- ja ympäristötekniikka

Vastuuopettaja/valvoja Professori Anna Mikola

Työn ohjaaja(t) TkT Henri Haimi ja TkT Timo Larsson

Päivämäärä 24.4.2023 **Sivumäärä** 117 **Kieli** englanti

Tiivistelmä

Typpioksiduulipäästöjen osuus on tyypillisesti yli 50 % jätevedenpuhdistamon kokonaishiilijalanjäljestä. Typpioksiduulia muodostuu nitrifikaation ja denitrifikaation aikana osana typpeä muuntavien mikro-organismien aineenvaihduntaa. Typpioksiduulipäästöjen tasossa on kuitenkin havaittu suurta vaihtelua puhdistamoiden välillä, minkä vuoksi tyypillisesti käytetyt vakiopäästökertoimet eivät anna luotettavaa kuvaa yksittäisen puhdistamon päästötasosta.

Tässä diplomityössä typpioksiduulipäästöjä mitattiin jätevedenpuhdistamoilla Akaassa, Mäntsälässä (Kirkonkylän puhdistamo) ja Tampereella (Viinikanlahden puhdistamo) puhdistamokohtaisten päästökertoimien määrittämiseksi. Kullakin puhdistamolla suoritettiin 1–2 mittauskampanjaa, jotka olivat kestoltaan 4–19 päivää. Päästöjä mitattiin aktiivilieteyksikköjen ilmastetuista lohkoista vapautuvasta kaasusta kaasua keräävällä kuvulla ja kaasuanalysaattorilla.

Tulevaan typpikuormaan suhteutetut päästökertoimet olivat Kirkonkylän puhdistamolla 0.04 % kesä-heinäkuussa 2022 ja 1.8 % tammikuussa 2023. Viinikanlahden puhdistamolla mitatut päästökertoimet olivat 0.4 % (syyskuu 2022) ja 0.08 % (marraskuu 2022). Akaan puhdistamolla mitattu päästökerroin oli 0.2 % joulukuussa 2022. Päästöissä oli selkeää vaihtelua eri puhdistamoiden ja samalla puhdistamolla suoritettujen mittauskampanjoiden välillä. Myös ajallinen ja paikallinen vaihtelu päästöissä oli selkeää. Kohtalaista tai vahvaa lineaarista korrelaatiota havaittiin typpioksiduulin ja tulovirtaaman, pH:n, happipitoisuuden sekä liuenneen nitriitin välillä. Typpioksiduulin havaittiin muodostuvan nitrifikaation aikana, eikä denitrifikaatiolla ollut merkittävää osuutta päästöjen muodostumiseen.

Prosessimalli Viinikanlahden puhdistamon jätevedenpuhdistusprosessista rakennettiin SUMO-prosessisimulointiohjelmalla, jotta voitiin tutkia mallinnuksen potentiaalia typpioksiduulipäästöjen kartoittamisessa. Simulointitulokset vähäisen kalibroinnin jälkeen osoittivat, ettei malli sellaisenaan tunnistanut mittaustulosten kaltaista päästöjen paikallista vaihtelua mutta ennusti päästöjen vuorokausivaihtelun oikein.

Avainsanat typpioksiduuli, jätevedenpuhdistus, päästökerroin, jatkuvatoiminen poistokaasumittaus, prosessimallinnus

Contents

Preface

This thesis was a part of a project named Direct greenhouse gases in wastewater treatment, funded by Finnish Water Utilities Association, Hämeenlinnan Seudun Vesi, Jyväskylä Seudun Puhdistamo, Tampereen Vesi, Turun Seudun Puhdistamo, Nivos and Aalto University whom I wish to thank for enabling my work within this project.

Most importantly, thank you to my supervisor, professor Anna Mikola and my advisors, D.Sc. (Tech.) Henri Haimi from FCG and D.Sc. (Tech.) Timo Larsson from Aalto University for your continuous support during my thesis project. I greatly value your feedback to my work and the expertise you have shared with me. Thank you also D.Sc. (Tech.) Raed Al-Juboori for your advising in the beginning of my thesis project.

Thank you to the personnel at the wastewater treatment plants in Akaa, Mäntsälä and Tampere for welcoming me to conduct nitrous oxide measurements at the plants, for sharing your knowledge and data related to the treatment processes and for your help with the measurement setup during the measurement campaigns.

From the Water Laboratory at Aalto University, I would like to express my gratitude to Antti Louhio, Aino Peltola, and Marina Sushko. Thank you, Antti Louhio, for your work to design the gas-collecting hood and for travelling to the treatment plants to help me with the setup of the measurements. Thank you, Aino Peltola, and Marina Sushko, for taking care that I had clean and sufficient equipment to conduct the measurement campaigns successfully. I am also grateful to M.Sc. (Tech.) Helena Hilander for familiarizing me with how to conduct the measurement campaigns and for providing me tools for data analysis.

Espoo, 24 April 2023
Milla Sieranen

Abbreviations

ADP	adenosine diphosphate
AMO	ammonia monooxygenase
AOB	ammonia-oxidizing bacteria
AOR	ammonia oxidation rate
AS	activated sludge
ASM	activated sludge model
ASM1	activated sludge model no 1
ASM-EC	activated sludge model with electron competition
ASM-ICE	activated sludge model with indirect coupling of electrons
ASMN	activated sludge model for nitrogen
ATP	adenosine triphosphate
BOD	biological oxygen demand
BOD_5	5-day biological oxygen demand
BOD_7	7-day biological oxygen demand
BOD/N	ratio of biological oxygen demand to nitrogen
BSM	benchmark simulation model
BSM2	benchmark simulation model no. 2
$CaCO_3$	calcium carbonate
$Ca(OH)_2$	calcium hydroxide
CO_2	carbon dioxide
COD	chemical oxygen demand
COD/N	ratio of chemical oxygen demand to nitrogen
CSTR	continuous stirred tank reactor
DO	dissolved oxygen
DNN	deep neural network
EF	emission factor
$FeCl_3$	ferric chloride
$Fe_2(SO_4)_3$	ferric sulfate
FTIR	Fourier transform infrared
GHG	greenhouse gas
HAO	hydroxylamine oxidoreductase
HDN	heterotrophic denitrifiers
HNO	nitrosyl
HNO_2	free nitrous acid
IC	inorganic carbon
IPCC	intergovernmental panel on climate change
IR	infared
IWA	international water association
K_La	volumetric mass transfer coefficient
LSTM	long short-term memory
MLSS	mixed liquor suspended solids
N_2	nitrogen gas
N_2O	nitrous oxide
N_2O-N	nitrous oxide nitrogen
NaR	nitrate reductase

NED	N-(1-napthyl)ethylenediamine
NH_2OH	hydroxylamine
NH_3	ammonia
NH_4^+	ammonium
NiR	nitrite reductase
NirK	nitrite reductase
NO	nitric oxide
NO_2^-	nitrite
NO_3^-	nitrate
NOB	nitrite-oxidizing bacteria
NoR	nitric oxide reductase
NoS	nitrous oxide reductase
O_2	oxygen
OHO	ordinary heterotrophic organism
PAC	polyaluminium chloride
PVC	polyvinyl chloride
RAS	return activated sludge
SA	sulfanilamide
SBR	sequencing batch reactor
SVM	support vector machine
SVR	support vector regression
VFA	volatile fatty acid
WAS	waste activated sludge
WRRF	wastewater resource recovery facility
WWTP	wastewater treatment plant

1 Introduction

Wastewater treatment has an important role in environmental protection by removing nutrients, most importantly nitrogen and phosphorus, and other substances from the wastewater. However, as a part of biological nitrogen removal, wastewater treatment processes have been found to produce and emit nitrous oxide (N_2O) from the biological treatment units and secondary settlers (Kosse et al., 2016). N_2O is a strong, ozone-depleting greenhouse gas (GHG) with a 100-year global warming potential approximately 300 times stronger than that of carbon dioxide (CO_2) (de Haas and Andrews, 2022). N_2O emissions account typically for the majority (50–70%) of the total carbon footprint of a wastewater treatment plant (WWTP) (Awaitey, 2020; Maktabifard et al., 2022). With increasing temperature leading to decreasing gas solubility, climate change can even increase the emission of N_2O during wastewater treatment (Poh et al., 2015).

N_2O emissions are often estimated based on fixed emission factors (EFs), even though the approach has been deemed unreliable, as the emissions vary significantly between WWTPs due to different treatment process configurations, influent characteristics, and operational conditions (Ahn et al., 2010b; Vasilaki et al., 2019; de Haas & Andrews, 2022). Furthermore, N_2O emissions from the treatment processes vary spatially and temporally (Ahn et al., 2010b). Temporal variation in the emissions can be both diurnal and seasonal. Therefore, direct measurement campaigns at WWTPs are required to quantify plant-specific emissions and plan mitigation measures (Vasilaki et al., 2019). However, measurement campaigns are resource-demanding, which limits their large-scale application. As a complementary method to direct measurement campaigns, mathematical models have been developed to support the estimation of N_2O emissions and the development of mitigation strategies (Spérandio et al., 2022).

The monitoring of N_2O emissions is currently not a common practice at Finnish WWTPs. Viikinmäki WWTP in Helsinki has monitored the emissions from the treatment process continuously since 2012 (Kosonen, 2013). From measurement campaigns at other treatment plants in Finland, Mikola et al. (2014) reported the emissions from four WWTPs and Hilander (2022) measured the emission level at two WWTPs. Thus, more effort is still required to define the N_2O emission level at Finnish WWTPs and understand the key parameters affecting the emissions before effective mitigation strategies can be developed and implemented at the WWTPs. Therefore, the research objectives of this thesis were to 1) provide additional information of the N_2O emission level at Finnish WWTPs and 2) assess the potential of N_2O modelling in emission quantification.

The first research objective was accomplished by conducting N_2O measurement campaigns at three Finnish WWTPs located in Akaa, Mäntsälä and Tampere. At each plant, the N_2O emissions were measured during 1–2 measurement campaigns with a duration of 4–19 days. The emissions were measured with a gas-collecting hood and Gasmet GT5000 Terra FTIR gas analyzer from the aerobic compartments of the biological treatment units which have been found to contribute the majority to the N_2O emissions (Ahn et al., 2010a). Based on the collected data, two plant-specific N_2O emission factors were calculated relating the measured N_2O-nitrogen (N_2O-N) load to the influent total nitrogen load and the removed total nitrogen load. Additionally, correlation was studied between the N_2O emissions and other variables, such as influent flow rate and dissolved oxygen (DO), to understand the spatial and temporal variability in the N_2O emissions. Another point of focus was to study how the emission factors between the three WWTPs compare to each other and to reported emission factors from other studies conducted at WWTPs in Finland and abroad. The following research questions were defined for this research objective

- What are the N_2O emission factors at the three WWTPs in Akaa, Mäntsälä and Tampere?
- Can correlation between N_2O and other variables (such as influent flow rate and DO) explain the variation in the emissions?
- How do the measured N_2O emission factors compare to each other and to other studies?

The second research objective was related to the potential of N_2O modelling in emission quantification and the focus was to conduct a literature review and a modelling experiment. The literature review was conducted to study the relevant modelling approaches related to N_2O emissions from wastewater treatment processes and the knowledge gaps that limit the applicability of N_2O modelling. The modelling experiment was conducted to study the applicability of N_2O modelling for a Finnish full-scale WWTP. A mechanistic model was constructed with SUMO wastewater treatment process modelling software based on the treatment process of one of the monitored WWTPs. Both research objectives link at this point of the study, as N_2O measurement data collected at the plant was needed to calibrate the model. The research questions related to this research objective were

- How can N_2O emission be modelled?
- What limits the applicability of N_2O modelling?
- How do the simulated and measured N_2O emissions compare to each other?
- What is the potential of N_2O modelling in the Finnish context?

An overview of the thesis is provided in figure 1 which visualizes the links between the thesis structure and the research objectives and questions. The thesis starts with a literature review in section 2 which provides a background for N_2O production and emission in wastewater treatment along with N_2O modelling approaches and knowledge gaps. Section 3 describes the measurement practices for the N_2O measurement campaigns, the studied WWTPs, the data analysis and the background for the modelling experiment. Section 4 presents the results of the N_2O measurement campaigns and the N_2O modelling experiment. The discussion in section 5 is divided into three parts, namely the discussion of the results and comparison to previous studies, sources of error in this research and the relevance of the results. Section 6 finishes the thesis by presenting the conclusions.

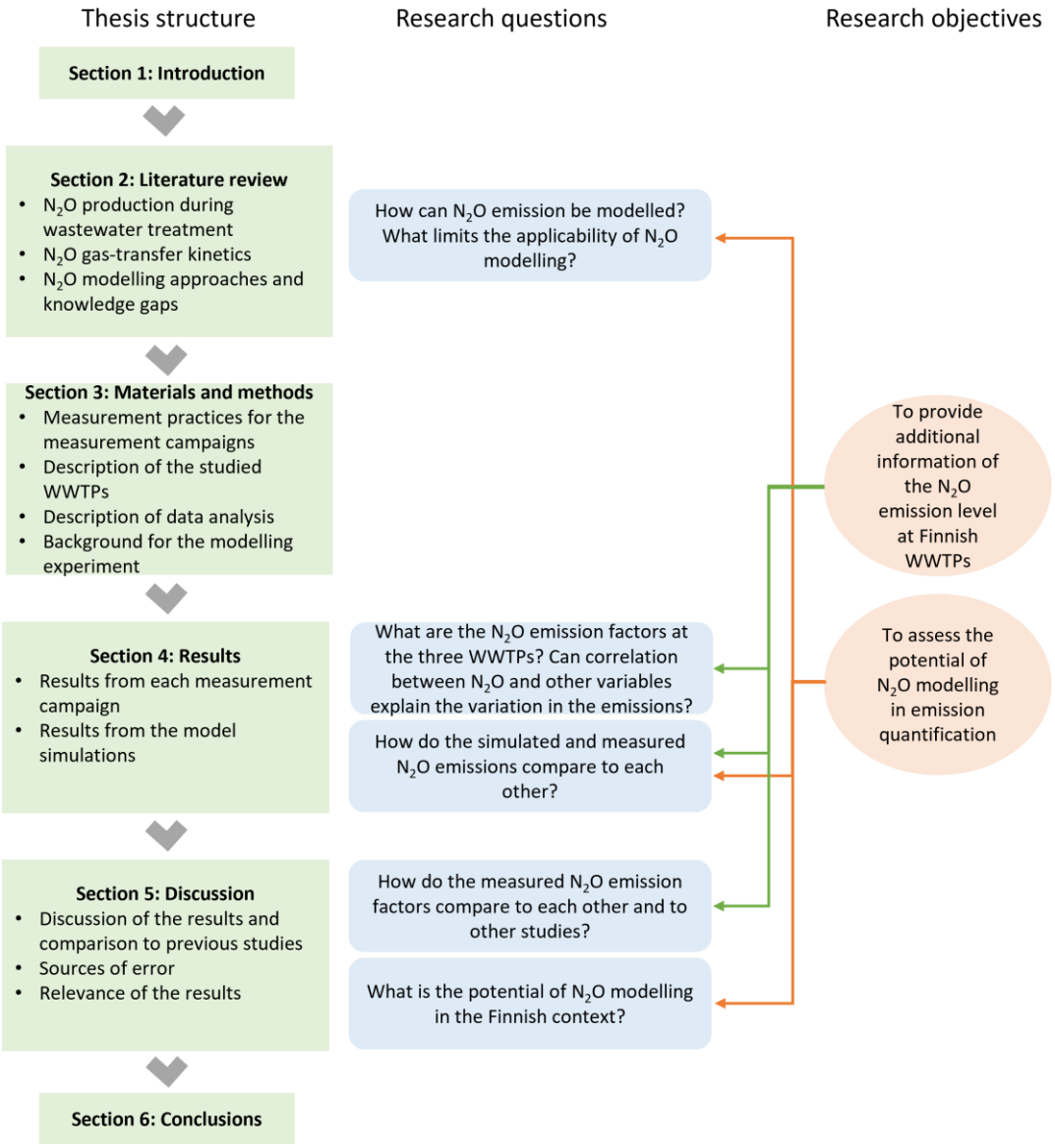

Figure 1 Overview of the thesis structure, research objectives and questions.

2 Nitrous oxide emission and modelling

Section 2 introduces the literature review which covers the background for N_2O production in biological nitrogen removal (section 2.1), the gas-transfer kinetics of N_2O (section 2.2), and different approaches to model N_2O production and the related knowledge gaps (section 2.3).

2.1 Nitrous oxide production in biological nitrogen removal

Biological nitrogen removal aims at converting the influent nitrogen, mainly in the form of ammonium/ammonia (NH_4^+/NH_3), into a form that is less harmful to the receiving waterbody and its biota (Law et al., 2012b). The key processes are microbial mediated nitrification and denitrification. Nitrification is a two-step process which consists of nitritation and nitratation (Pijuan and Zhao, 2022). In nitritation, NH_3 is oxidized to nitrite (NO_2^-) via hydroxylamine (NH_2OH) which is an intracellular intermediate. NO_2^- is further oxidized to nitrate (NO_3^-) during nitratation. Denitrification is a multi-step reduction of NO_3^- to nitrogen gas (N_2): the intermediates in the process are NO_2^-, nitric oxide (NO) and N_2O (Richardson et al., 2009).

The nitrogen-conversion processes are mainly performed by ammonia-oxidizing bacteria (AOB) in nitritation and nitrite-oxidizing bacteria (NOB) in nitratation (Okabe et al., 2011). The diverse group of microorganisms performing denitrification is referred to as heterotrophic denitrifiers (HDN) (Pijuan and Zhao, 2022). Moreover, each step is catalyzed by reaction-specific reductases that have been discovered in the genetics of the nitrogen-converting microorganisms (Stein and Yung, 2003). Figure 2 summarizes the conversion of nitrogen compounds during nitrification and denitrification, and the respective microbial groups performing the reactions.

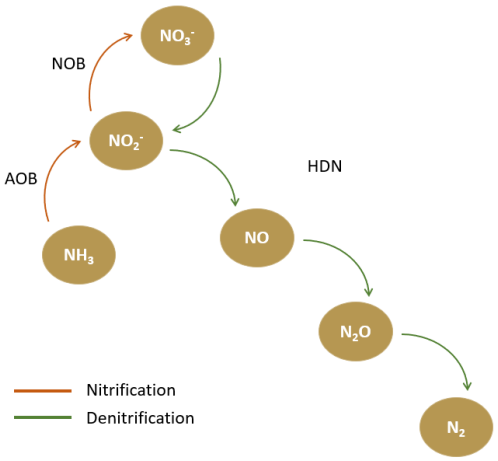

Figure 2 Nitrogen conversion reactions in nitrification and denitrification.

N_2O can be produced both in nitrification and denitrification (Kampschreur et al., 2009). The main production pathways are hydroxylamine oxidation, i.e., NH_2OH oxidation, and nitrifier denitrification and heterotrophic denitrification (Pijuan and Zhao, 2022). NH_2OH oxidation and nitrifier denitrification occur in nitrification, mainly due to the metabolism of AOB (Law et al., 2012b). Heterotrophic denitrification refers to denitrification by HDN. Additionally, N_2O can be produced via abiotic pathways which include different chemical reactions (Zhu-Barker et al., 2015). However, Su et al. (2019) found that abiotic N_2O production has an irrelevant contribution to the total emissions under the near-neutral pH range of conventional wastewater treatment processes.

2.1.1 Hydroxylamine oxidation

NH_2OH is an intermediate in nitritation, i.e., the first oxidation reaction of nitrification (Pijuan and Zhao, 2022). NH_3 is first oxidized to NH_2OH which is further oxidized to NO_2^- (Massara et al., 2017). The reactions are catalysed by the enzymes ammonia monooxygenase (AMO) and NH_2OH oxidoreductase (HAO), respectively (Pijuan and Zhao, 2022).

During nitrification, incomplete oxidation of NH_2OH to NO_2^- can result in the production of N_2O (Chen et al., 2020). However, there is some uncertainty regarding the exact pathways producing N_2O during NH_2OH oxidation. Duan et al. (2017) propose that a HAO-catalysed reaction involving NH_2OH generates nitrosyl (HNO) as an intermediate. N_2O is eventually formed, when HNO reacts with another NH_2OH molecule in a chemical reaction (Duan et al., 2017). According to Stein (2011), HAO oxidizes NH_2OH to NO which is reduced to N_2O by NorS, a homologue of NO reductase (NoR). Figure 3 visualizes N_2O production via the NH_2OH oxidation pathway.

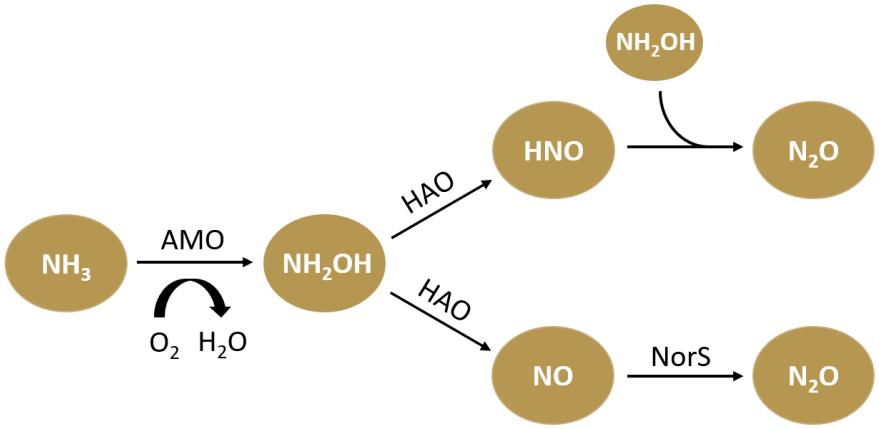

Figure 3 Possible pathways for N_2O production via the NH_2OH oxidation pathway (adapted from Pijuan and Zhao, 2022).

Peng et al. (2015) studied an enriched nitrifying culture and found that NH_2OH oxidation was the dominant pathway only under high DO concentrations, above 3.5 mg/l, along with low NO_2^- concentrations. Similarly, Tumendelger et al. (2014) detected a significant contribution to N_2O production via NH_2OH oxidation only at a high DO level of 2.5 mg/l in a conventional activated sludge process. Moreover, the laboratory studies by Wunderlin et al. (2012) and Law et al. (2012b) suggest that NH_2OH accumulation due to increased ammonia oxidation rate (AOR) can enhance N_2O production.

2.1.2 Nitrifier denitrification

In addition to NH_2OH oxidation, AOB are also responsible for N_2O production through nitrifier denitrification (Pijuan and Zhao, 2022). In nitrifier denitrification, AOB reduce NO_2^- to NO and NO further to N_2O (Chen et al., 2020), as summarized in figure 4. The involved enzymes in the reduction reactions are NO_2^- and NO reductases NirK and NoR, respectively (Pijuan and Zhao, 2022). Unlike HDN in heterotrophic denitrification, AOB are unable to reduce N_2O further to N_2 due to the lack of N_2O reductase (NoS) in their genetics (Klotz and Stein, 2011). However, nitrifier denitrification occurs without the need for organic carbon, in contrast to heterotrophic denitrification (Pijuan and Zhao, 2022).

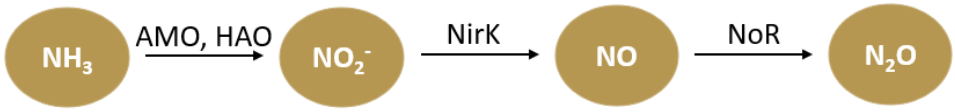

Figure 4 Nitrifier denitrification pathway for N_2O production.

Nitrifier denitrification is typically the predominant source of N_2O during nitrification and it is especially stimulated by low DO levels (Law et al., 2012b). In oxygen limiting conditions, AOB save oxygen (O_2) for the oxidation of NH_3 to NH_2OH and use NO_2^- as the electron acceptor in the nitrifier denitrification pathway (Kampschreur et al., 2009). Peng et al. (2015) found that nitrifier denitrification is especially stimulated by DO levels below 1.5 mg/l. They also studied the effect of NO_2^- accumulation and discovered that high NO_2^- levels (3–5 mg-N/l) enhance nitrifier denitrification.

2.1.3 Heterotrophic denitrification

In heterotrophic denitrification, N_2O is an obligate intermediate, as the reduction from NO_3^- to N_2 has three intermediates, namely NO_2^-, NO and N_2O (Richardson et al., 2009). The four enzymes involved in the reduction reactions are NO_3^- reductase (NaR), NO_2^- reductase (NiR), NoR and N_2O

reductase (NoS) (Pijuan and Zhao, 2022), as presented in figure 5. The reduction of N_2O to N_2 is the last step of the process and an incomplete denitrification will cause accumulation of N_2O (Chen et al., 2020). However, HDN can also consume N_2O by reducing it to N_2. Therefore, heterotrophic denitrification can be an N_2O sink by consuming N_2O produced not only during heterotrophic denitrification but also during nitrification (Conthe et al., 2019). Laboratory studies by Itokawa et al. (2001) and Conthe et al. (2019) revealed that the N_2O reduction rate can be 2–5-fold compared to the N_2O production rate.

Figure 5 Heterotrophic denitrification as a pathway for N_2O emissions (adapted from Pijuan and Zhao, 2022).

Heterotrophic denitrification takes place under anoxic conditions, as HDN typically favour O_2 over NO_2^- and NO_3^- as the final electron acceptor (Chen et al., 2020). Tallec et al. (2008) found that the N_2O production rate of heterotrophic denitrification reached its maximum at a low DO level of 0.3 mg/l. Similarly to nitrifier denitrification, the accumulation of NO_2^- can enhance N_2O production during heterotrophic denitrification by causing the accumulation of NO and N_2O (Schulthess et al., 1995).

Moreover, HDN require biodegradable organic carbon to reduce the nitrogen compounds (Okabe et al., 2011). One measure for the availability of organic carbon is the ratio of chemical oxygen demand (COD) to nitrogen (COD/N). Henze et al. (2002) and Pan et al. (2013a) have proposed that the ratio should be above 4–6 to ensure the sufficiency of organic carbon and promote complete denitrification. However, the COD/N ratio does not give an indication of the share of readily biodegradable organic matter in COD which is better described with the ratio of biological oxygen demand (BOD) to nitrogen (BOD/N). Zhang et al. (2012) studied the effect of BOD/N ratio on N_2O production in two identical sequencing batch reactors (SBRs) treating the separated liquid fraction of anaerobically digested pig manure and synthetic wastewater simulating the separated liquid. The BOD was analyzed as 5-day BOD (BOD_5). The synthetic wastewater had a higher BOD_5/N ratio (2.9) than the separated liquid (0.7), but both had a similar COD/N ratio (around 3.0). The lower BOD_5/N ratio was concluded to contribute to the approximately 24% higher N_2O emission rate in the SBR treating the separated liquid than in the SBR treating the synthetic wastewater.

Moreover, a low COD/N ratio can also intensify intracellular electron competition among the denitrification reductases (Pan et al., 2013a). Pan et al. (2013a) studied a denitrifying culture utilizing methanol as the carbon source and found that electron competition occurred both under carbon-limiting and carbon-abundant conditions. The results suggest that lower carbon loading leads to a lower fraction of electrons distributed to the NoS reductase, consequently enhancing N_2O accumulation.

2.1.4 Variation in nitrous oxide production and emissions

The nitrogen-converting processes and their effective completion are affected by several operational conditions and environmental factors which can lead to significant variation in the N_2O emissions (Pijuan and Zhao, 2022). The most important factors, such as DO and NO_2^- concentrations, are detailed in sections 2.1.1–2.1.3 together with the three production pathways. In addition, pH and temperature are key parameters affecting N_2O production. Massara et al. (2017) suggest that optimal ranges for pH and temperature are around 7 for pH and 20 °C for temperature to ensure the completion of nitrification and the N_2O consumption through heterotrophic denitrification. Significantly lower or higher pH and temperature values can increase the N_2O emissions by for example affecting the enzyme activities, solubility of N_2O and AOR (Massara et al., 2017). Furthermore, varying emission levels are typically detected in different bioreactor configurations utilizing a variety of biological nitrogen removal alternatives (Ahn et al., 2010a).

Another highly relevant aspect is the effect of microbial population dynamics on the variation in N_2O emissions, as activated sludge contains several microbial species performing nitrification and denitrification which can be grouped, e.g., to AOB and NOB (Ren et al., 2019). The microbial population undergoes seasonal variation due to changes in temperature and other conditions (Gruber et al., 2021b). Furthermore, the sludge retention time directly affects the abundance and selection of species in the activated sludge (Vasilaki et al., 2019). Gruber et al. (2021b) found links between the microbial population dynamics and seasonal N_2O emission patterns, as high emission peaks were not detected from SBRs with stable microbial communities, whereas large community shifts correlated with increased N_2O emissions.

Due to the multivariate dependency of N_2O emissions on different process parameters and influent characteristics, the root causes for N_2O emissions and their variation are difficult to define exactly. The variation can be significant both on daily and seasonal level (Gruber et al., 2021a). The N_2O emissions are typically characterized with an emission factor which describes the emitted N_2O-N load relative to the total influent nitrogen load, described in detail in section 3.5.1. The intergovernmental panel on climate change (IPCC)

has suggested a default emission factor of 1.6 % relative to the influent total nitrogen load for WWTPs treating domestic wastewater (IPCC, 2019). The default emission factor was derived based on data from N_2O measurement campaigns at full-scale WWTPs and it was significantly increased from the original default emission factor of 0.05% suggested by IPCC in 2006.

The revised default emission factor as well as several studies quantifying the emission factors from wastewater treatment confirm the high variability in N_2O emissions. A review by Kampschreur et al. (2009) found a variation in the emission factors between 0–14.6% of the influent total nitrogen load detected at full-scale WWTPs, mainly measured with grab samples. Ahn et al. (2010a) quantified the N_2O emissions from 12 full-scale WWTPs where the emission factors varied between 0.01–1.6% of the influent total nitrogen load. Gruber et al. (2021a) reviewed the results of six continuous measurement campaigns at WWTPs with a minimum duration of one year and the reported emission factors were between 0.8–2.9% of the influent total nitrogen load. In lab-scale studies, the variation is typically even greater, between 0–95% of the influent total nitrogen load (Kampschreur et al., 2009).

2.2 Gas-transfer kinetics of nitrous oxide

In wastewater treatment, N_2O is produced in the water in soluble form and emitted if the dissolved N_2O is transferred to gas phase. Conventional wastewater treatment processes have been reported to emit N_2O from the aerobic and anoxic compartments of the biological treatment units and secondary clarifiers where the biological activity continues (Foley et al., 2010; Mikola et al., 2014). However, the majority of N_2O is emitted in the aerobic compartments, as aeration intensifies the stripping of the dissolved N_2O (Ahn et al., 2010a; Zhang et al., 2012; Marques et al., 2016). Therefore, dissolved N_2O produced during heterotrophic denitrification in the anoxic compartments can also be stripped to the gas-phase when the water is conducted to an aerobic compartment (Kampschreur et al., 2009). However, some of the produced N_2O may not be stripped during the treatment process and thus remains dissolved in the effluent. Therefore, N_2O can also be emitted in the effluent-receiving waterbodies even though Foley et al. (2010) estimated that approximately only 5% of the produced N_2O would be emitted after the treatment process.

The gas-transfer kinetics of N_2O have received little attention in comparison to O_2 transfer which has been the focus of scientific research due to the energy intensity of aeration (Amaral et al., 2019). However, the O_2 gas-transfer kinetics can be applied in estimating the kinetics of N_2O gas-transfer, as both gases have been classified to have a low solubility in water (Henry's law constants for O_2 and N_2O are $1.2 * 10^{-5}$ and $2.4 * 10^{-4}$ mol/(m^3*Pa), respectively)

(Amaral et al., 2019). Typically, the transfer from liquid to gas phase is characterized with a volumetric mass transfer coefficient (K_La) or an α-factor which can be utilized to relate the O_2 gas-transfer kinetics to those of N_2O (Amaral et al., 2019). As the K_La and the α-factor lump together several unknown phenomena of the system, this approach is likely to cause underestimation or overestimation to the gas transfer of N_2O (Amaral et al., 2019). Factors such as the aerator immersion depth, aeration bubble size, diffuser layout, liquid viscosity, salinity and fouling of the aerators affect the magnitude of the K_La and the α-factor (Marques et al., 2016). Moreover, temperature affects the solubility and gas-transfer of N_2O, as increasing temperature decreases the solubility of N_2O (Poh et al., 2015).

2.3 Modelling of nitrous oxide production and emission

Mathematical models have been widely utilized to study nitrogen removal in wastewater treatment and are increasingly applied to predict the production and emission of N_2O (Spérandio et al., 2022). Various activated sludge models (ASMs) have been developed to study the conventional activated sludge processes, originally introduced by the International Water Association (IWA) (Henze et al., 2000). The production and emission of N_2O can be integrated into the existing ASMs by extending the nitrification and denitrification reactions (Massara et al., 2017). For example, in the first version of the ASMs, the Activated Sludge Model No 1. (ASM1), nitrification is modelled as a one-step process and thus, it is unable to account for the accumulation of NO_2^- (Hiatt and Grady, 2008a). Similarly, denitrification is modelled as a one-step reduction of NO_3^- to N_2 in ASM1 (Pan et al., 2013b).

Several models have been proposed to describe the N_2O production pathways (sections 2.1.1–2.1.3) related to nitrification and denitrification. The nitrification related models are either single-pathway models including one of the two emission pathways occurring during nitrification or two-pathway models including both pathways. Sections 2.3.1–2.3.3 introduce the most relevant mechanistic models for nitrification and denitrification related N_2O production. Section 2.3.4 considers data-driven and hybrid models which are more novel in wastewater treatment modelling than the mechanistic models. A short description is included in section 2.3.5 related to the integration of N_2O modelling into plantwide models if the GHG emissions of a WWTP are assessed on a comprehensive scale. Section 2.3.6 covers the knowledge gaps in N_2O modelling that limit its potential in reliable emission quantification.

2.3.1 Nitrification related single-pathway models

There are three types of pathway models describing N_2O production during nitrification: 1) single-pathway models for NH_2OH oxidation, 2) single-

pathway models for nitrifier denitrification, and 3) two-pathway models including both NH_2OH oxidation and nitrifier denitrification (Chen et al., 2020). Altogether four single-pathway models have been proposed for the nitrifier denitrification pathway by Ni et al. (2011), Mampaey et al. (2013), Pocquet et al. (2013) and Guo and Vanrolleghem (2014). Single-pathway models for NH_2OH oxidation have been introduced by Law et al. (2012a) and Ni et al. (2013b). Comprehensive two-pathway models including both nitrification related N_2O pathways have been proposed by Ni et al. (2014), Peng et al. (2016), Domingo-Félez and Smets (2016) and Pocquet et al. (2016). An overview of the single-pathway models is provided in table 1 which is followed by more detailed descriptions of the models.

Table 1 An overview of the nitrification related single-pathway N_2O models.

Model reference	**NH_2OH oxidation**	**Nitrifier denitrification**	**Applicability and notes**
Ni et al. (2011)		**X** (incl. NH_2OH, NO to N_2O)	• NO_2^- accumulation • Low DO enhances N_2O production
Mampaey et al. (2013)		**X** (excl. NH_2OH, NO to N_2O)	• NO_2^- accumulation • No inhibitive effect of DO on NO_2^- and NO reduction
Guo and Vanrolleghem (2014)		**X** (excl. NH_2OH, NO to N_2O)	• NO_2^- accumulation • Modified from Mampaey et al. (2013): enhancement of N_2O production at low DO added
Pocquet et al. (2013)		**X** (incl. NH_2OH, NO to N_2O)	• NO_2^- accumulation • Modified from Ni et al. (2011): oxygen inhibiting factor removed, effect of pH variation added
Law et al. (2012a)	**X** (NOH to N_2O)		• High DO, low NO_2^-
Ni et al. (2013b)	**X** (NO to N_2O)		• High DO, low NO_2^-

Ni et al. (2011) used the standard kinetic expressions and parameters of the well-known ASMs (ASM1, ASM2, ASM2d and ASM3) as the basis and made extensions to include N_2O modelling related to the nitrifier denitrification pathway. N_2O emitted during heterotrophic denitrification was also included in the model, but the NH_2OH oxidation pathway was ignored due to the assumption that nitrifier denitrification is the major contributor to N_2O emissions during nitrification (Ni et al., 2011). In the model, nitrifier denitrification consists of four reactions, each catalyzed by AOB and the respective

enzymes (Ni et al., 2011). NH_4^+ oxidation to NO_2^- is a two-step process with NH_2OH as the intermediate and O_2 as the terminal electron acceptor. N_2O emissions occur when NO is produced by reducing NO_2^- and NO is further reduced to N_2O. Ni et al. (2011) assumed biomass production only during the oxidation of NH_2OH to NO_2^-, but not during NO or N_2O production. Additionally, the model considers the specific substrate removal rate lower when NO_2^- is used as the final electron acceptor instead of O_2 (Ni et al., 2011). Moreover, the model enhances N_2O production at low DO levels with an oxygen inhibiting factor (Ni et al., 2011). Ni et al. (2011) calibrated and validated the model based on four experimental case studies concerning N_2O dynamics. The cases were studied individually with the model, and therefore the obtained parameter values were different for each case.

The nitrifier denitrification related model by Mampaey et al. (2013) directly oxidizes NH_3 to NO_2^-, and ignores NH_2OH as an intermediate, in contrast to the model by Ni et al. (2011). N_2O is produced via NO reduction after NO has been reduced from NO_2^- (Mampaey et al., 2013). Mampaey et al. (2013) included two scenarios for the electron donor: either NH_3 or biomass donates the electrons to the reduction reactions. The model does not consider the inhibitive effect of DO on NO_2^- and NO reduction, again in contrast to Ni et al. (2011). The model was not extensively calibrated, but simulations were performed with continuous and intermittent aeration patterns to study NO and N_2O emission from a partial nitritation reaction (Mampaey et al., 2013).

The other two single-pathway models related to nitrifier denitrification are modified versions from the models by Ni et al. (2011) and Mampaey et al. (2013). Pocquet et al. (2013) modified the model by Ni et al. (2011) by removing the oxygen inhibiting factor with an increasing effect on N_2O production at decreasing DO concentrations. To link pH variation to N_2O production, NH_3 and free nitrous acid (HNO_2) were considered as the substrates of nitrifier denitrification instead of NH_4^+ and NO_2^- used by Ni et al. (2011).

Guo and Vanrolleghem (2014) modified the model by Mampaey et al. (2013) regarding the DO kinetic term and growth reduction factors of the two steps of nitrifier denitrification. Based on research suggesting that the maximum N_2O production rate via nitrifier denitrification occurs under relatively low DO levels, Guo and Vanrolleghem (2014) introduced a DO kinetic term which stimulates N_2O production at low DO levels and inhibits it at high DO levels. The term replaced the DO kinetic term by Mampaey et al. (2013) which enhanced N_2O production with increasing DO concentration. Additionally, growth reduction factors were used for both NO_2^- and NO reduction, whereas Mampaey et al. (2013) used the factor only for NO_2^- reduction.

Single-pathway models to simulate N_2O production via NH_2OH oxidation have been proposed by Law et al. (2012a) and Ni et al. (2013b). Law et al. (2012a) studied how AOR affects N_2O production in an enriched AOB culture and formulated a model to identify if NH_2OH oxidation was the main source of N_2O under the studied conditions. NH_2OH oxidation was modelled as a two-step process with NH_2OH oxidized to NO_2^- via HNO (Law et al., 2012a). HNO was modelled to either chemically decompose to form N_2O or oxidize to NO_2^- (Law et al., 2012a). O_2 was used as the electron acceptor. The experimental data obtained by Law et al. (2012a) was the basis for model calibration. Indeed, the developed model could simulate N_2O emissions similarly to the results obtained from the experiments (Law et al., 2012a). In contrast, nitrifier denitrification single-pathway models, such as the model by Ni et al. (2011), could not reproduce the experimental results.

Ni et al. (2013b) used NO as the intermediate in NH_2OH oxidation, in comparison to HNO used by Law et al. (2012a). NH_4^+ is first oxidized to NH_2OH and a following oxidation reaction results in NO formation. NO is either oxidized to NO_2^- or reduced to N_2O (Ni et al., 2013b). In N_2O production, NH_2OH is the electron donor. Furthermore, the model assumes that DO has no inhibitory effect on NO reduction to N_2O and that the AOB have a lower specific reaction rate when they use NO as the electron acceptor instead of O_2 (Ni et al., 2013b). The model was calibrated based on literature and data collected during a sampling campaign at a full-scale WWTP. Ni et al. (2013b) validated the model with additional data collected from two WWTPs.

2.3.2 Nitrification related two-pathway models

The single-pathway models are unable to reproduce N_2O emissions based on experimental results under varying operational conditions, as for example NH_4^+, NO_2^- and DO concentrations affect the dominance of the emission pathways (Ni et al., 2013a). Therefore, selecting a suitable single-pathway model requires case-specific analysis to identify the most relevant nitrification related pathway (Ni et al., 2013a). Alternatively, two-pathway models considering both emission pathways have been proposed to more accurately model N_2O production during nitrification (Ni et al., 2014; Peng et al., 2016; Domingo-Félez and Smets, 2016; Pocquet et al., 2016). The two-pathway models can be categorized into decoupling-based and direct coupling-based approaches. In the decoupling-based models, the oxidation and reduction reactions are decoupled by utilizing electron carriers, whereas direct coupling-based models couple these reactions directly. The decoupling-based models have been proposed by Ni et al. (2014) and Peng et al. (2016). The two-pathway models by Domingo-Félez and Smets (2016) and Pocquet et al. (2016) are based on direct coupling. An overview of the four two-pathway models is presented in table 2, followed by more detailed descriptions of the models.

Table 2 An overview of the nitrification related two-pathway N_2O models.

Model reference	Direct/Indirect coupling approach	Applicability and notes
Ni et al. (2014)	Indirect (Electron competition with carriers)	• Varying DO and NO_2^- levels • Biomass growth excluded • NH_2OH to N_2O via NO, NO_2^- to N_2O
Peng et al. (2016)	Indirect (Energy balance with ATP and ADP)	• Modified from Ni et al. (2014): Effect of IC variation on N_2O added • Biomass growth included • NH_2OH to N_2O via NO, NO_2^- to N_2O
Domingo-Félez and Smets (2016)	Direct	• NO precursor for N_2O production via both pathways • Varying DO, NH_3 and HNO_2 levels • Biomass growth included
Pocquet et al. (2016)	Direct	• Based on single-pathway models by Ni et al. (2011), Mampaey et al. (2013) and Ni et al. (2013b) • NH_2OH to N_2O via NO, HNO_2 to N_2O • Effect of HNO_2 and DO on N_2O production

In the model by Ni et al. (2014), NH_3 is first oxidized to NH_2OH while O_2 is reduced to H_2O. NH_2OH is further oxidized to NO_2^- via NO. Alternatively, NO is reduced to N_2O to model N_2O production via the NH_2OH oxidation pathway. Furthermore, nitrifier denitrification is modelled by directly reducing NO_2^- to N_2O. By excluding NO as the intermediate in nitrifier denitrification, a loop between NO oxidation to NO_2^- and NO_2^- reduction to NO is avoided. The electron transport processes between the oxidation and reduction reactions are modelled with electron carriers. The carriers are either in reduced or oxidized form which limits the electron availability for the different processes. This approach enables prediction of the contribution of each pathway, as different kinetic values can be assigned to the processes with respect to the electron carriers (Spérandio et al., 2022). A schematic representation of the model is presented in figure 6. The model calibration and validation were based on batch tests conducted under varying NO_2^- and DO concentrations with two independent nitrifying cultures (Ni et al., 2014). Limitations of the model include the exclusion of biomass growth, based on the assumption that biomass growth is negligible in short batch tests. In addition, the model is not assumed to accurately simulate N_2O emissions during shifts from anoxic to aerobic conditions, as the complex mechanisms are partially unknown and therefore not considered by the model (Ni et al., 2014).

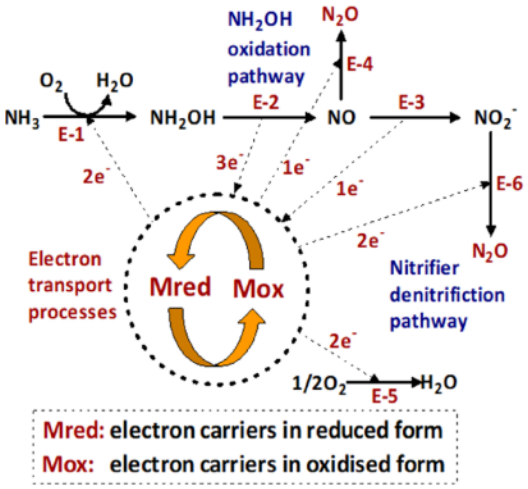

Figure 6 A schematic representation of the two-pathway model by Ni et al. (2014). Figure adapted from Spérandio et al. (2022).

The second two-pathway model utilizing the decoupling and electron carrier approach (figure 7) has been developed by Peng et al. (2016). The model extends the model proposed by Ni et al. (2014) by including the dependency between N_2O production by AOB and inorganic carbon (IC) concentration. IC, typically CO_2, acts as a carbon source for cell synthesis, and therefore affects the rate of biomass growth (Peng et al., 2016). The new state variables by Peng et al. (2016) are adenosine triphosphate (ATP) and adenosine diphosphate (ADP) to include energy balance in the model. During NH_3 oxidation and NO_2^- and O_2 reduction, energy is yielded to produce ATP, aided by proton translocation. Biomass growth and maintenance require ATP, electron carriers and CO_2. Thus, different kinetic rates of the energy yielding process are affected by the IC variation, which indirectly changes the contributions of the pathways to total N_2O production.

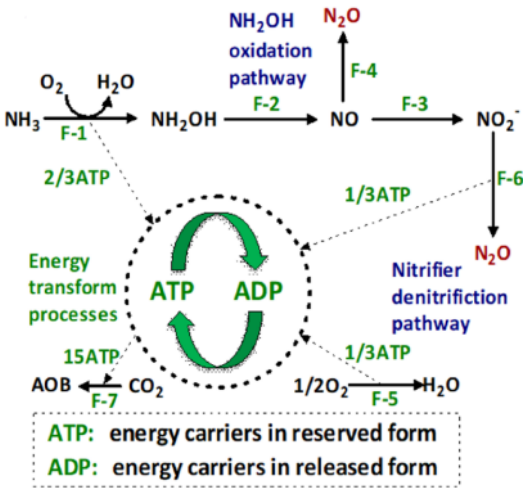

Figure 7 A schematic representation of the two-pathway model by Peng et al. (2016). Figure adapted from Spérandio et al. (2022).

The direct coupling based two-pathway models by Domingo-Félez and Smets (2016) and Pocquet et al. (2016) do not decouple the oxidation and reduction reactions with electron carriers, in contrast to Ni et al. (2014) and Peng et al. (2016). In the model by Domingo-Félez and Smets (2016), NO is the precursor for N_2O production both via NH_2OH oxidation and nitrifier denitrification, contrary to Ni et al. (2014) and Peng et al. (2016). NH_3 is oxidized to NH_2OH with O_2 as the electron acceptor. NH_2OH can be either completely oxidized to HNO_2 or partly to NO and HNO_2 (Domingo-Félez and Smets, 2016). As a part of the nitrifier denitrification pathway, HNO_2 is also reduced to NO with NH_2OH as the electron donor (Domingo-Félez and Smets, 2016). N_2O production follows the reduction of NO, again with NH_2OH as the electron donor. Figure 8 visualizes the pathway model by Domingo-Félez and Smets (2016). The contribution of each pathway to N_2O production is determined by the distribution of NO produced in NH_2OH oxidation and in nitrifier denitrification (Domingo-Félez and Smets, 2016). Different DO, NH_3, and HNO_2 dependencies govern the dominance of the pathways, as the model enhances NH_2OH oxidation at high NH_3 and DO concentrations, whereas low DO and high HNO_2 levels promote nitrifier denitrification (Domingo-Félez and Smets, 2016). As a part of the model development process, the model was not calibrated and validated.

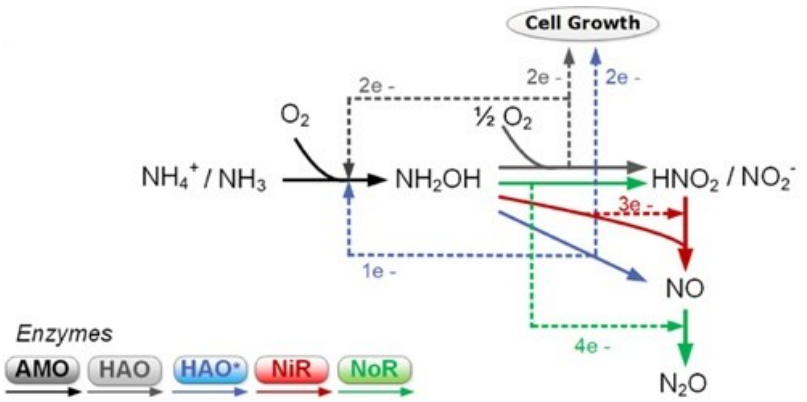

Figure 8 A schematic representation of the two-pathway model by Domingo-Félez and Smets (2016). Figure adapted from Spérandio et al. (2022).

The two-pathway model by Pocquet et al. (2016) was based on the single-pathway model for NH_2OH oxidation by Ni et al. (2013b) and the models for nitrifier denitrification developed by Ni et al. (2011) and Mampaey et al. (2013). Five enzymatic reactions (figure 9) were included in the model: NH_3 was used as the substrate for the oxidation to NH_2OH. NH_2OH was further oxidized to HNO_2 via NO with O_2 receiving the electrons in all reactions (Pocquet et al., 2016). NO reduction to N_2O was the emission pathway during NH_2OH oxidation. For nitrifier denitrification, N_2O was produced directly from HNO_2 reduction without the NO intermediate to avoid the NO loop, similarly to Ni et al. (2014) and Peng et al. (2016). Both N_2O-producing

reactions are coupled with NH_2OH oxidation to HNO_2, according to the direct-coupling approach (Pocquet et al., 2016). The model was not supplied with inhibition factors of NH_3 and HNO_2 on AOB growth, but the effect of HNO_2 on N_2O production and DO on nitrifier denitrification was considered. Model calibration and validation were performed with data obtained from batch tests conducted in a lab-scale SBR (Pocquet et al., 2016).

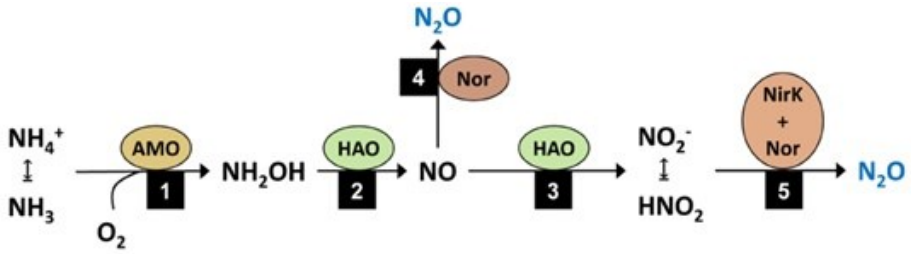

Figure 9 A schematic representation of the two-pathway model by Pocquet et al. (2016). Figure adapted from Spérandio et al. (2022).

2.3.3 Denitrification pathway models

N_2O emitted in heterotrophic denitrification must be modelled as a multiple-step process to include the intermediates present during the reactions (Spérandio et al., 2022). Four-step models for heterotrophic denitrification have been proposed by Hiatt and Grady (2008a), Pan et al. (2013b) and Domingo-Félez and Smets (2020). The accumulation of the intermediates and electron competition between them affects N_2O emissions (Pan et al., 2013b). The models developed by Pan et al. (2013b) and Domingo-Félez and Smets (2020) decouple nitrogen reduction and carbon oxidation to consider electron competition. The reactions are directly coupled in the model by Hiatt and Grady (2008a). An overview of the models is provided in table 3.

Table 3 An overview of the heterotrophic denitrification related N_2O models.

Model reference	**Coupling/decoupling approach**	**Applicability and notes**
Hiatt and Grady (2008a)	Coupling	• Direct coupling of carbon oxidation and nitrogen reduction reactions • No electron competition • Enzyme kinetics ignored
Pan et al. (2013b)	Decoupling with electron carriers	• Effect of electron competition and enzyme kinetics on N_2O production • Methanol as model carbon source
Domingo-Félez and Smets (2020)	Decoupling with multi-resistor electric circuit analogy	• Electron competition • Less parameters than in ASM-ICE by Pan et al. (2013b)

Hiatt and Grady (2008a) developed an activated sludge model for nitrogen (ASMN). They based the model on ASM1, as several processes were directly incorporated from ASM1 to ASMN. The most significant extensions regarded nitrification and denitrification (Hiatt and Grady, 2008a). Regarding denitrification, the model adopts a direct coupling approach by directly coupling carbon oxidation and the reduction reactions of the nitrogen compounds (Spérandio et al., 2022), as illustrated by figure 10. The four reactions are the reduction of NO_3^-, NO_2^-, NO and N_2O with them acting simultaneously as the electron acceptors for oxidation of organic carbon compounds (Hiatt and Grady, 2008a). The ASMN uses reaction-specific parameters for each denitrification step, including the growth rate of heterotrophic microorganisms, half-saturation coefficient for electron acceptor and inhibition coefficient for oxygen (Hiatt and Grady, 2008a). However, Spérandio et al. (2022) note that the model assumes that the electron supply will always be equal to the predicted total electron demand. Therefore, the ASMN does not consider the effect of intracellular electron competition on N_2O emissions. Moreover, the direct coupling approach ignores the different enzyme kinetics related to the reduction and oxidation reactions and thus, their rate-limiting effect on denitrification is not accounted for (Spérandio et al., 2022). Hiatt and Grady (2008b) evaluated the performance of the ASMN by conducting steady-state and dynamic simulations for a modified Ludzak-Ettinger process configuration. The varying wastewater characteristics were based on characterisation data from several industrial wastewater treatment facilities (Hiatt and Grady, 2008b).

Figure 10 A schematic representation of ASMN by Hiatt and Grady (2008a). Figure adapted from Spérandio et al. (2022).

Pan et al. (2012) detected that the ASMN could not accurately model the N_2O emissions during carbon limitation which likely resulted from electron competition. Responding to the need to include electron competition in denitrification related N_2O modelling, Pan et al. (2013b) developed a denitrification model incorporating electron competition. The model is referred to as activated sludge model with indirect coupling of electrons (ASM-ICE). Pan et al. (2013b) divide nitrogen reduction (i.e., denitrification) into four processes. Furthermore, carbon oxidation uses methanol as a model carbon source, and the oxidation is modelled by two processes (methanol conversion to CO_2 and methanol assimilation to biomass). As new state variables, electron carriers

(reduced mediator Mred and oxidized mediator Mox) are introduced to model the electron transfer between carbon oxidation and nitrogen reduction (Pan et al., 2013b). Figure 11 is a schematic illustration of the ASM-ICE. The electron competition between the reduction processes is modelled by assigning different values to the affinity constants of the enzymes involved in the reactions (Pan et al., 2013b). The model was calibrated and validated with experimental data from a lab-scale denitrifying culture receiving methanol as the sole carbon source. Pan et al. (2013b) note that the calibration and validation should be further developed by using full-scale sludge characteristics including varying microbial groups and carbon sources.

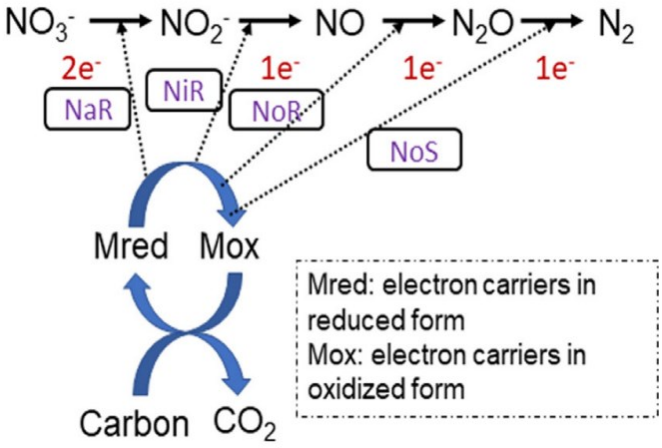

Figure 11 A schematic representation of ASM-ICE by Pan et al. (2013b). Figure adapted from Spérandio et al. (2022).

By applying the principles related to multi-resistor electric circuits, Domingo-Félez and Smets (2020) proposed an activated sludge model with electron competition (ASM-EC) where the electron competition and distribution during denitrification are analogous to the intensity of electric current through parallel resistors (Spérandio et al., 2022). The ASM-EC is illustrated by figure 12. In the circuit analogy, HDN and a pair of electron acceptor and electron donor create a potential, and parallel resistors describe the electron transport from organic carbon oxidation to the four denitrification reductases and to an oxygen-reducing oxidase (Domingo-Félez and Smets, 2020). The resistance of the resistor is inversely related to the substrate concentration and the resulting intensity of the current through a resistor is equivalent to the rate of the reaction (Domingo-Félez and Smets, 2020). Individual resistances for each denitrification reductase enable the modelling of the intracellular electron competition between the reductases (Domingo-Félez and Smets, 2020). In addition, oxygen is included in the model as an inhibitor, as aerobic conditions would inhibit denitrification and enhance oxygen reduction (Domingo-Félez and Smets, 2020). The ASM-EC was calibrated and validated with data from batch experiments which produced reduction rates of

the denitrification steps with varying heterotrophic denitrifying communities and carbon sources (Domingo-Félez and Smets, 2020). Comparing the ASM-EC and the ASM-ICE by Pan et al. (2013b), the ASM-EC is a simpler model with 12 parameters and the ASM-ICE is the more complex one with 17 parameters (Domingo-Félez and Smets, 2020). Thus, using the ASM-EC could help to avoid difficulties with overparameterization and calibration (Domingo-Félez and Smets, 2020).

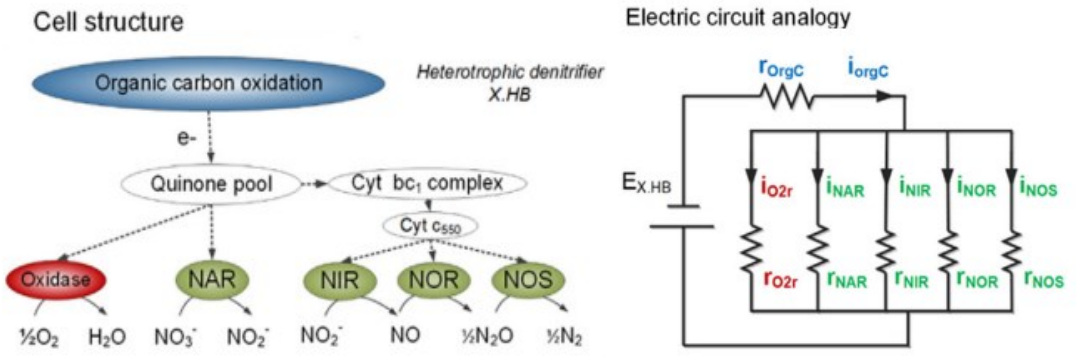

Figure 12 A schematic representation of ASM-EC by Domingo-Félez and Smets (2020). Figure adapted from Spérandio et al. (2022).

2.3.4 Data-driven and hybrid model structures

Mechanistic models, the ones focused on N_2O described in sections 2.3.1–2.3.3, are the most common approach in wastewater treatment process modelling. Another increasingly relevant approach is data-driven modelling techniques, such as multivariate statistics and machine learning algorithms, which can be applied on their own to model WWTPs or in hybrid modelling by integrating them with mechanistic, typically ASM-based, models (Vasilaki et al., 2019; Hwangbo et al., 2021). Essentially different from mechanistic models, data-driven modelling techniques are targeted to identify patterns and hidden structures related to N_2O emissions and their relations to other parameters (Vasilaki et al., 2020). However, currently only few studies have applied such modelling approaches to study N_2O emissions from wastewater treatment processes.

A deep learning approach by Hwangbo et al. (2021) was utilized to quantitatively describe N_2O emissions from Avedøre WWTP in Denmark, based on approximately 750 000 data points from the influent flow rate, air flow rate, temperature, NH_4^+, NO_3^-, DO and N_2O. According to Hwangbo et al. (2021), deep learning is one of the most powerful machine-learning tools to study hierarchical features and representations of long-term data by considering deep architectures. The deep neural network (DNN) model was targeted to predict liquid-phase N_2O concentration from the input data (influent flow

rate, air flow rate, temperature, NH_4^+, NO_3^- and DO) with an objective function minimizing the difference between the measured liquid-phase N_2O concentration and a single value from the output layer. The model considered six hidden layers studying the relationships between the N_2O concentration and the six parameters the input data covered. Each layer had 4–32 hidden neurons which encompassed an activation function (a hyperbolic tangent sigmoid function) (Hwangbo et al., 2021). The DNN model was found to have a good fit ($R^2 > 0.8$) for both low and high N_2O concentrations. Different approaches were tested to determine the N_2O emission rate, one of them being a mathematical model calculating the emission rate from the predicted liquid phase N_2O concentration. Furthermore, data processing, including a data smoothing process, was found to have a key role in accurate DNN model development. Hwangbo et al. (2021) also compared the forecasting ability of the DNN-approach to long short-term memory (LSTM) recurrent neural networks and concluded that the LSTM-based model performed even better in forecasting than the DNN-based model.

Multivariate statistical techniques were utilized by Vasilaki et al. (2018) to study their applicability to relate N_2O emissions with online operational variables (DO, NH_4^+, NO_3^-, NO_2^-, temperature and influent flow rate). The data originated from Kralingseveer WWTP in the Netherlands which is a full-scale plant with a plug-flow reactor followed by two parallel carrousel reactors (Vasilaki et al., 2018). The data had been collected from several locations in the reactors, and all reactors were covered to collect the off-gas to measure the N_2O emissions (Vasilaki et al., 2018). The data was divided into distinctive sub-periods based on the variability in the N_2O emissions by using Binary Segmentation. The methodological framework included Spearman's correlation analysis, k-means clustering, hierarchical clustering, and Principal component analysis. The results suggested that multivariate analysis has great applicability in identifying the conditions where low or high ranges of N_2O emissions occur based on long-term historical data from operational variables (Vasilaki et al., 2018). The approach was deemed to have also potential in N_2O emission mitigation (Vasilaki et al., 2018).

A data-driven knowledge discovery framework was developed by Vasilaki et al. (2020) to study the dynamics of N_2O in a full-scale sidestream SBR treating anaerobic supernatant. The structured data analysis included abnormal events detection with features extraction and density-based clustering, classification with support vector machines (SVMs), and regression analysis with support vector regression (SVR), was applied for knowledge discovery from the input data set including, e.g., pH, DO and influent loadings (Vasilaki et al., 2020). An important conclusion of the study was the capability of low-cost sensors typically used in WWTP monitoring to predict the behaviour of

N_2O dynamics when combined with knowledge discovery techniques (Vasilaki et al., 2020).

Detailed spatial submodels utilizing computational fluid dynamics were developed by Bellandi et al. (2018) to understand the mechanisms behind N_2O production at Eindhoven wastewater resource recovery facility (WRRF) in the Netherlands. According to Bellandi et al. (2018), accurate hydrodynamic studies allow for a better representation of local conditions and recirculation patterns in activated sludge tanks to which the nitrogen conversion processes are highly sensitive. The models were not calibrated but it was concluded that the models had an increased ability to represent local N_2O concentrations in the tanks in comparison to an ASM-based model (Bellandi et al., 2018).

A hybrid model combining a mechanistic model (ASM1) and a deep learning approach was developed by Li et al. (2022) to model N_2O emissions at a full-scale WWTP in South Australia. The adopted deep learning model was based on LSTM architecture which was used for time-series predictions (Li et al., 2022). The mechanistic model and the deep learning model were also tested separately for comparison. The key finding was that the hybrid model had the most potential due to reduced calibration effort in comparison to the mechanistic model and less need for data when compared to the pure deep learning model (Li et al., 2022).

2.3.5 Integration of nitrous oxide emission into plant-wide models

The main source for N_2O emissions at WWTPs is the biological treatment unit, and thus, mathematical modelling is mainly focused on the water treatment lines. However, if the total carbon footprint of a WWTP is to be assessed, a plant-wide model must be applied to also account for the direct and indirect GHG emissions emitted due to, e.g., sludge treatment and aeration. A plant-wide model can be an efficient tool to improve the plant operation by planning mitigation strategies for GHG emissions, while maintaining high effluent quality and realistic operational costs (Mannina et al., 2019).

The mechanistic N_2O models (sections 2.3.1–2.3.3) can be combined with ASM-type models, which is the most conventional approach to simulate N_2O emissions from full-scale WWTPs (Spérandio et al., 2022). Typically, a single- or two-pathway model for nitrification related N_2O emission is combined with the denitrification-related ASMN (Spérandio et al., 2022). Furthermore, the modelling of the water treatment lines must be complemented with models for solid and gaseous lines (Mannina et al., 2016). For this purpose, benchmarking models (BSMs) can be utilized, as they combine different process models to represent a virtual WWTP (Mannina et al., 2016). The first BSM covering all relevant treatment processes of a WWTP, Benchmark

Simulation Model No. 2 (BSM2), was published by the IWA Task Group on Benchmarking of Control Strategies for Wastewater Treatment Plants in 2018 (Alex et al., 2018).

2.3.6 Knowledge gaps in nitrous oxide modelling

Several mechanistic models exist to simulate N_2O production during wastewater treatment processes. The large variation mostly results from incomplete understanding of the mechanisms behind the N_2O production pathways, especially regarding NH_2OH oxidation and nitrifier denitrification. Furthermore, each nitrification related pathway model has been specified operational conditions regarding DO and NO_2^- in which it is applicable (Spérandio et al., 2022). Especially the use of single-pathway models requires careful consideration of the operational conditions to determine the dominant pathway in the system. Two-pathway models provide a more comprehensive description of nitrification related N_2O production. However, these models typically suffer from overparameterization, resulting in the need for heavy calibration (Vasilaki et al., 2019). Furthermore, short-term calibration and validation likely result in model accuracy only under specific conditions, e.g., dry weather, and limit the applicability of the model to study the effect of changes in the treatment system (Vasilaki et al., 2019).

Furthermore, regarding model calibration and validation, Snip et al. (2014) and Spérandio et al. (2016) identified a problem with performing model calibration with data obtained from batch experiments. The operational conditions in the batch tests are typically well-controlled and do not correspond to the highly dynamic operational conditions at WWTPs (Snip et al., 2014). In addition, the cultivated sludge for the experiments is exposed to a sudden change in the batch test conditions, which can lead to transient behaviour (Spérandio et al., 2016). Similarly, the microbial population dynamics in the activated sludge at full-scale WWTPs exhibit strong seasonality, which were found to contribute to the seasonal N_2O emission patterns by Gruber et al. (2021b). Therefore, long-term operational data from WWTPs is needed for model calibration to improve the accuracy of the N_2O emission simulations.

The gas-transfer kinetics of N_2O (section 2.2) are an important part of N_2O modelling, as the kinetics determine the amount of N_2O that is stripped to gaseous form from the liquid. Massara et al. (2017) note that reliable description of the gas-transfer kinetics of N_2O should be included in N_2O related modelling for accurate emission quantification. However, the reviewed articles in sections 2.3.1–2.3.3 do not seem to cover the modelling of the gas-transfer kinetics in detail. Therefore, it is suggestable to pay more attention to this area in N_2O modelling.

Vasilaki et al. (2019) suggest the co-application of data-driven and mechanistic models, complemented with long-term data from N_2O monitoring campaigns, to improve the understanding and effective control of emissions at WWTPs. According to Hwangbo et al. (2021), the problem with incomplete understanding of the N_2O production pathways could be overcome by data-driven N_2O modelling. However, also the conventional multivariate statistical tools, such as principal component analysis and k-means clustering, can be limited in the ability to quantitatively describe the long-term data dynamics typical to full-scale WWTPs (Hwangbo et al., 2021). Thus, the applicability of data-driven models in N_2O modelling should be studied further.

3 Research material and methods

Section 3 introduces the measurement equipment, treatment plants, data analysis related to the measurement campaigns and the background for the N_2O modelling experiment. Section 3.1 includes a description of the measurement equipment that was utilized during the N_2O measurement campaigns at the treatment plants, i.e., the gas analyzer, gas-collecting hood, and the laboratory analysis procedure to analyze NO_2^- from wastewater samples. Sections 3.2–3.4 introduce each of the treatment plants where the measurement campaigns were conducted, namely Kirkonkylä, Viinikanlahti and Akaa WWTPs. Section 3.5 details the equations and other principles regarding the processing of N_2O and aeration data to produce the results. In section 3.6, the background is provided for the process model of Viinikanlahti WWTP.

3.1 Measurement practices

3.1.1 Gasmet GT5000 Terra FTIR gas analyzer

Gasmet GT5000 Terra FTIR gas analyzer was used to measure the concentration of N_2O in the off-gas released from the biological treatment units. The gas analyzer includes a sampling probe with a hydrophobic polytetrafluoroethylene filter (Gasmet Technologies, n.d.). The probe collects the sample gas which is pumped to a sample cell with an internal pump. There is also an outlet to conduct the sample gas to the open air from the sample cell. The gas analyzer and the sampling probe are shown in figure 13.

Figure 13 Gasmet GT5000 Terra FTIR gas analyzer and the sampling probe.

The Gasmet GT5000 Terra FTIR gas analyzer identifies individual gases based on Fourier Transform Infrared (FTIR) spectroscopy. Due to unique molecular structures, different gases absorb infrared (IR) light with unique patterns (Gasmet Technologies, 2018). Figure 14 visualizes the FTIR spectroscopy that is utilized in the gas analyzer. The core is an interferometer which consists of a beam splitter, a moving mirror, and a fixed mirror (Gasmet Technologies, 2018). The interferometer and an IR light source are used to expose the gas molecules in the sample cell to all IR wavelengths simultaneously. The intensity of the IR light is measured with a detector after it has passed through the sample cell that contains the IR absorbing sample gas. The background without the sample gas should be measured with 5.0 purity N_2 gas every 24 hours (Gasmet Technologies, n.d.).

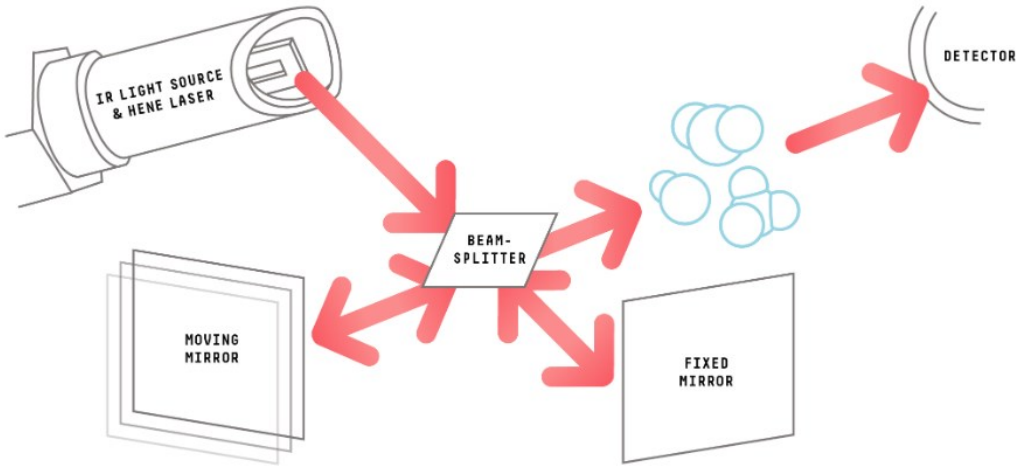

Figure 14 A visualization of the FTIR spectroscopy (Gasmet Technologies, 2018). The blue gas molecules represent the sample cell of the gas analyzer.

The intensity signal is converted from a time domain signal to a frequency domain signal with Fourier transform (Gasmet Technologies, 2018). Gasmet provides the resulting spectrum as the measured absorbance as a function of the wavenumber. The complete IR spectrum is collected 10 times per second and the minimum measurement interval is one minute. The collected spectra are combined into a co-add spectrum, which improves the accuracy of the gas analysis by increasing the signal-to-noise ratio (Gasmet Technologies, 2018). The spectrum is compared to the background spectrum to identify the absorbance of the sample gas at different wave numbers.

Individual gases and their concentrations in the sample gas are analyzed by utilizing a modified Classical Least Squares analysis algorithm and characteristic absorption spectra of individual gases (Gasmet Technologies, 2018). Such spectra have been measured from a known concentration of an IR absorbing gas diluted in nitrogen. The unique absorbance patterns of individual

gases and the absorbance peaks in relation to the reference spectra enable the simultaneous identification of multiple gases and the quantification of their concentration in the sample gas. Figure 15 is an example visualization of an analysis where four gases and their concentrations have been identified from a measurement spectrum. To analyze the measured spectra and store the results, the gas analyzer is connected to a computer installed with Calcmet software which is also a product by Gasmet Technologies (2018). Calcmet gives the concentrations of the gases in parts per million by volume (ppmv). The measurement range for N_2O is 0–1000 ppmv.

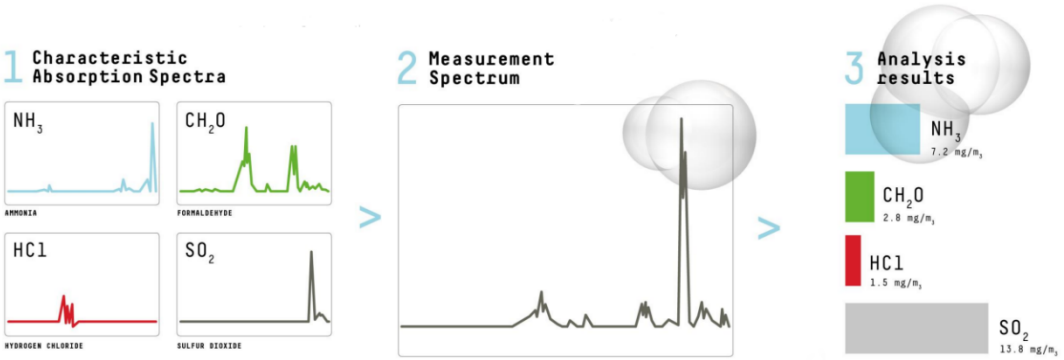

Figure 15 An example visualization of the analysis of a measurement spectrum with characteristic absorption spectra to identify the gases and their concentrations in the sample gas (Gasmet Technologies, 2018).

The operating temperatures for the gas analyzer are -5–40°C for short term periods and 5–30°C for long term periods (Gasmet Technologies, n.d). The conditions for the sample gas are ambient pressure and ambient temperature (between -5–40°C, non-condensing). The performance specifications of the gas analyzer are detailed in table 4.

Table 4 Performance specifications of the Gasmet GT5000 Terra FTIR gas analyzer (Gasmet Technologies, n.d.).

Parameter	Performance specification
Zero-point drift	< 2% of measuring range per 24h background measurement interval
Sensitivity drift	None
Linearity deviation	< 2% of measuring range
Temperature drift	< 1% of measuring range per 10K temperature change. Ambient temperature changes are measured and compensated.
Pressure influence	< 1% change of measuring value for 1% sample pressure change. Ambient pressure changes are measured and compensated.

3.1.2 Gas-collecting hood

A gas-collecting hood was built to collect the stripped off-gas from the aerobic compartments of the biological treatment unit. The frame of the hood was a 1.17 m x 1.17 m square built from polyvinyl chloride (PVC) pipes. The frame was covered with a polyethylene tarp, tied to place with yarn. The off-gas was collected from an area of a square meter inside the frame. The hood was stabilized by connecting the frame to a vertically aligned PVC pipe with metal wires. Figure 16 shows the structure of the hood. A seven-meter PVC pipe was connected to the top of the hood to transfer the off-gas to the gas analyzer.

Figure 16 The structure of the gas-collecting hood.

3.1.3 Measurement practice on-site

The measurement locations were the aerobic compartments in the biological treatment units, as it is assumed that N_2O, produced both by nitrification and heterotrophic denitrification, is mainly emitted during aeration due to intensified gas stripping, as discussed in section 2.2. Parallel biological treatment units, i.e., aeration lines, with similar configurations were assumed identical if the flows and loads were divided equally and there were no other known differences between the lines. Therefore, the measurements mainly focused on one aeration line.

Principally, a compartment in the beginning and end of the aerobic phase were monitored to study the spatial variation in the emissions. To study the contribution of nitrification and denitrification to the N_2O emissions, it was assumed that high N_2O concentrations in the beginning of the aerobic phase would indicate that N_2O was produced during denitrification in the anoxic compartments and was stripped from the liquid phase to the gas phase at the

start of aeration. Respectively, high N_2O concentrations at the end of the aerobic phase would suggest that N_2O production occurred during nitrification.

The gas-collecting hood was placed in one compartment of the aeration line at a time. The hood was kept in place by tying it to the nearest railings with thin ropes. The pipe transported the off-gas to the gas analyzer which was covered with a wooden box for protection. Figure 17 visualizes the measurement setup.

The off-gas measurement was continuous and the minimum measurement interval of one minute was used during all measurements. A measurement break of 30 minutes occurred daily due to the background measurement. Otherwise, the measurements were paused mainly due to the shutdown of the computer and when the measurement setup was moved between the compartments.

(a) (b)

Figure 17 The measurement setup on-site for N_2O measurement campaigns.

3.1.4 Laboratory analysis of nitrite

Dissolved NO_2^- was analyzed from wastewater samples during the measurement campaigns to study the correlation between dissolved NO_2^- and the measured N_2O concentrations, as suggested by literature covered in sections 2.1.1–2.1.3. The NO_2^- samples were collected and analyzed approximately three times per day to estimate temporal variation.

The NO_2^- analysis was conducted according to SFS 3029:1976. The NO_2^- analysis included the following steps

- A wastewater sample was collected near the N_2O measurement in the aerobic compartment from a depth of 20 cm to 50 cm.
- The wastewater sample was filtered with a 0.45 µm filter.
- The sample for analysis was prepared by pipetting 5 ml of the filtered wastewater sample or its dilution to a sampling tube.
- The sample was dosed with 125 µl of sulfanilamide (SA) solution and the sample was mixed.
- After 4–6 minutes, 125 µl of N-(1-Napthyl)ethylenediamine (NED) was added to the sample. The sample was again mixed after which it was placed into darkness for 20 minutes to 2 hours.
- The absorbance of the sample was measured in a UV spectrophotometer (Shimadzu UV-VIS Spectrophotometer UV-1201) with a 10 mm optical glass cuvette at a wavelength of 545 nm.

The NO_2^- concentration of the sample was calculated with equation 1. If the analyzed sample was diluted, the dilution factor was accounted for to obtain the NO_2^- concentration in the collected wastewater sample.

$$c_{NO_2^-} = 294.1 * abs - 0.794 \quad (1)$$

Where

c_{NO2^-}	NO_2^- concentration of the sample [µg/l]
abs	Absorbance of the sample at 545 nm within a range of 0–1.8 [-]

3.2 Kirkonkylä WWTP, Mäntsälä

3.2.1 Treatment process

Kirkonkylä WWTP is operated by Nivos Vesi ja Lämpö in Mäntsälä in southern Finland. The size of the plant is approximately 14 000 PE, and the design inflow is 4 500 m^3/d. Regarding nitrogen removal, the environmental permit of Kirkonkylä WWTP requires that the plant removes 70% of the influent total nitrogen. Additionally, the nitrification rate should be above 90% and the effluent NH_4^+-nitrogen concentration should be limited to 4 mg/l. The fulfillment of the requirements is supervised with monthly water samples collected at the plant.

The treatment process of Kirkonkylä WWTP consists of mechanical, chemical, and biological treatment. A simplified process figure of the treatment process is presented in figure 18. The influent wastewater is first treated mechanically, including screening, aerated grit removal and primary

clarification. The primary clarifier is partially bypassed for 9–16 hours every day, depending on the temperature of the wastewater. The bypassed flow is directly introduced into the biological treatment to support denitrification with a higher load of organic carbon source.

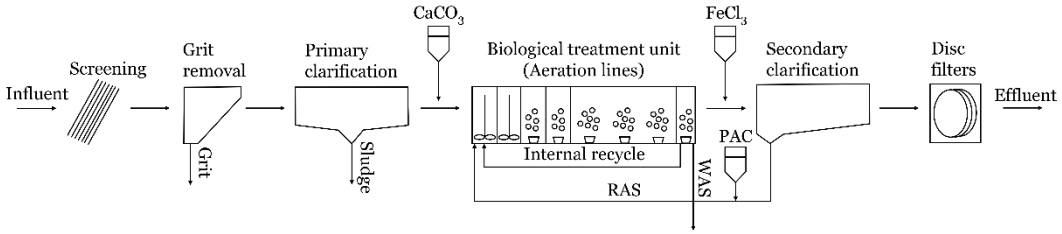

Figure 18 The main treatment process at Kirkonkylä WWTP.

The biological treatment is an activated sludge (AS) process consisting of biological treatment units (aeration lines) and secondary clarifiers. Before the biological treatment, calcium carbonate ($CaCO_3$) is dosed to adjust the pH and alkalinity. The AS process has two identical parallel aeration lines with a total treatment volume of 1 900 m^3. Each aeration line is divided into six compartments which are either anoxic and denitrifying or aerobic and nitrifying. Depending on the temperature of the wastewater, 1–3 of the compartments are anoxic in the beginning of the lines and the latter 3–5 compartments are aerobic. An internal recycle from the last compartment to the first compartment recycles NO_3^- produced during nitrification to the denitrifying compartments for total nitrogen removal.

Two secondary clarifiers, one for each aeration line, settle the sludge from the treated water. The dosing point for ferric chloride ($FeCl_3$) is prior to the clarifiers to precipitate phosphorus during the clarification. The settled sludge is recycled back to the beginning of the aeration lines as return activated sludge (RAS). RAS is dosed with polyaluminium chloride (PAC) to minimize the amount of floating sludge in the process. To retain the desired sludge age in the biological treatment, a fixed portion of the sludge is removed from the end of the aeration lines as waste activated sludge (WAS). WAS and the sludge removed from the primary clarifier are dewatered in a centrifuge and stored to await delivery to further treatment.

The last treatment step at Kirkonkylä WWTP is tertiary treatment with two units of disc filters, each unit consisting of eight discs. The tertiary treatment has been added to the process to improve the treatment results and increase the treatment capacity. During disturbances in the process, the water can be dosed with PAC and polymer to coagulate and flocculate colloidal particles. The particles are filtered out in the disc filters and the treated effluent is discharged to river Mäntsälänjoki.

3.2.2 Measurement campaigns

Two measurement campaigns were conducted at Kirkonkylä WWTP, in June–July 2022 and January 2023. In June–July, the campaign lasted for four days, and it took place between Tuesday 28 June and Friday 1 July. The measurement location was compartment 5 of aeration line 2 which was the second to last aerobic compartment, as visualized in figure 19. During the measurements, 59 hours (2.5 days) of data was collected.

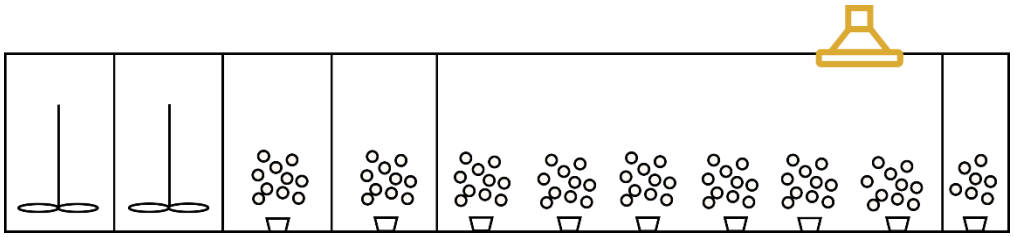

Figure 19 The measurement location in aeration line 2 during the measurement campaign at Kirkonkylä WWTP in June–July 2022.

The winter measurement campaign was conducted from 9 to 24 January 2023. The measurements started in compartment 5 of aeration line 2, similarly to the first measurement campaign. Additionally, N_2O was monitored from the third compartment of line 2. Figure 20 visualizes the measurement locations in the aeration line. At the start of the measurement campaign, the first compartment was anoxic while the latter five compartments were aerobic. However, in the middle of the measurement campaign, on 13 January, aeration started also in the first compartment to prepare the treatment process for increased inflows due to a rainstorm. Thus, all compartments were aerobic during the last four measurement days in compartment 5 and all measurements in compartment 3.

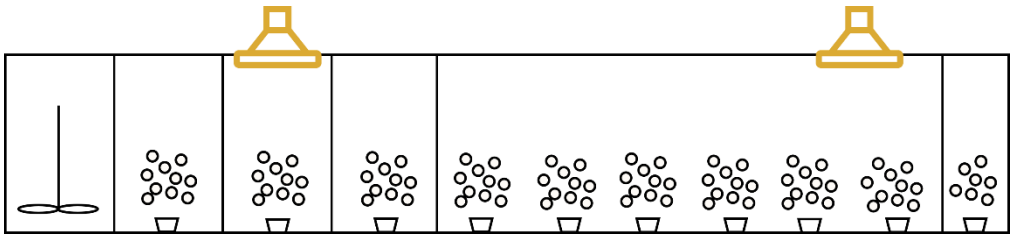

Figure 20 The measurement locations in aeration line 2 during the measurement campaign at Kirkonkylä WWTP in January 2023. On 13 January, the first compartment was switched from anoxic to aerobic and thus, compartment 3 was measured when all compartments were aerobic.

In total, 283 hours (11.8 days) of data was collected during January, of which 180 hours (7.5 days) from compartment 5 and 161 hours (6.7 days) from compartment 3. However, during N_2O monitoring in compartment 3, difficulties

were faced with the measurement setup due to cold temperatures, as the pipe did not transport the off-gas to the gas analyzer properly. Therefore, 55 hours (2.3 days) of data collected from compartment 3 had to be excluded from the data analysis as unrepresentative.

The parameters in table 5 describe the operational conditions and influent and effluent quality during the measurement campaigns. The BOD was analyzed as the 7-day BOD (BOD_7). The pH was below 7 during both measurement campaigns, which represents the normal operating conditions at Kirkonkylä WWTP, as the pH is typically 6.2–6.5. Even though the pH is relatively low, it has not been detected to affect the treatment process or the treatment results negatively. However, the rainstorm that occurred during January caused a drop in pH to a slightly abnormal level of 5.8–6.1 between 14 and 17 January.

The rainstorm in the middle of the January measurement campaign caused inflows two to three times the typical inflow of 2 500 m^3/d between 13 and 16 January (figure 21). To prepare for the increased inflows, the bypass of the primary clarifier was stopped to treat all water in the clarifier and all six compartments were switched to aerobic in the biological treatment unit. The changes were made on 13 January and remained as such until the end of the measurement campaign. From 14 to 18 January, 100–300 m^3/h of the inflow bypassed the AS process and was conducted directly from the primary clarifier to the disc filters. Table 5 includes the flow rate to the biological treatment to consider only the inflow undergoing the nitrogen conversion processes which are also responsible for N_2O production.

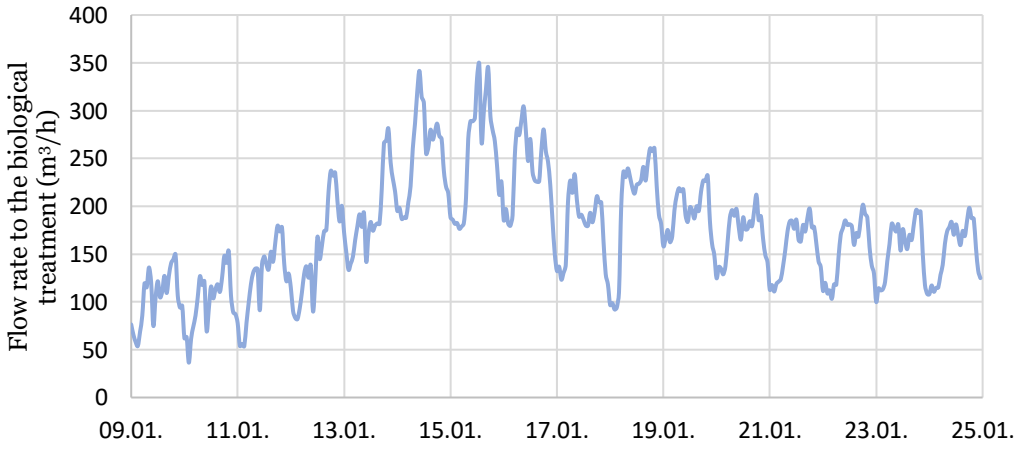

Figure 21 The flow rate to the biological treatment during the January measurement campaign at Kirkonkylä WWTP. The flow rates increased between 13 and 16 January due to a rainstorm.

Table 5 Operational conditions and influent and effluent quality during the measurement campaigns at Kirkonkylä WWTP.

Parameter	Average value (Minimum-maximum)	
	June–July 2022	**January 2023**
Influent flow rate to biological treatment (m^3/h)	110 (40–180)	170 (40–350)
Temperature in biological treatment (°C)	15 (15–16)	8 (7–10)
pH in biological treatment	6.4 (6.3–6.4)	6.2 (5.8–6.4)
Sludge content in biological treatment (g/l)	4.6 (4.3–5.8)	5.9 (5.0–7.0)
DO in compartment 5 of aeration line 2 (mg/l)	2.5 (2.2–2.9)	3.0 (1.0–4.7)
DO in compartment 3 of aeration line 2 (mg/l)	-	3.2 (2.2–5.3)
NO_3^- after biological treatment (mg/l)	14 (11–18)	18 (4–36)
NH_4^+ after biological treatment (mg/l)	0 (–)	3.2 (0–17)
Influent total nitrogen (mg/l)	65 (-)	45 (28–61)
Effluent total nitrogen (mg/l)	10 (-)	20 (13–26)
Influent BOD_7 (mg/l)	270 (-)	210 (180–240)
Effluent BOD_7 (mg/l)	3.4 (-)	8.0 (3.0–13)
Influent COD (mg/l)	560 (-)	415 (350–480)
Effluent COD (mg/l)	36 (-)	43 (32–53)
BOD_7/N ratio after primary clarification	2.7 (-)	3.4 (3.1–3.6)
COD/N ratio after primary clarification	6.7 (-)	8.2 (8.0–8.3)
Influent alkalinity (mmol/l)	5.2 (-)	5.4 (-)
Effluent alkalinity (mmol/l)	2.8 (-)	1.8 (-)

3.3 Viinikanlahti WWTP, Tampere

3.3.1 Treatment process

Viinikanlahti WWTP is operated by Tampereen Vesi and it is located in Tampere in western Finland. The size of Viinikanlahti WWTP is 350 000 PE and the average daily inflow is 65 000 m^3/d. Regarding nitrogen removal, the environmental permit of Viinikanlahti WWTP requires a minimum nitrification rate of 90% and to limit the effluent NH_4^+-N concentration to a maximum of 4 mg/l. Thus, the plant is not obliged to total nitrogen removal. The fulfillment of the requirements is supervised with biweekly water samples collected at the plant.

The treatment process is summarized in figure 22. The mechanical treatment in the beginning of the process includes screening, aerated grit removal and primary clarification to remove the largest solids, grit, and a part of the organic matter from the wastewater. The chemicals that are added to the treatment process include ferric sulfate ($Fe_2(SO_4)_3$), $CaCO_3$ and polymer. $Fe_2(SO_4)_3$ is used to precipitate phosphorus and it is first dosed before grit removal.

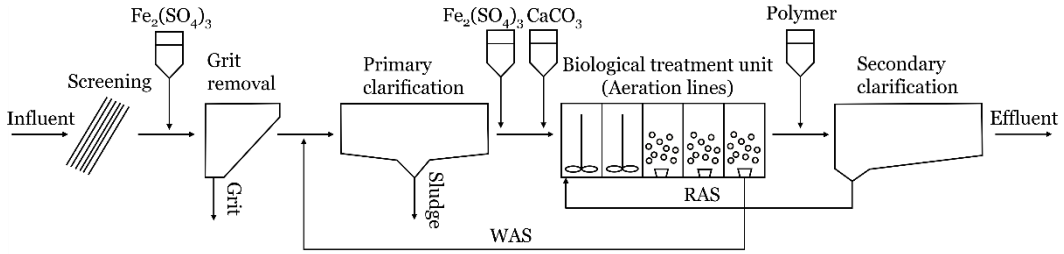

Figure 22 The main treatment process of Viinikanlahti WWTP.

The biological treatment is an AS process, and it follows the primary clarification. The AS process is a combination of eight biological treatment units (aeration lines) and 16 secondary clarifiers. The eight identical parallel aeration lines have a total treatment volume of 17 000 m^3. Each line is divided into five compartments. During the warm-period conditions, the first two compartments are mechanically mixed to denitrify, and three compartments are aerated to nitrify. The process is run as fully nitrifying in the cold-period conditions with all compartments aerated. Before the aeration lines, $Fe_2(SO_4)_3$ is dosed for phosphorus removal and $CaCO_3$ to adjust pH and alkalinity.

Secondary clarifiers, two for each aeration line, complete the treatment process. Polymer is added to the water entering the secondary clarifiers to enhance the settling of sludge and residual phosphorus. The settled sludge is

conducted from the clarifiers back to the beginning of the aeration lines as a RAS flow. To control the sludge age, WAS is removed from the end of the aeration lines and conducted to the primary clarifier where the sludge is settled and removed from the treatment process. The effluent water after the secondary clarifiers is discharged to Lake Pyhäjärvi.

3.3.2 Measurement campaigns

The measurement campaigns at Viinikanlahti WWTP were conducted in September and November 2022. During both measurement campaigns, there were aeration lines with varying configurations. Three lines (lines 3, 5 and 7) had the configuration as intended by the plant operators, i.e., two anoxic compartments and three aerobic compartments, as visualized by figure 23(a). Four lines (lines 1, 4, 6 and 8) had only one anoxic compartment and four aerobic compartments, visualized by figure 23(b), due to impaired mixers. The configuration of aeration line 2 changed during the September measurement campaign from all aerobic compartments to one anoxic compartment (compartment 2) and four aerobic compartments. In November, aeration line 2 was fully aerated with five aerobic compartments, as visualized by figure 24(c).

The measurement campaign in September was conducted between 12 and 30 September and included measurement data from 19 days. In total, 396 hours (16.5 days) of data was collected during September. The measured compartments are marked in figure 23. Compartments 3 and 5 were measured from line 3. The measurements started from compartment 5 which was measured for 184 hours (7.7 days) after which compartment 3 was measured for 129 hours (5.4 days). The last measurement location, compartment 3 from line 4, was measured for 83 hours (3.5 days).

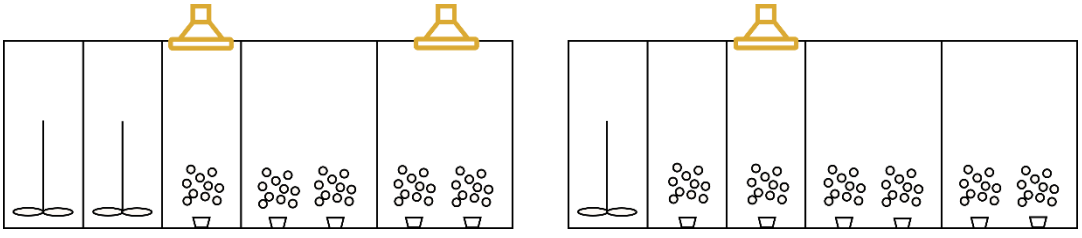

(a) (b)

Figure 23 The measurement locations in aeration line 3 (a) and in line 4 (b) at Viinikanlahti WWTP in September 2022.

The second measurement campaign was a 17-day campaign from 14 to 30 November 2022. In total, 348 hours (14.5 days) of measurement data was collected from four measurement locations. The measurement locations are visualized by figure 24. Similarly to September, compartments 3 and 5 of

aeration line 3 were monitored. Measurement data from these compartments was 183 hours (7.6 days) from compartment 5 and 66 hours (2.8 days) from compartment 3. Additionally, compartment 5 in line 7 was monitored for 17 hours to compare the N_2O emission level to the same compartment in line 3. In addition, compartment 3 aeration line 2 was monitored for 82 hours (3.4 days) to compare the emissions between lines of different configurations.

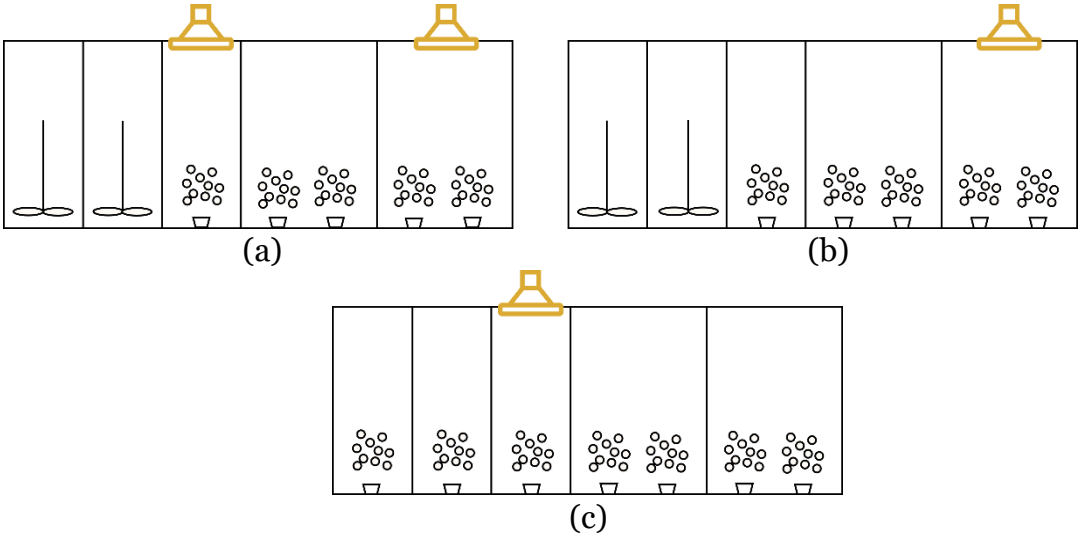

Figure 24 The measurement locations in aeration line 3 (a), in line 7 (b) and in line 2 (c) at Viinikanlahti WWTP in November 2022.

Parameters describing the operational conditions and influent and effluent quality during the measurement campaigns are collected to table 6. The COD concentration of the water after primary clarification was estimated from the influent COD concentration according to the principles detailed in section 3.6. The COD/N ratio after primary clarification describes the ratio of the water conducted to the biological treatment, as primary clarification significantly reduces the influent COD load. Thus, also the COD/N ratio of the influent is decreased during primary clarification.

Viinikanlahti WWTP receives industrial wastewater from a board mill, which explains the relatively high fluctuation in the temperatures detected during both measurement campaigns. As the temperature of the industrial wastewater is assumably around 30 °C, it also results in relatively warm temperatures in the biological treatment at Viinikanlahti WWTP. For a reference, the average temperature at Akaa WWTP was 10 °C in December 2022, while the average temperature a month earlier was 15 °C at Viinikanlahti WWTP.

Table 6 Operational conditions and influent and effluent quality during the measurement campaigns at Viinikanlahti WWTP.

Parameter	Average value (Minimum-maximum)	
	September 2022	**November 2022**
Influent flow rate (m^3/h)	2550 (1180–4510)	2700 (1230–3700)
Temperature in biological treatment (°C)	18 (14–20)	15 (11–17)
pH in biological treatment	7.0 (6.9–7.2)	7.0 (6.8–7.1)
Sludge content in biological treatment (g/l)	4.6 (4.2–5.7)	4.6 (4.2–5.0)
DO in compartment 3 of aeration line 2 (mg/l)	3.1 (0.4–4.1)	2.0 (1.8–2.6)
DO in compartment 3 of aeration line 3 (mg/l)	1.8 (1.0–2.5)	2.0 (1.8–2.2)
DO in compartment 5 of aeration line 3 (mg/l)	2.0 (0.9–3.2)	2.0 (1.7–2.4)
DO in compartment 3 of aeration line 4 (mg/l)	1.8 (0.4–3.1)	2.0 (1.8–2.3)
DO in compartment 5 of aeration line 7 (mg/l)	3.1 (1.0–6.1)	2.9 (1.5–6.1)
Influent total nitrogen (mg/l)	59.0 (53.0–65.0)	56.0 (54.0–57.0)
Effluent total nitrogen (mg/l)	36.5 (34.0–41.0)	34.5 (34.0–35.0)
Influent BOD_7 (mg/l)	310 (260–370)	310 (280–340)
Effluent BOD_7 (mg/l)	1.9 (1.5–3.5)	2.0 (1.5–3.5)
Influent COD (mg/l)	740 (-)	540 (-)
Effluent COD (mg/l)	33 (-)	36 (-)
BOD_7/N ratio after primary clarification	1.3 (-)	1.1 (-)
COD/N ratio after primary clarification, estimation	9.3 (-)	6.8 (-)
Influent alkalinity (mmol/l)	5.3 (4.7–5.6)	5.1 (5.0–5.2)
Effluent alkalinity (mmol/l)	2.6 (2.3–2.9)	2.4 (2.3–2.5)

3.3.3 Carbon footprint of Viinikanlahti WWTP

The carbon footprint of Viinikanlahti WWTP has been estimated for the year 2021, including estimations for N_2O emissions. The direct greenhouse gas emissions from the wastewater treatment process were in total 9 565 metric tonnes of CO_2 equivalents of which the share of N_2O was 7 520 metric tonnes of CO_2 equivalents and the share of methane (CH_4) was 2 045 metric tonnes of CO_2 equivalents (Mäki, 2022). Additionally, biogas emissions of 50 metric tonnes of CO_2 equivalents occurred during disturbances in sludge digestion. Indirect emissions originated from district heating and were in total 222 metric tonnes of CO_2 equivalents. The contract for electricity is carbon neutral and therefore, electricity has no share in the carbon footprint. Moreover, the emissions from fuel consumption by vehicles were estimated but these emissions were allocated to Tampereen Vesi and were not included in the carbon footprint of Viinikanlahti WWTP, or other treatment facilities operated by Tampereen Vesi.

Figure 25 visualizes the carbon footprint of Viinikanlahti WWTP. The estimated N_2O emissions account for 76% of the total carbon footprint. An emission factor of 0.0212083 kg-N_2O/kg of nitrified nitrogen was used to estimate the N_2O emissions, derived from long-term N_2O monitoring data from Viikinmäki WWTP (Mäki, 2022).

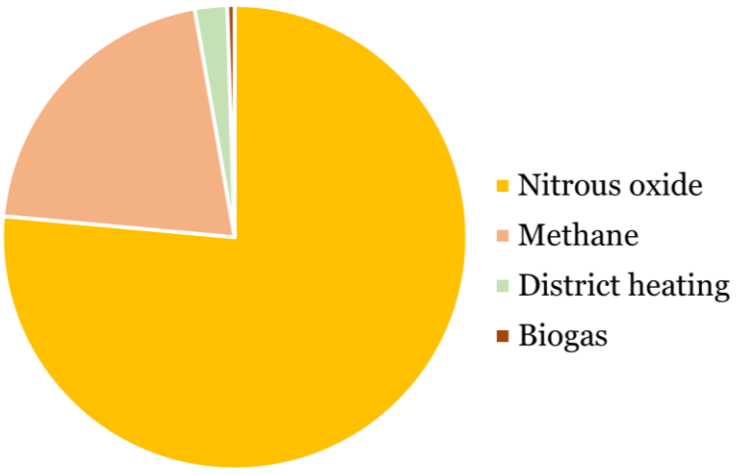

Figure 25 The shares of GHG emission sources at Viinikanlahti WWTP.

3.4 Akaa WWTP, Akaa

3.4.1 Treatment process

Akaa WWTP is under the operation of Hämeenlinnan Seudun Vesi and located in Akaa in western Finland. Akaa WWTP is of size 70 000 PE and the

design inflow is 13 000 m³/d. However, the realized inflow has been 4 500–5 500 m³/d in 2012–2021, and thus less than a half of the design inflow. Furthermore, the realized PE, calculated based on the incoming BOD_7 loads, was approximately 20 000 PE in 2021. Thus, there is also a significant gap between the design PE and the realized PE.

Regarding nitrogen removal, the environmental permit of Akaa WWTP requires that the plant removes 50% of the influent total nitrogen, when the temperature in the biological treatment is above 12 °C. Furthermore, the effluent total nitrogen and NH_4^+-nitrogen concentrations should be below 20 mg/l and 8 mg/l, respectively. The fulfillment of the requirements is supervised with monthly water samples collected at the plant.

In the beginning of the main treatment process, the influent wastewater is screened to remove the coarsest impurities before grit removal and primary clarification. To adjust pH and alkalinity in the process, calcium hydroxide ($Ca(OH)_2$) is added to the water entering the primary clarification. Figure 26 summarizes the main treatment process at Akaa WWTP.

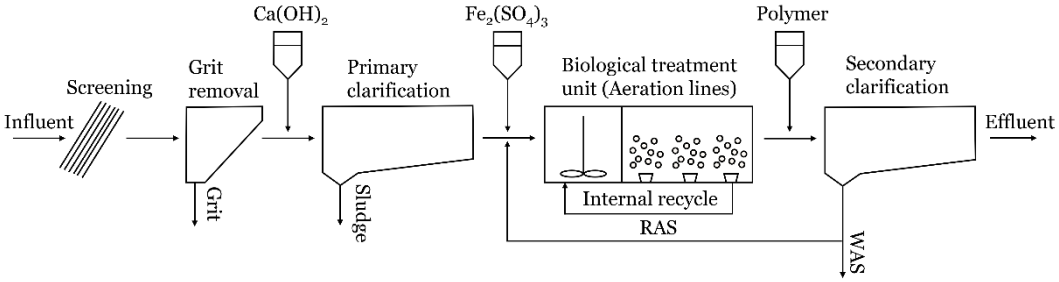

Figure 26 The main treatment process at Akaa WWTP.

The biological treatment is an AS process which is a combination of biological treatment units (aeration lines) and secondary clarifiers. The aeration lines consist of an anoxic compartment in the beginning of the unit and an aerobic compartment in the latter part of the unit. There are four parallel aeration lines with a total volume of 2 040 m³. Approximately 30% of the treatment volume is anoxic to enable denitrification and 70% of the volume is aerobic for nitrification. An internal recycle pumps water and activated sludge from the end of the aerobic compartment to the beginning of the anoxic compartment. To ensure phosphorus removal, $Fe_2(SO_4)_3$ is dosed prior to the aeration lines.

The secondary clarifiers finish the main treatment process. There are two clarifiers, i.e., one clarifier per two aeration lines. Secondary clarification separates the sludge from the effluent water which is discharged to River Nahkialanjoki. Polymer is dosed before the secondary clarifiers to enhance

sludge settling. The settled sludge is partly recycled back to the beginning of the aeration lines as RAS and partly removed as WAS and conducted to sludge treatment. The RAS and WAS flows are controlled according to the desired sludge age in the AS process.

Akaa WWTP has a separate treatment unit to treat the by-pass waters that are not treated in the main treatment process. However, the treatment unit is targeted to only remove solids and phosphorus, and it is therefore not a potential source for N_2O emissions.

3.4.2 Measurement campaign

A measurement campaign of 17 days was conducted at Akaa WWTP from 5 until 21 December 2022. The aerobic compartments of lines 1 and 3 were the focus of the measurement campaign. As the aerobic compartment was not divided into smaller compartments at Akaa WWTP, N_2O emissions were monitored at the beginning and end of the compartment.

The measurement was first placed to the end of the aerobic compartment in line 3 for 136 hours (5.7 days) and then moved to the beginning of the compartment for 98 hours (4.1 days). Similarly, the same measurement locations were monitored for 92 hours (3.4 days) and 21 hours (0.9 days) in line 1. The measurement locations are visualized in figure 27.

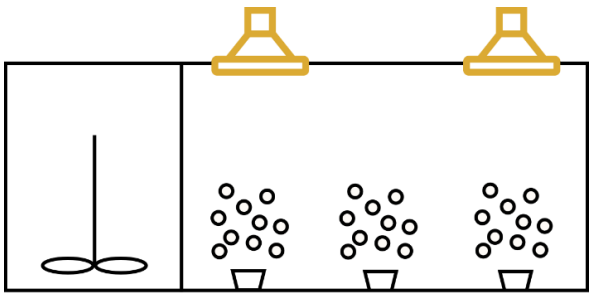

Figure 27 Measurement locations in aeration lines 1 and 3 at Akaa WWTP.

The key parameters during the measurement campaign are collected to table 7. The measurement campaign included DO measurements with a DO probe in the beginning of the aerobic compartments, as an online measurement was only placed at the end of the compartments.

A fault in $CaCO_3$ dosing occurred at the start of the measurement campaign, causing a decreased pH (5.4–6.4) between 5 and 13 December after which the normal pH level of 6.5–7.0 was reached again. Furthermore, the influent sample is collected from a point where the influent has been mixed with reject waters from the treatment process which affect the laboratory analysis results of the influent sample.

Table 7 Operational conditions and influent and effluent quality during the measurement campaign at Akaa WWTP.

Parameter	Value		
	Average	Minimum	Maximum
Influent flow rate (m^3/h)	138	60	602
Temperature in biological treatment (°C)	10	8	11
pH in biological treatment	6.5	5.4	7.0
Sludge content in biological treatment (g/l)	5.1	3.9	7.2
DO in aeration line 1 (mg/l), online measurement at the end of the aerobic compartment	1.7	0.5	4.2
DO in aeration line 1 (mg/l), 7 measurements in the beginning of the aerobic compartment	1.5	1.1	2.2
DO in aeration line 3 (mg/l), online measurement at the end of the aerobic compartment	4.3	3.1	5.1
DO in aeration line 3 (mg/l), 23 measurements in the beginning of the aerobic compartment	0.9	0.5	2.2
NH_4^+ in secondary clarification (mg/l)	0.3	0	1
NO_3^- in secondary clarification (mg/l)	33	17	45
Influent total nitrogen (mg/l)	86	-	-
Effluent total nitrogen (mg/l)	37	-	-
Influent BOD_7 (mg/l)	330	-	-
Effluent BOD_7 (mg/l)	4.8	-	-
Influent COD (mg/l)	760	-	-
Effluent COD (mg/l)	32	-	-
BOD_7/N ratio after primary clarification	2.8	-	-
COD/N ratio after primary clarification	6.6	-	-
Influent alkalinity (mmol/l)	7.0	-	-
Effluent alkalinity (mmol/l)	1.6	-	-

3.5 Data analysis

3.5.1 Equations to quantify nitrous oxide emissions

The data from the measurement campaigns was used to quantify the level of N_2O emissions by calculating the emitted N_2O-N load, and two emission factors. The parameters were calculated according to Loosli and Joss (2021).

The N_2O-N load gives the mass of nitrogen emitted as N_2O-N. The hourly N_2O-N load is calculated according to equation 2.

$$L_{N_2O-N} = c_{N_2O-N,off-gas} * Q_{air} = \frac{N_2O_{measured}}{10^6} * Q_{air} * \frac{p_N}{R * T_N} * M_N \qquad (2)$$

Where

L_{N2O-N}	Emitted N_2O-N load per time interval [gN/h]
$c_{N2O-N,off-gas}$	N_2O-N concentration in the off-gas [gN/Nm³]
Q_{air}	Averaged air flow rate in the aeration tank, in standard cubic meters per hour [Nm³/h]
$N_2O_{measured}$	Measured N_2O concentration in the off-gas [ppmv]
p_N	Standard pressure: 101 325 Pa [Pa]
T_N	Standard temperature: 298 K [K]
R	Universal gas constant: 8.314 J/mole/K [J/mole/K]
M_N	Molar mass of N_2O-N: 28 gN/mole [gN/mole]

Emission factor is the most used parameter for comparing N_2O emissions between different plants and plant configurations (Loosli and Joss, 2021). Typically, the emission factor is derived by relating the emitted N_2O-N load to the nitrogen load in the influent wastewater, according to equation 3.

$$EF_{N_2O-N} = \frac{L_{N_2O-N}}{L_N} * 100 \qquad (3)$$

Where

EF_{N2O-N}	Emission factor relative to influent nitrogen load [%]
L_{N2O-N}	Emitted N_2O-N load [gN/d]
L_N	Influent nitrogen load, including external co-substrates [gN/d]

An additional emission factor can be calculated relative to the amount of nitrogen removed during the wastewater treatment process. This emission factor especially describes how efficiently the treatment process removes the influent nitrogen load. Equation 4 was derived by applying equation 3.

$$EF_{N,removed} = \frac{L_{N_2O-N}}{L_{N,removed}} * 100 = \frac{L_{N_2O-N}}{L_N - L_{N,effluent}} * 100 \quad (4)$$

Where

$EF_{N,removed}$	Emission factor relative to removed nitrogen load [%]
L_{N_2O-N}	Emitted N_2O-N load [gN/d]
$L_{N,removed}$	The mass of nitrogen removed in the treatment process [gN/d]
L_N	Nitrogen load in the influent [gN/d]
$L_{N,effluent}$	Nitrogen load in the effluent [gN/d]

The nitrogen load in the influent is typically analyzed from 24-hour composite samples, thus the N_2O-N load is aggregated to daily values to calculate the emission factor (Loosli and Joss, 2021). The influent nitrogen load is calculated with equation 5.

$$L_N = c_N * Q_{inflow} + L_{N,co-substrate} \quad (5)$$

Where

L_N	Nitrogen load in the influent [gN/d]
c_N	Nitrogen concentration in the inflow according to flow proportional sample [gN/m³]
Q_{inflow}	Influent flow to the WWTP over the sampling duration [m³/d]
$L_{N,co-substrate}$	Nitrogen load fed to digester as co-substrate [gN/d]

The additional nitrogen load from co-digestion of external substrates ($L_{N,co-substrate}$) should not be included in the influent nitrogen load if reject water from sludge-dewatering is treated separately and the N_2O emissions from the separate treatment process are not monitored (Loosli and Joss, 2021). The term is not relevant for the WWTPs monitored during this thesis, as only Viinikanlahti WWTP has digesters to which they do not receive external substrates. Kirkonkylä WWTP and Akaa WWTP deliver the sludge for further treatment to other facilities.

The effluent nitrogen load (equation 6) can be calculated similarly to the influent nitrogen load, but the term $L_{N,co-substrate}$ is excluded.

$$L_{N,effluent} = c_N * Q_{inflow} \quad (6)$$

Where

$L_{N,effluent}$	Nitrogen load in the effluent [gN/d]
c_N	Nitrogen concentration in the effluent according to flow proportional sample [gN/m³]
Q_{inflow}	Influent flow to the WWTP over the sampling duration [m³/d]

3.5.2 Processing of the measured nitrous oxide concentrations

During the measurement campaigns, the N_2O concentrations were measured as ppmv. For better interpretation, the concentrations were converted into g/Nm³, describing the mass of N_2O in a normalized cubic meter of the off-gas released from the aerobic compartments. The unit conversion was found by applying equation 2 which includes a conversion from ppmv to gN/Nm³. By replacing the molar mass of nitrogen with the molar mass of N_2O, equation 7 was found.

$$c_{N_2O,off-gas} = \frac{N_2O_{measured}}{10^6} * \frac{p_N}{R * T_N} * M_{N_2O} \quad (7)$$

Where

$c_{N2O,off-gas}$	N_2O concentration in the off-gas [g/Nm³]
$N_2O_{measured}$	Measured N_2O concentration in the off-gas [ppmv]
p_N	Standard pressure: 101 325 Pa [Pa]
T_N	Standard temperature: 298 K [K]
R	Universal gas constant: 8.314 J/mole/K [J/mole/K]
M_{N2O}	Molar mass of N_2O: 44 g/mole [g/mole]

The N_2O concentrations were not measured from the measured compartments for each hour for every day of the week due to measurement breaks and limited duration of the measurement campaigns. Therefore, the concentrations for the missing hours were estimated based on the measured data. If there was a maximum of three hours of missing N_2O concentrations in between the measured data, the concentrations were estimated by linearly interpolating between the last measured concentration before the measurement break and the first measured concentration after the break. Otherwise, the missing concentration was calculated as the average of the measured concentrations from the same hour of the other weekdays. If the missing concentration was from the weekend, the measured concentration from the same

hour of the other day of the weekend was primarily used as the estimate for the missing concentration.

Furthermore, the measurement campaigns included measurements from 1–4 aerobic compartments which meant that not all compartments could be measured. The N_2O concentrations were assumed to change linearly between the compartments. Thus, the N_2O concentrations for the unmeasured compartments could be estimated with linear regression analysis based on the data collected from the measured compartments. As a simple example, if there was data from compartments 3 and 5, the N_2O concentrations for compartment 4 were calculated as the average of the concentrations measured from compartments 3 and 5. Hourly N_2O concentrations were calculated for each compartment for each hour of the measurement campaign. However, if only one compartment was monitored during the measurement campaign, the same N_2O concentrations were assumed for each aerobic compartment.

Certain assumptions were made regarding the configurations of the aeration lines and the allocation of the N_2O emissions, due to the limited data availability to estimate compartment-specific air flows (section 3.5.3). Compartment-specific N_2O concentrations and air flows were needed to calculate the N_2O-N loads and emission factors. In the results for Viinikanlahti WWTP, all lines were assumed to have a configuration of two anoxic compartments and three aerobic compartments, even though there were lines with more aerobic compartments due to impaired mixers. Assumably, the lines with more than three aerobic compartments emit N_2O from all aerobic compartments, instead of only compartments 3–5. However, the increased emissions from these lines were accounted for in the emission calculations, as the total air flow distributed between compartments 3–5 was higher than in lines where there were only three aerobic compartments. Furthermore, the N_2O-N load and emission factor calculations were based on the measurement data from line 3, as most of the measurements were conducted in that line. The N_2O data collected from other aeration lines was compared with the emission level measured in line 3.

During the measurement campaign at Kirkonkylä WWTP in January 2023, the number of aerobic compartments in the aeration lines increased from five aerobic compartments (compartments 2–6) to six aerobic compartments (compartments 1–6). Five aerobic compartments were assumed in the calculations, as compartment-specific air flow could only be estimated for compartments 2–6. As in the results for Viinikanlahti WWTP, the increase in the emissions due to an additional aerobic compartment was accounted for by distributing the higher total air flow between compartments 2–6.

At Akaa WWTP, the aerobic compartment of the aeration lines is not divided into smaller compartments. As the measurement campaign included measurements from two locations in the aerobic compartment, average hourly N_2O concentrations were estimated for the compartment to calculate the N_2O-N load and emission factors. The hourly average concentration was calculated as the average of the measured concentrations from the two locations. In addition, two of the four aeration lines were monitored for N_2O during the measurement campaign. Thus, the hourly N_2O concentration averages from the measured lines were assumed to be the N_2O concentrations in the two lines that were not measured.

3.5.3 Processing of aeration data

The air flow rate to the aerobic compartments is used to calculate the N_2O-N load (equation 2) which is needed to calculate the emission factors. At Viinikanlahti WWTP, the total air flow to each aeration line is measured, but it is not measured how the total air flow is distributed between the aerobic compartments. At Kirkonkylä WWTP and at Akaa WWTP, air flow rates were not directly measured and were therefore estimated based on the available data.

The built model of the treatment process of Viinikanlahti WWTP (section 3.6) was utilized to divide the total air flow between the aerobic compartments (compartments 3–5). The model calculated the air flow to the compartments based on the measured DO concentrations in each compartment. The air flow data provided by the model was the basis to calculate the distribution of the total air flow between the aerobic compartments. The results showed that most of the total air flow (approximately 39%) was taken up by compartment 4. Respectively, the shares of compartments 3 and 5 were 31% and 30%.

For Kirkonkylä WWTP, the air flow rate was estimated based on the data collected from the frequency converter which is used to control the generated air flow by the compressor. The measured frequency was used to calculate the rotation speed of the compressor according to equation 8.

$$nG = \frac{f}{50\ Hz} * 3696 \frac{1}{min} \quad (8)$$

Where

nG	Rotation speed of the compressor [1/min]
f	Frequency of the frequency converter [Hz]

Furthermore, the rotation speed and the air flow rate have a linear relationship, presented in equation 9. The equation was derived based on the performance chart of the compressor.

$$Q = 0.0114 * nG - 4.279 \quad (9)$$

Where

Q	Air flow rate [m^3/min]
nG	Rotation speed of the compressor [1/min]

The total air flow rate calculated for Kirkonkylä WWTP includes air flow to grit removal and the biological treatment. The air flow to grit removal was estimated according to Tchobanoglous et al. (2003). To derive an estimate of the air flow to the biological treatment, the calculated air flow to grit removal was subtracted from the total air flow.

The air flow to the biological treatment unit was halved between the two aeration lines and then divided between the aerobic compartments according to a report by Haimi et al. (2022) examining the aeration in the AS process during 2021. The estimated distribution of the total air flow between compartments 3–5 is 33%, 27% and 40%, respectively (Haimi et al., 2022). The distribution with compartments 2–5 aerated is 18%, 22%, 20% and 40%, respectively (Haimi et al., 2022). In the calculations, compartment 6 was assumed anoxic. However, during both measurement campaigns at Kirkonkylä WWTP, compartment 6 was aerobic. The air flow to compartment 6 was estimated based on its share of the total aerobic volume which was 8–9%. The share was first reduced from the total air flow after which the air flow to the rest of the aerobic compartments was calculated. The simplified approach to estimate the air flow to compartment 6 was deemed sufficient, as its share of the total aerobic volume is small, which likely results in a low share of the total air flow rate.

During the measurement campaign at Kirkonkylä WWTP in January 2023, the frequency data was available only from 16 to 24 January. Thus, the frequencies for the first week of the measurements (9–15 January) had to be estimated based on the available data. There was little variation in the available data and the frequencies followed a similar diurnal pattern every day, reaching the maximum peak around midnight. The hourly averages of the available frequency data were calculated to obtain estimates for the missing days. As the available data was from a time when all six compartments in the aeration lines were aerobic, the difference in the frequencies could not be studied between compartments 2–6 and compartments 1–6 being aerobic. From 9 to 13 January, only compartments 2–6 were aerobic, which likely

would result in lower frequencies than provided by the available data, and thus also lower total air flow to the aeration lines. As a conclusion, the estimated frequency data for 9–13 January can be expected to cause some overestimation to the calculated N_2O-N loads which are included in section 4.1.2.

Similarly to Kirkonkylä WWTP, the air flow rates of Akaa WWTP were estimated based on the frequency data from the frequency converter and the performance diagram for the compressor in use at the treatment plant. The maximum rotation speed of the compressor is 1800 1/min, and the maximum frequency provided by the converter is 50Hz. Thus, a frequency of 50 Hz corresponds to the maximum rotation speed. Equation 10 gives an estimation for the rotation speed, by assuming a linear relationship between the frequency and rotation speed.

$$nG = \frac{f}{50\ Hz} * 1800 \frac{1}{min} \tag{10}$$

Where

nG	Rotation speed of the compressor [1/min]
f	Frequency of the frequency converter [Hz]

Based on the performance diagram, equation 11 was derived to relate the rotation speed to the air flow rate.

$$Q = 0.0417 * nG - 8.2386 \tag{11}$$

Where

Q	Air flow rate [m^3/min]
nG	Rotation speed of the compressor [1/min]

Furthermore, the aeration data from Kirkonkylä and Akaa WWTPs had to be standardized from cubic meters (m^3/h) to standard cubic meters (Nm^3/h) to be applied in N_2O-N load calculation (equation 2). The standardization was performed according to Hilander (2022) by assuming ideal gas law and the conservation of substance. Thus, air flow in cubic meters could be converted to standard cubic meters with equation 12. The equation contains two unknown variables, V1 and T2, which were solved with an optimization function.

$$V2 = V1 \frac{P1}{P2} \frac{T2}{T1} \quad (12)$$

Where

V1	Aeration flow in standard unit [Nm^3/h]
V2	Aeration flow measured from the pipe [m^3/h]
P1	Standard pressure: 101.32 kPa [kPa]
P2	Pressure at the aeration flow measurement location [kPa]
T1	Standard temperature: 273.15 K [K]
T2	Air temperature at the measurement location [K]

3.6 Modelling background

The treatment process of Viinikanlahti WWTP was modelled to simulate N_2O production and compare the simulated data to the measurement data collected during the measurement campaign in September 2022. The wastewater modelling software used in the modelling experiment was SUMO (version 22.0.0), an open-source wastewater simulation software with a graphical interface by Dynamita. Related to N_2O emissions, SUMO includes Sumo4N model which models the three main N_2O production pathways (sections 2.1.1–2.1.3) (Takács, 2022). The key parameters of the model are presented in table 8. The pathways are modelled according to Hiatt and Grady (2008a) and Pocquet et al. (2016), described in sections 2.3.2–2.3.3.

The model of the treatment process of Viinikanlahti WWTP (section 3.3.1) included the AS process consisting of the biological treatment units (aeration lines) and secondary clarifiers. The chemical dosages were also included in the model. The built model is visualized in figure 28. One of the eight aeration lines at Viinikanlahti WWTP, aeration line 3, was included in the model, as most of the measured N_2O data was collected from line 3. Each continuous stirred tank reactor (CSTR) corresponds to either an anoxic or aerobic compartment of the aeration line. The two identical secondary clarifiers following the aeration line were included in the model as a singular secondary settling unit summarizing the treatment area of the two settlers. Primary clarification was excluded, as data for COD fractionation was available only for the wastewater that has gone through the primary clarification. In addition, primary clarifiers are not relevant treatment units for nitrogen removal and N_2O production which were the focus of the modelling experiment. Also due to the focus of the modelling, phosphorus removal and pH were not paid attention to.

Table 8 Key parameters of the Sumo4N model.

Parameter	Description of the parameter
$i_{CV, XB}$	COD of biodegradable substrate in volatile solids
$i_{CV,XU}$	COD of particulate unbiodegradable organics in volatile solids
$i_{CV,BIO}$	COD of biomass in volatile solids
$i_{CV,XE}$	COD of endogenous products in volatile solids
μ_{algae}	Maximum specific growth rate of algae
b_{algae}	Decay rate of algae
$i_{CIT,algae}$	Inorganic carbon content of algae
$i_{N,algae}$	N content of algae
$i_{P,ALGAE}$	P content of algae
$\eta_{AOB,NO,N2O}$	Reduction factor for NO reduction to N_2O by AOB (NH_2OH oxidation pathway)
μ_{AOB}	Maximum specific growth rate of AOB
$\eta_{AOB,NO2,N2O}$	Reduction factor for HNO_2 reduction to N_2O by AOB (nitrifier denitrification pathway)
$K_{O2,AOB,AS}$	Half-saturation of O_2 for AOB (AS)
$K_{O2,NH2OH,AOB,AS}$	Half-saturation of O_2 for NH_2OH oxidation by AOB (AS)
$K_{O2,NHx,AOB,AS}$	Half-saturation of O_2 for NH_x oxidation by AOB (AS)
$K_{O2,NOB,AS}$	Half-saturation of O_2 for NOB (AS)
$K_{NHx,ALGAE}$	Half-saturation of NH_x for algae
$K_{NH2OH,AOB,AS}$	Half-saturation of NH_2OH for AOB (AS)
$K_{NHx,NH2OH,AOB,AS}$	Half-saturation of NH_x to NH2OH for AOB (AS)
$K_{NHx,AOB,AS}$	Half-saturation of NH_x for AOB (AS)
μ_{NOB}	Maximum specific growth rate of NOB
μ_{OHO}	Maximum specific growth rate of OHOs
$K_{VFA,NO2,AS}$	Half-saturation of VFA for OHOs on NO_2 (AS)
$K_{SB,AS}$	Half-saturation of readily biodegradable substrate for OHOs (AS)
$K_{SB,NO3,AS}$	Half-saturation of readily biodegradable substrate for OHOs on NO_3 (AS)
$K_{SB,NO2,AS}$	Half-saturation of readily biodegradable substrate for OHOs on NO_2 (AS)
$K_{VFA,NO3,AS}$	Half-saturation of VFA for OHOs on NO_3 (AS)
$K_{SB,NO,AS}$	Half-saturation of readily biodegradable substrate for OHOs on NO (AS)
$K_{NO2,NOB,AS}$	Half-saturation of NO_2 for NOB (AS)
$K_{VFA,N2O,AS}$	Half-saturation of VFA for OHOs on N_2O (AS)
$K_{SB,N2O,AS}$	Half-saturation of readily biodegradable substrate for OHOs on N_2O (AS)
$K_{VFA,NO,AS}$	Half-saturation of VFA for OHOs on NO (AS)
$K_{O2,OHO,AS}$	Half-saturation of O_2 for OHOs (AS)
$K_{O2,OHO,NO3,AS}$	Half-saturation of O_2 for OHOs on NO_3 (AS)
$K_{O2,OHO,N2O,AS}$	Half-saturation of O_2 for OHOs on N_2O (AS)
$K_{O2,OHO,NO2,AS}$	Half-saturation of O_2 for OHOs on NO_2 (AS)
$K_{O2,OHO,NO,AS}$	Half-saturation of O_2 for OHOs on NO (AS)
μ_{CASTO}	Maximum specific growth rate of CASTOs
$q_{PAO,PP}$	Maximum polyphosphate uptake rate of PAOs
$K_{PO4,PAO,AS}$	Half-saturation of PO_4 for PAOs (AS)
q_{HYD}	Rate of hydrolysis

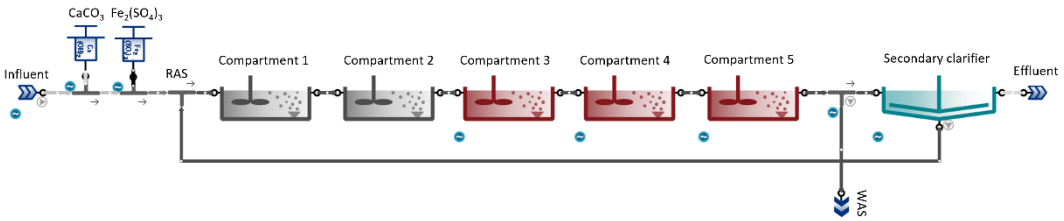

Figure 28 The SUMO model of the treatment process of Viinikanlahti WWTP.

Input data to the model was based on online measurements and laboratory analyses. Hourly online data was available for influent inflow, temperature, dissolved oxygen in compartments 3–5, dosages of $CaCO_3$ and $Fe_2(SO_4)_3$ and the RAS and WAS flows which were put into the model. $Fe_2(SO_4)_3$ is dosed before and after the primary clarifier, and it was assumed that a half of the $Fe_2(SO_4)_3$ dosed prior to the clarifier was removed with the settled sludge. Due to the lack of $CaCO_3$ component in SUMO, $CaCO_3$ was entered to the model as $Ca(OH)_2$ in unit kgCa/d.

Concentrations of total nitrogen and COD in the influent were available from laboratory analyses. To include these parameters in dynamic form into the model, the relationship was studied between them and the total influent inflow to the plant. The assumption was that a higher inflow dilutes the total nitrogen and COD concentrations, which was confirmed by studying the available data. The dynamic data series for the influent total nitrogen and COD concentrations were derived directly from the total influent inflow by formulating a linear relationship between the inflow and laboratory-analyzed total nitrogen and COD concentrations in January-September 2022.

The calculated total nitrogen concentration was assumed to be the same for the influent and primary settled water, as primary clarifiers do not primarily remove nitrogen. However, COD was estimated separately for the primary settled water. At Viinikanlahti WWTP, COD is analyzed with a dichromate method from the influent water but not from the water that has gone through primary clarification. COD is analyzed with a permanganate method from both influent and primary settled water. To estimate the dichromate-based COD of the primary settled water, the permanganate-based COD of the influent was compared to that of the primary settled water. Approximately 55% of the permanganate-based COD was reduced in primary clarification. Thus, the dichromate-based COD of the primary settled water was assumed to be 45% of the influent COD.

The basis for the COD fractionation was a report by Pöyry Environment (2008) who analyzed the primary settled water from Viinikanlahti WWTP as a part of a modelling project. The COD fractions for the primary settled water are presented in table 9.

Table 9 The COD fractionation of the primary settled water at Viinikanlahti WWTP, provided by Pöyry Environment (2008).

COD fraction	Fraction of total COD (%)
Soluble biodegradable substrate (RBCOD)	20
Soluble unbiodegradable COD	15
Slowly biodegradable substrate	49
Particulate unbiodegradable COD	16
Heterotrophic biomass	0

The COD fractionation in table 9 could not be input into the Sumo4N model as such, as the structure of the COD fractionation was different in the model. Thus, the COD fractionation was modified to be applied in SUMO, as presented by table 10. An assumption was made regarding the distribution of the slowly unbiodegradable substrate into colloidal and particulate matter, as it was assumed that the slowly unbiodegradable substrate contains an equal amount of colloids and particles. The assumption was made to calculate the fraction of filtered COD in total COD and further the fractions of volatile fatty acids (VFAs) and soluble unbiodegradable organics in filtered COD. In the case that the fractions would seem unrepresentative in the model simulations, they could be further modified to increase the accuracy of the simulation results.

Table 10 The input COD fractionation to SUMO.

COD fraction	Fraction (%)
Filtered COD in total COD	60
Flocculated filtered COD in total COD	35
VFA in filtered COD	33
Soluble unbiodegradable organics in filtered COD	25
Particulate unbiodegradable organics in total COD	16
Heterotrophs in total COD	0

Separate calibration and validation procedures were not possible, as there was only available data from laboratory analyses collected at Viinikanlahti WWTP during the measurement campaign. The data was not accurate enough to allow proper calibration and validation of the model, as it did not provide information regarding the diurnal variation in the analyzed parameters. Thus, general guidelines (table 11) were constructed for six parameters to calibrate the model, based on the calibration procedure proposed by Rieger et al. (2012) for a nitrogen removal model. However, all proposed parameters could not be included in the calibration due to the limited data availability. Regarding the biological treatment unit, attention was paid to

the mixed liquor suspended solids (MLSS) concentration to ensure that the sludge content was on the correct level in the treatment unit. The effluent quality was checked for total nitrogen, NO_2^-, NO_3^-, NH_4^+, total suspended solids (TSS) and COD. The nitrogen compounds, TSS and COD were analyzed from 24-hour composite samples and the MLSS in compartment 5 from grab-samples. The samples were collected and analyzed biweekly, despite effluent COD which was analyzed once during the measurement campaign.

Table 11 Guidelines to calibrate the Sumo4N model of Viinikanlahti WWTP.

Parameter	**Guideline for calibration**
MLSS in compartment 5 (g/l)	4.3–5.2
Effluent total nitrogen (mg/l)	31–41
Effluent NO_2^- (mg/l)	0
Effluent NO_3^- (mg/l)	29–39
Effluent NH_4^+ (mg/l)	0.12–0.43
Effluent TSS (mg/l)	2.0–4.0
Effluent COD (mg/l)	33

Furthermore, the simulated N_2O concentrations in the off-gas from compartments 3 and 5 were compared to the measured concentrations in aeration line 3 during September 2022. By adjusting the key parameters of the Sumo4N model (table 8), an attempt was made to fit the simulated N_2O concentrations to the measured concentrations. The adjusted parameters were

- μ_{AOB}, the maximum specific growth rate of AOB
- μ_{OHO}, the maximum specific growth rate of ordinary heterotrophic organisms (OHOs) which represent HDN in the model
- $\eta_{AOB,NO,N2O}$, the reduction factor for NO reduction to N_2O by AOB (NH_2OH oxidation pathway)
- $\eta_{AOB,NO2,N2O}$, the reduction factor for HNO_2 reduction to N_2O by AOB (nitrifier denitrification pathway)

The growth rates were adjusted to adjust the rate of nitrification and heterotrophic denitrification in the model, as the rates can also affect the N_2O production rates in different compartments. Furthermore, the two reduction factors listed above are the key factors to calibrate the N_2O production simulated by the model according to Spérandio et al., 2022. However, extensive calibration was not performed, as the primary goal was to obtain preliminary results of how the model simulates the N_2O production and emission.

4 Results

The results from the measurement campaigns at Kirkonkylä WWTP, Viinikanlahti WWTP and Akaa WWTP are presented in sections 4.1–4.3, respectively. Section 3.5 includes a more detailed description of the data analysis and assumptions that were made to produce the results. The following results are included for each measurement campaign

- The measured off-gas N_2O concentrations (g/Nm^3) from all measured compartments
- The emitted N_2O-N loads (gN/h) estimated for each aerobic compartment of the biological treatment unit (aeration line)
- The plant-wide N_2O-N loads as hourly averages for each weekday. The plant-wide load summarizes the estimated N_2O-N loads from the aerobic compartments of all aeration lines, and thus gives an estimate of the total amount of nitrogen emitted as N_2O-N at the treatment plant
- The emission factors relative to influent total nitrogen and removed total nitrogen
- Pearson correlation factors between the measured N_2O concentrations and other parameters as an indication of possible linear correlation.

Additionally, two measurement campaigns conducted at the same treatment plant were compared to each other to study the variation in the emissions. The comparisons are included in the results of Kirkonkylä WWTP (section 4.1.3) and Viinikanlahti WWTP (section 4.2.3). Furthermore, section 4.4 presents the results from the modelling experiment to simulate the N_2O emissions measured at Viinikanlahti WWTP in September 2022.

4.1 Kirkonkylä WWTP, Mäntsälä

4.1.1 Measurement campaign in June–July 2022

The N_2O concentrations measured from 59 hours at Kirkonkylä WWTP are presented in figure 29. The monitored compartment was compartment 5 in aeration line 2 which was the third aerobic compartment, as compartments 1 and 2 were anoxic. On average, the N_2O concentration was 0.002 g/Nm^3. Respectively, the measured minimum and maximum N_2O concentrations were 0.0002 and 0.01 g/Nm^3. The maximum concentration was 50-fold compared to the minimum concentration, indicating clear variation in the emission levels, even though the measured N_2O concentrations were relatively low.

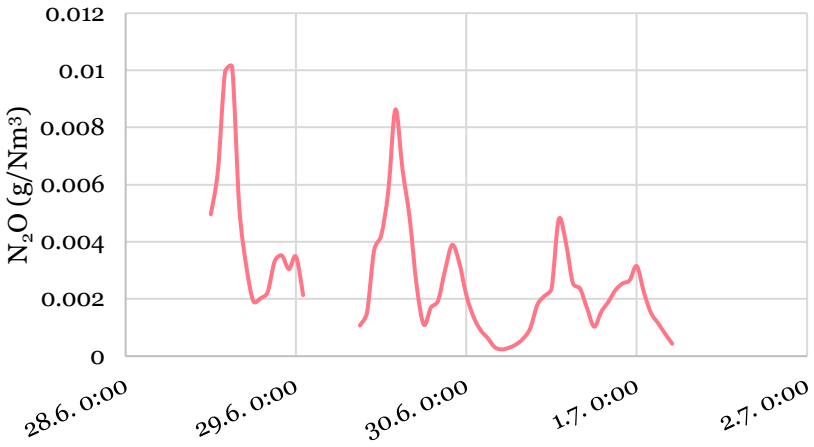

Figure 29 The measured N_2O concentrations from compartment 5 of line 2 during the June–July measurement campaign at Kirkonkylä WWTP in 2022.

The missing N_2O concentrations were estimated based on the measured data, according to the principles detailed in section 3.5.2. The same concentration of N_2O in the off-gas was assumed for all compartments, as the measurement campaign included measurements only from one compartment. Therefore, the differences in the N_2O emissions between the compartments are due to the compartment-specific air flows. The estimated N_2O-N loads for all aerobic compartments (compartments 3–6) are presented in figure 30. The highest N_2O-N load seemed to originate from the largest compartment (compartment 5) at a maximum hourly load around 2 gN/h. Respectively, the lowest N_2O-N loads were from compartment 6 with the smallest volume. In compartment 6, the maximum hourly load was around 0.5 gN/h.

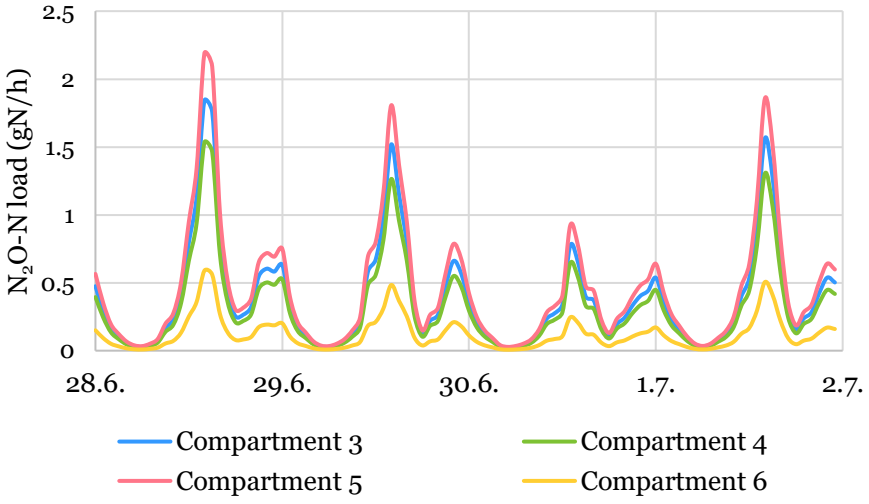

Figure 30 The estimated N_2O-N loads from each aerobic compartment in aeration line 2 during the measurement campaign at Kirkonkylä WWTP in June–July 2022.

The estimated N_2O-N loads from the whole plant during the measurement campaign from Tuesday to Friday are presented in figure 31. The average load was 2.6 gN/h. Each day, the highest emission peaks occurred between 12 PM and 5 PM. The maximum peak was reached approximately at 2 PM. Another smaller emission peak was measured in the evenings around 10 PM. The highest N_2O-N load of 12 gN/h was emitted on Tuesday and the lowest on Thursday (5 gN/h). The average and maximum N_2O-N loads on Tuesday were three to four times higher than the measured concentrations on Thursday. Each day, the loads were close to 0 gN/h for a few hours of the day, approximately between 4 AM and 7 AM.

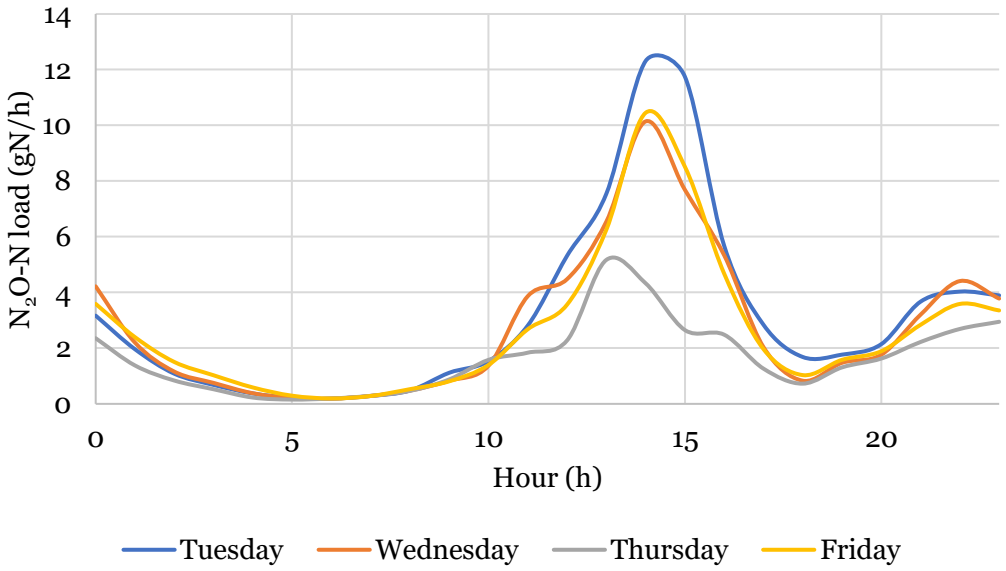

Figure 31 The average hourly plantwide N_2O-N loads emitted during the measurement campaign at Kirkonkylä WWTP in June–July 2022.

The emission factors were 0.04% and 0.05% relative to the influent nitrogen load and the removed total nitrogen, respectively. During the measurement campaign, the total nitrogen concentration in the influent was 65 mg/l and in the effluent 10 mg/l, both analyzed from a 24-hour composite sample.

A possible link was found between the N_2O emissions and the bypass of the primary clarification. During the measurement campaign, approximately 60% of the influent bypassed the primary clarification daily for 16 hours from 12 AM to 4 PM. Thus, the highest N_2O emission peak occurs during the bypass and the emissions start to decrease with a one-hour delay after the bypass has finished, as can be seen from figure 29. The primary clarification is bypassed to supply heterotrophic denitrification with more organic carbon. However, the bypass can also negatively affect nitrification if the COD load of the bypass contains a high share of slowly biodegradable matter. The

oxidation of this matter in the aerobic compartments is a competitive process for nitrification and could therefore enhance N_2O production.

Between the measured N_2O concentrations and DO in compartment 5, a low positive correlation was found with a Pearson correlation factor of 0.3. Thus, there was no clear link between them. The DO remained at the desired level of 2–3 mg/l which is also a desirable DO level to mitigate N_2O emission (Peng et al., 2015). Similarly, only low Pearson correlation (r = 0.4) was found between the N_2O concentrations and flow rate with a time lag of -7 hours. Negative time lags were studied, as the flow rate is measured prior to the disc filters which is the last treatment step after the aeration lines and secondary clarifiers. Furthermore, the NO_2^- concentration in all samples (N = 6) was below 0.1 mg/l and there was no correlation with N_2O. The low NO_2^- and effluent total nitrogen concentrations indicate a good performance of nitrification which support the finding of a consistently low N_2O emission level.

4.1.2 Measurement campaign in January 2023

The N_2O concentrations measured during the campaign are presented in figure 32. The measurement campaign included N_2O monitoring from compartments 3 and 5 in aeration line 2. The measurements started from compartment 5 when it was the fourth aerobic compartment and there was one anoxic compartment (compartment 1). On January 13, aeration was started also in compartment 1 and the last days of the measurements in compartment 5 as well as all measurements in compartment 3 were conducted when there were no anoxic compartments in the aeration line. The conditions during the measurement campaign are detailed in section 3.2.2.

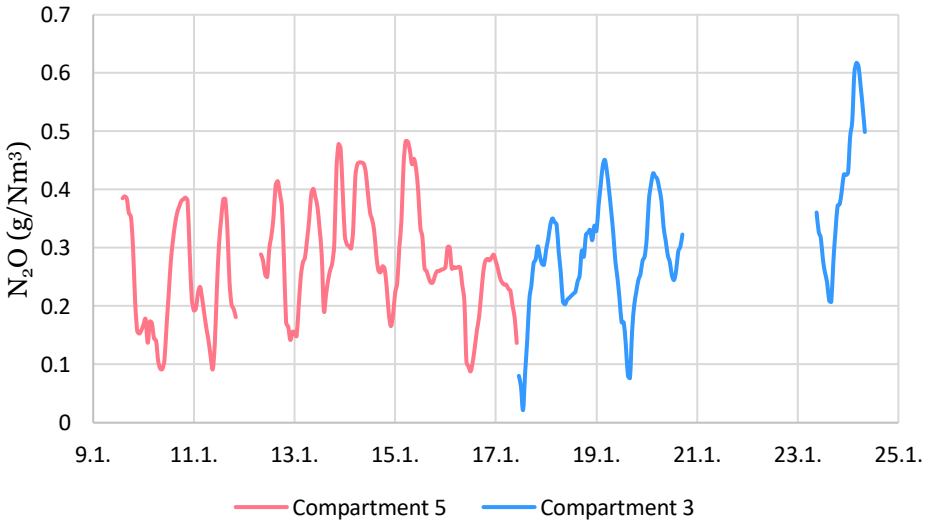

Figure 32 The measured N_2O concentrations from compartments 3 and 5 of line 2 during the January measurement campaign at Kirkonkylä WWTP.

The average, minimum and maximum concentrations from compartment 3 were 0.31, 0.02 and 0.62 g/Nm^3, and the respective concentrations from compartment 5 were 0.27, 0.09 and 0.48 g/Nm^3. The measured maximum concentration was 30-fold compared to the minimum concentration in compartment 3. The respective difference was only 5-fold in compartment 5, indicating a more varying emission level in compartment 3. The maximum concentration was measured in compartment 3 near the end of the measurement campaign. Generally, the average emission level seemed relatively similar between the measured compartments, as the average N_2O concentrations were almost equal. However, the dynamic conditions during the measurement campaign, complicated the study of the spatial variation between the compartments.

Based on the measured N_2O data from compartments 3 and 5, the N_2O concentrations were estimated for the other aerobic compartments, i.e., compartments 2, 4 and 6. Compartment 1 was assumed to be anoxic in the calculations. Figure 33 presents the N_2O-N loads for compartments 2–6 in line 2 during the first week of the measurement campaign. Generally, the highest N_2O-N loads were emitted from the largest compartment (compartment 5) with a maximum hourly load around 65 gN/h and an average load of 30 gN/h. Respectively, the lowest N_2O-N loads were from compartment 6 with the smallest volume where the average hourly load was around 7 gN/h. Loads of similar magnitude were emitted from compartments 2–4, each compartment emitting approximately 20 g of N_2O-N per hour.

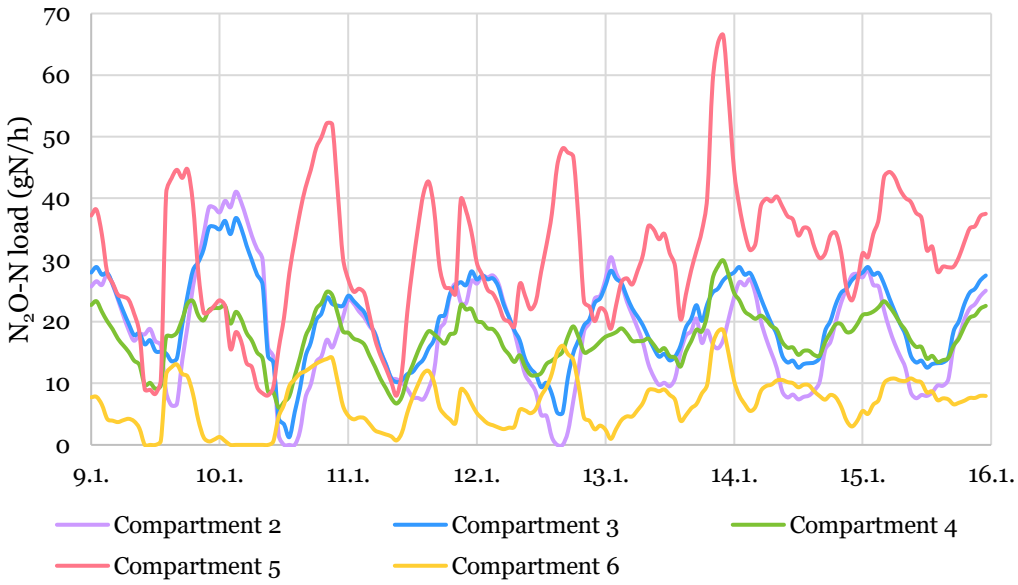

Figure 33 The estimated N_2O-N loads from each aerobic compartment in aeration line 2 during the first week of the measurement campaign at Kirkonkylä WWTP in January 2023.

The plantwide average hourly N_2O-N loads during the measurement campaign are presented in figure 34 for each weekday. The average load was 190 gN/h. The minimum loads varied from 60 to 140 gN/h, and they occurred approximately between 9 AM and 12 PM from Monday to Thursday. From Friday to Sunday, the minimum loads were emitted between 12 PM and 4 PM. Towards the evening, the loads started to increase each day, being at the maximum between 7 PM and 2 AM. The highest N_2O-N load of 350 gN/h was emitted on Friday, while the minimum average loads (60–70 gN/h) were detected on Wednesday and Thursday.

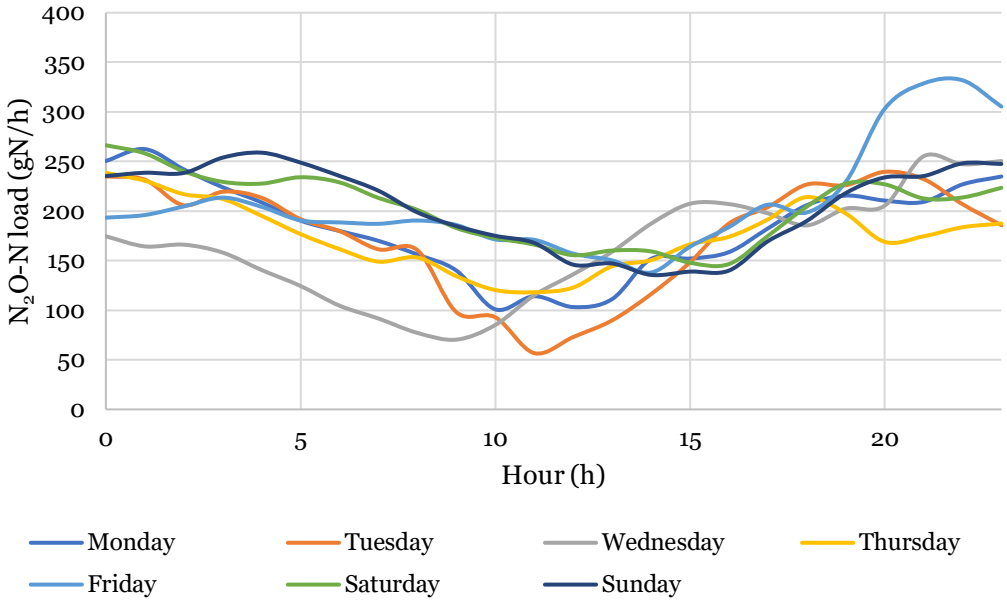

Figure 34 The average hourly plantwide N_2O-N loads emitted during the measurement campaign at Kirkonkylä WWTP in January 2023.

The emission factors were 1.8% and 3.0% relative to the influent nitrogen load and the removed total nitrogen, respectively. During the measurement campaign, the total nitrogen concentration in the influent was 61 mg/l and in the effluent 26 mg/l, both analyzed from a 24-hour composite sample. Another 24-hour composite sample collected between 16 and 17 January revealed that the influent and effluent total nitrogen concentrations were 28 and 13 mg/l, respectively, indicating dilution by the increased inflows during the rainstorm.

During the measurement campaign, the primary clarification was bypassed only from 9 to 13 January after which all influent was treated in the clarifier. Figure 35 shows the measured N_2O concentrations during these days. The bypass occurred for 12 hours from 12 AM to 12 PM and it was 40% of the influent flow. Between 10 and 12 January, the emissions started to increase

between 8 and 10 AM, indicating that the increase began near the end of the bypass.

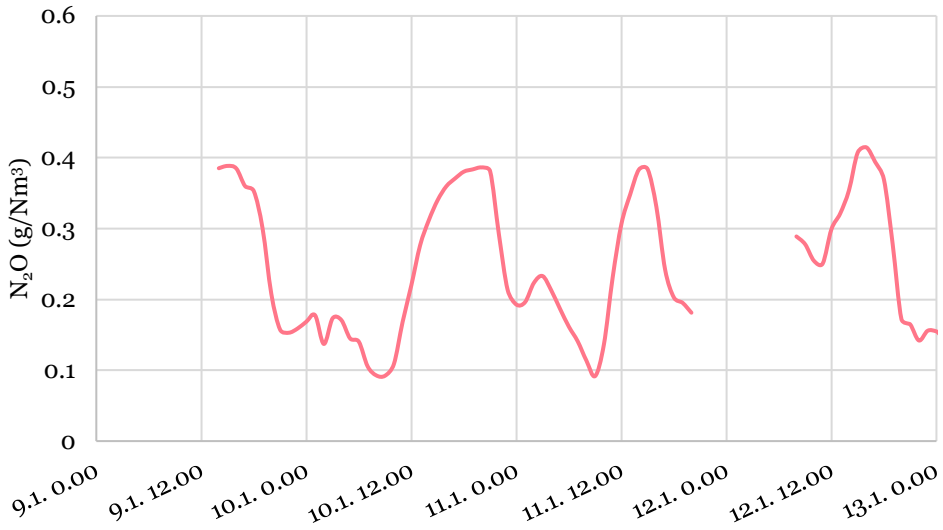

Figure 35 The measured N_2O concentrations from compartment 5 during the days the bypass of the primary clarification (from 12 AM to 12 PM) occurred.

The measured N_2O and NO_2^- concentrations showed moderate positive correlation in both compartments 3 and 5. The Pearson correlation factor between N_2O and NO_2^- was 0.6 (N = 18) in compartment 5 and 0.5 (N = 11) in compartment 3. Figure 36 visualizes the relationship between the measured N_2O and NO_2^- concentrations in compartment 5 and a similar visualization is presented in figure 37 for the data collected from compartment 3.

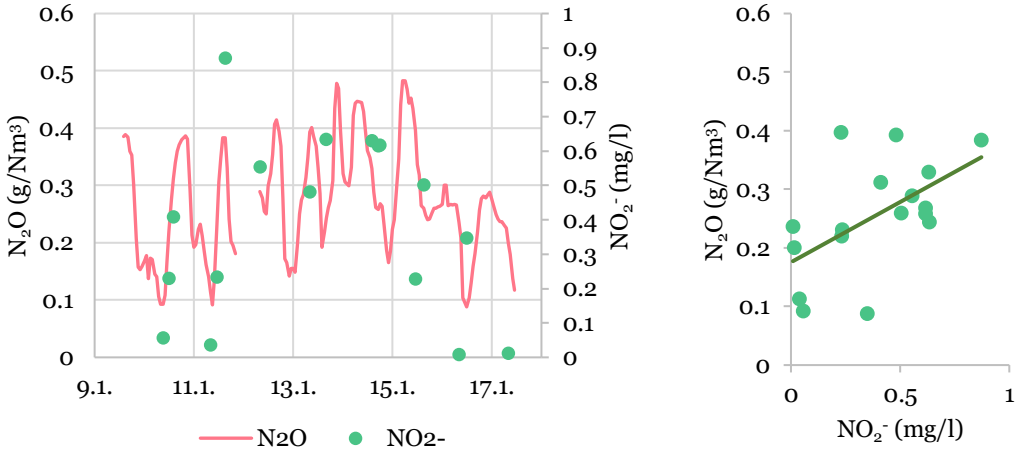

(a) (b)

Figure 36 The relationship between the measured N_2O and NO_2^- concentrations in compartment 5 during the measurement campaign.

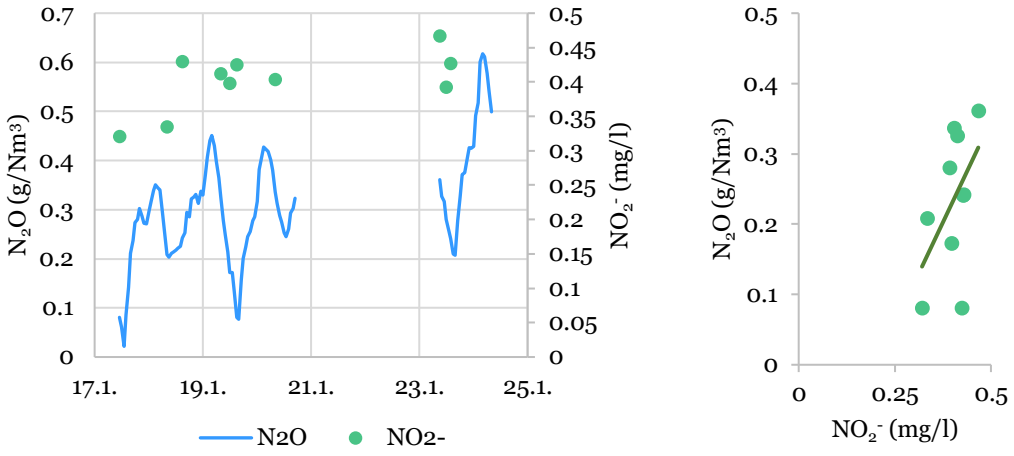

Figure 37 The relationship between the measured N_2O and NO_2^- concentrations in compartment 3 during the measurement campaign.

Between the N_2O concentrations and flow rate, only low correlation was found both for the concentrations measured in compartment 3 and 5. The highest Pearson correlation factor was 0.4 and it was calculated between the flow rate and the N_2O concentrations from compartment 5 with a time lag of -3 hours. As the flow rate is measured prior to the disc filters, the correlation was studied with negative time lags. Similarly, the Pearson correlation between N_2O and DO was low in both compartments. Low positive Pearson correlation ($r = 0.2$) was calculated between N_2O and DO in compartment 3, while low negative correlation ($r = -0.3$) was calculated for compartment 5.

4.1.3 Comparison between the measurement campaigns

The average, minimum and maximum N_2O concentrations during the two measurement campaigns at Kirkonkylä WWTP are compared in figure 38. There was a significant difference in the emission levels between the two measurement campaigns, which is indicated by the high variation in the measured concentrations. Compartment 5 was measured during both measurement campaigns and the average N_2O concentration in the off-gas was 135 times higher in January 2023 than in June–July 2022.

The significant difference in the measured emission levels is also depicted by the emission factors which were 0.04–1.8% relative to influent total nitrogen load and 0.05–3.0% relative to removed total nitrogen. The emission factor relative to removed total nitrogen was higher than the emission factor relative to influent total nitrogen during both measurement campaigns but especially during January 2023, indicating that the process struggled more with total nitrogen removal then than in June–July 2022. The emission factors

are collected to table 12 together with other variables describing the conditions during the measurements. The influent total nitrogen, BOD_7 and COD loads were 30–40% higher in January than in June–July, indicating an increased loading in the treatment process in January, which could be a cause for the high emission of N_2O in January. However, the BOD_7 and COD loads are not entirely representative of the loading to the biological treatment due to the different operation of the bypass of the primary clarification.

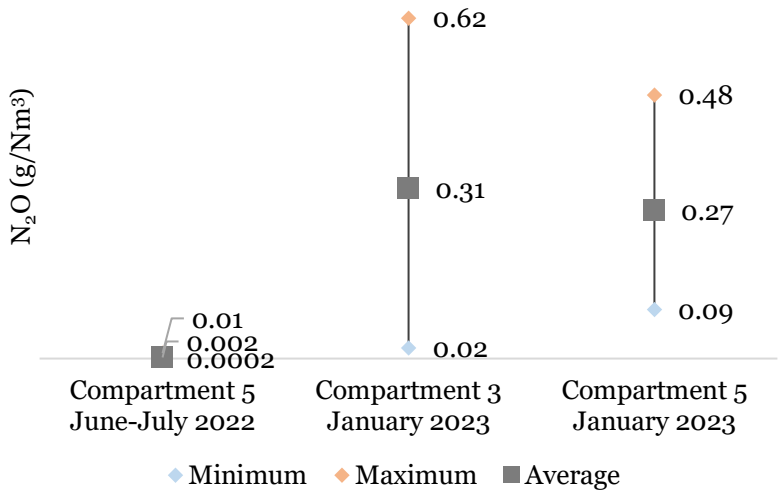

Figure 38 Comparison of the measured N_2O concentrations during the two measurement campaigns at Kirkonkylä WWTP.

Table 12 The emission factors measured at Kirkonkylä WWTP and loading in the treatment process during the two measurement campaigns.

Parameter	June–July 2022	January 2023
Emission factor relative to influent total nitrogen (%)	0.04	1.8
Emission factor relative to removed total nitrogen (%)	0.05	3.0
Influent total nitrogen load (kgN/d)	160	210
Influent BOD_7 load (kg/d)	660	920
Influent COD load (kg/d)	1400	1800
BOD_7/N ratio after primary clarification	2.7	3.4
COD/N ratio after primary clarification	6.7	8.2
Temperature in the biological treatment (°C)	15–16	7–10

An apparent difference was detected also in the temperature in the biological treatment between the two measurement campaigns. In June–July, the temperature was around 15 °C, and thus under the warm-period conditions. The temperatures in January (7–10 °C) were under the cold-period conditions. The low temperatures are typically not favorable for biological nitrogen removal (Massara et al., 2017), which was also indicated by the higher effluent total nitrogen concentration (26 mg/l) in January than in June–July (10 mg/l). Thus, N_2O production might be generally linked to the overall efficiency of nitrogen removal in the treatment process.

The bypass of the primary clarification could be linked to the highest daily peaks in the N_2O emissions measured during the campaigns. The relation seemed especially distinct during June–July when the duration of the bypass was longer and its share of the inflow higher than in January. While denitrification is boosted by the increased organic loading as a result of the bypass, nitrification and the oxidation of organic matter both take place in the aerobic compartments. Thus, the organic matter loading may enhance N_2O production by impacting nitrification. The COD/N ratio (table 12) after primary clarification was around 7–8 during both campaigns, indicating a sufficient ratio for the completion of heterotrophic denitrification according to Henze et al. (2002) and Pan et al. (2013b). The BOD_7/N ratio around 3 also suggests a good share of the COD load is readily available for biodegradation during denitrification. Thus, it could be assumed that heterotrophic denitrification was not a likely source of N_2O, even though no data could be collected to study whether denitrification produced N_2O in the anoxic compartments.

The DO in the measured compartments remained mostly at a high level between 2–5 mg/l during both measurement campaigns. The DO showed only low correlation to the measured N_2O concentrations, not indicating a strong connection between the variability in the DO levels and N_2O concentrations. Similarly, low correlation ($r = 0.4$) was found between the flow rate and the N_2O concentrations. A moderate positive correlation ($r = 0.5–0.6$) was found between N_2O and NO_2^- during the measurement campaign in January but not in June–July. Thus, the studied variables were not able to explicitly explain the variability in the N_2O emissions. Flow rate is typically a good measure of the variability in the nutrient loadings under dry-weather conditions, as the concentrations of, e.g., influent nitrogen remain relatively stable. However, the loading in the biological treatment also varied according to the bypass of the primary clarification. Therefore, the flow rate alone would not describe the diurnal variability in the loading in the biological treatment. In addition, a rainstorm occurred during the measurement campaign in January 2023, and thus, not all measurements were conducted under dry-weather conditions at Kirkonkylä WWTP.

4.2 Viinikanlahti WWTP, Tampere

4.2.1 Measurement campaign in September 2022

The measurement data collected from three measurement locations during the campaign in September is presented in figure 39 as the concentration of N_2O in the off gas. The main focus of the measurements was aeration line 3, where the average, minimum and maximum concentrations were 0.008, 0.0004 and 0.01 g/Nm^3 in compartment 3 and 0.09, 0.0001 and 0.56 g/Nm^3 in compartment 5, respectively. Thus, significant variation was found in the measured concentrations between the two measurement locations in line 3.

The highest N_2O concentrations were measured from compartment 5. The maximum concentration measured in compartment 5 was 60 times higher than that measured in compartment 3. Furthermore, there was approximately 10-fold difference between the average concentrations. In both compartments, N_2O concentrations near zero were also measured. In addition, the variation in the emissions was more significant in compartment 5 than in compartment 3. For example, there was approximately a 6000-fold difference between the minimum and maximum N_2O concentrations in compartment 5, whereas the respective difference was 25-fold in compartment 3.

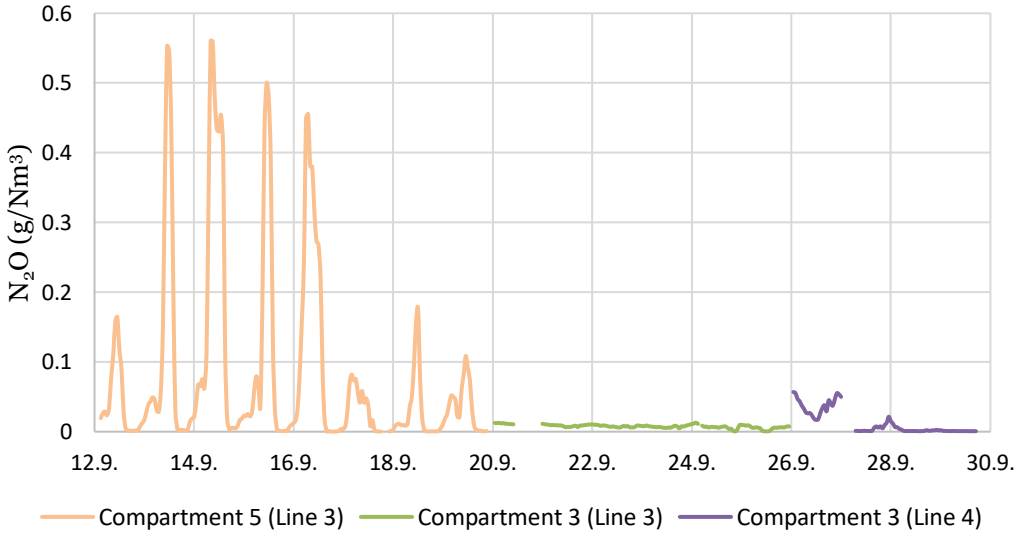

Figure 39 The measured N_2O concentrations at Viinikanlahti WWTP during the measurement campaign in September 2022.

The estimated N_2O-N loads emitted from the three aerobic compartments in aeration line 3 are presented in figure 40 for the first week of the measurement campaign. The highest N_2O-N load originated from compartment 5 at a maximum hourly load around 220 gN/h. Generally, the loads from

compartments 4 and 5 were on a similar level, as the average load from compartment 5 was 37 gN/h and the average load from compartment 4 was 25 gN/h. In contrast, the loads from compartment 3 were clearly the lowest. The loads varied between 0.1 and 5.3 gN/h, being 2.6 gN/h on average.

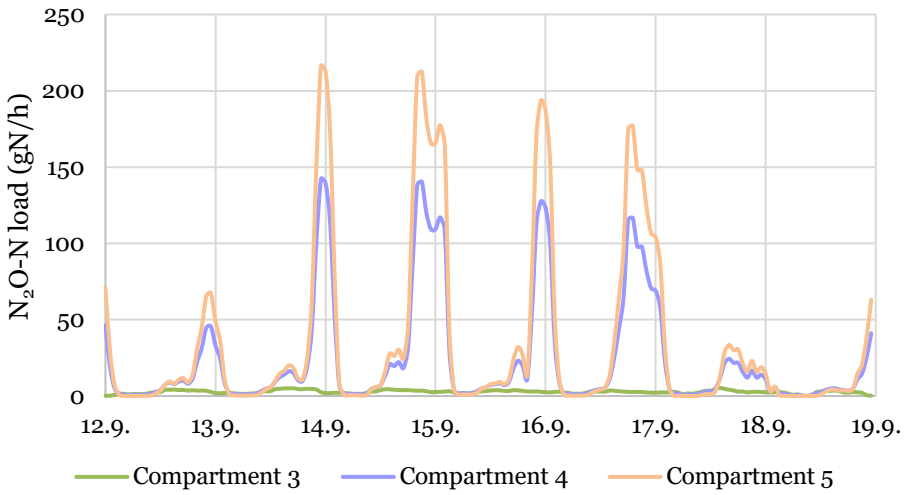

Figure 40 The estimated N_2O-N loads from each aerobic compartment in aeration line 3 during the first week of the measurement campaign.

The plantwide average hourly N_2O-N loads during the measurement campaign are presented in figure 41 for each weekday. The average load was 570 gN/h. Each day, the minimum loads (around 30–50 gN/h) occurred approximately from 4 AM to 8 AM. Towards the evening, the loads started to increase, being at the maximum level between 7 PM and 2 AM. The highest N_2O-N load of 3500 gN/h was emitted on Wednesday, while the lowest average loads throughout the day were detected on Saturday and Sunday.

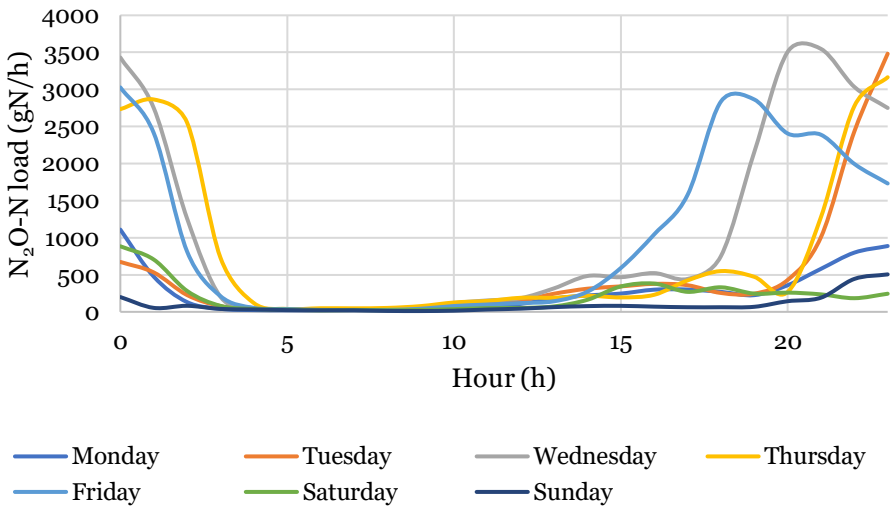

Figure 41 The average hourly plantwide N_2O-N loads for each weekday.

The emission factors were 0.4% and 1.1% relative to the influent total nitrogen and the removed total nitrogen loads, respectively. The average total nitrogen concentration in the influent was 59 mg/l and in the effluent 36.5 mg/l, both analyzed biweekly from 24-hour composite samples.

Between the N_2O concentrations and inflow rate (figure 42), a moderate positive correlation (r = 0.6) was found in compartment 5 with a 2-hour time lag. Thus, the highest N_2O concentrations were generally emitted during the highest inflows. In compartment 3, only low correlation (r = 0.4) was found between the N_2O concentration and inflow without a time lag.

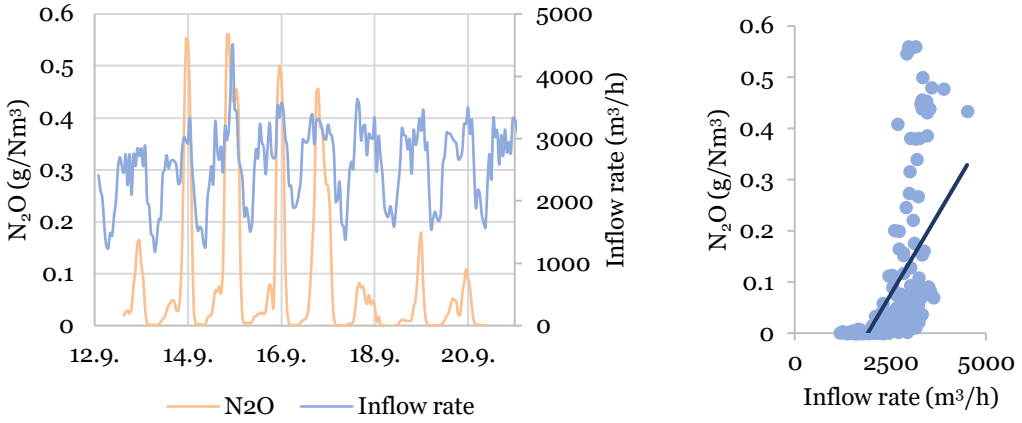

(a) (b)

Figure 42 The relationship between the N_2O concentrations measured in compartment 5 (aeration line 3) and inflow rate with a time lag of 2 hours.

The DO and dissolved NO_2^- concentrations were found to strongly correlate with the measured N_2O concentrations in compartment 5. The Pearson correlation factor for the DO and N_2O concentrations was -0.8 and for NO_2^- and N_2O concentrations 0.9 (N = 17). Figure 43 visualizes the N_2O, DO and NO_2^- concentrations in compartment 5.

Similarly to compartment 5, correlation was studied with the data obtained from compartment 3 in aeration line 3. In compartment 3, the N_2O emissions and DO exhibited only low correlation (r = 0.2), contrary to compartment 5, even though low DO levels of 1 mg/l were detected in both compartments. Between the N_2O and NO_2^- concentrations in compartment 3 (figure 44), the Pearson correlation factor was 0.6, indicating moderate correlation. The NO_2^- concentrations were relatively stable, varying between 0.7–0.9 mg/l, as well as relatively high throughout the day. As compartment 3 was the first aerobic compartment, nitrification was likely in the early stages, which could cause the high NO_2^- concentrations but low production of N_2O. The off-gas N_2O concentration in compartment 3 varied between 0–0.01 g/Nm³.

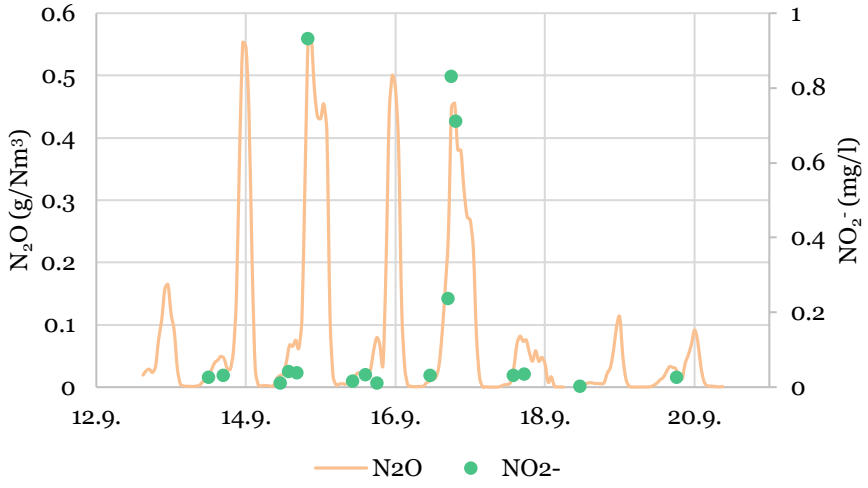

(a)

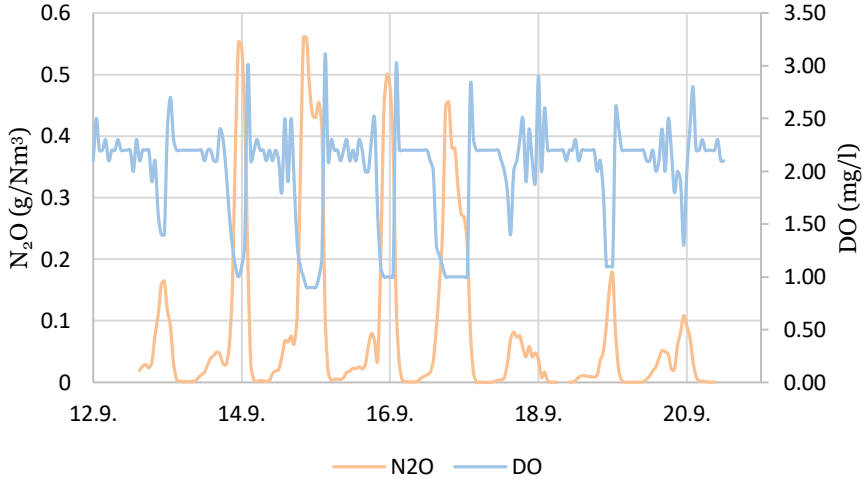

(b)

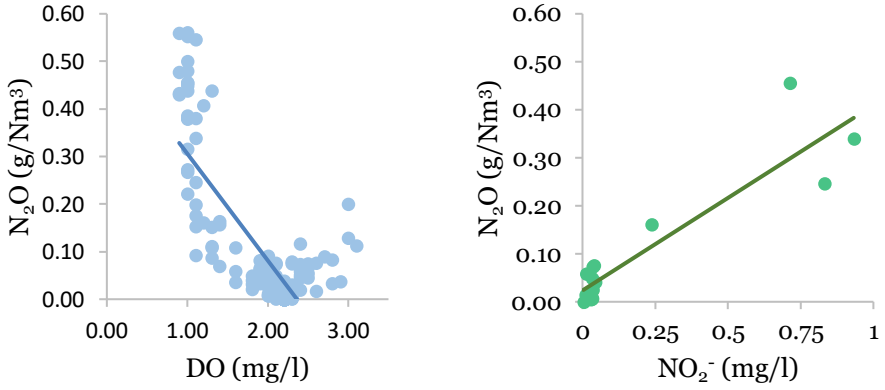

(c) (d)

Figure 43 The relationship between the measured N_2O concentrations and DO and NO_2^- in compartment 5 (the last aerobic compartment) in aeration line 3.

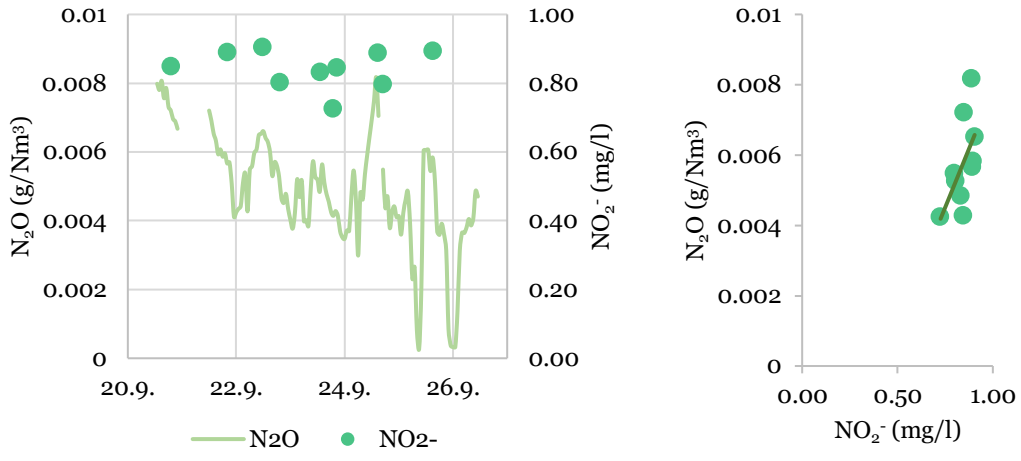

(a) (b)

Figure 44 The relationship between N_2O and NO_2^- in compartment 3 (the first aerobic compartment) of aeration line 3.

To compare the N_2O emissions between aeration lines of different configurations, the variation was studied between the N_2O concentrations measured in compartment 3 of lines 3 and 4. Figure 45 presents the measured N_2O concentrations in both measurement locations. The average, minimum and maximum concentrations were 0.01, 0.0006 and 0.06 g/Nm³ in line 4 and 0.008, 0.0004 and 0.01 g/Nm³ in line 3, respectively. Generally, the emission level was slightly higher in aeration line 4. In line 4, compartment 3 was the second aerobic compartment, whereas in line 3 it was the first aerobic compartment. Thus, nitrification had proceeded further in line 4 than in line 3, likely also enhancing the N_2O concentrations to a higher level.

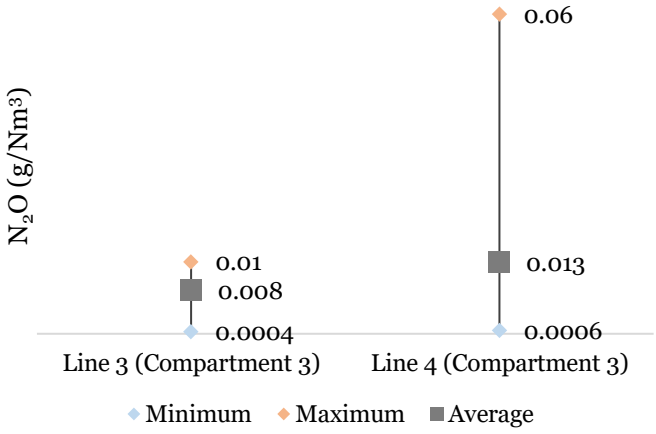

Figure 45 Comparison between the N_2O emission levels in compartment 3 in aeration lines 3 and 4. Compartment 3 was the first aerobic compartment in line 3 and the second aerobic compartment in line 4.

4.2.2 Measurement campaign in November 2022

The measured N_2O concentrations from four measurement locations, detailed in section 3.3.3, are presented in figure 46. The N_2O monitoring was mainly conducted in line 3, where the average, minimum and maximum concentrations were 0.005, 0.003 and 0.007 g/Nm^3 in compartment 3 and 0.02, 0.0006 and 0.11 g/Nm^3 in compartment 5, respectively. On average, the concentrations were four times higher in compartment 5 than in compartment 3. Respectively, the maximum concentration in compartment 5 was 14-fold compared to that measured in compartment 3.

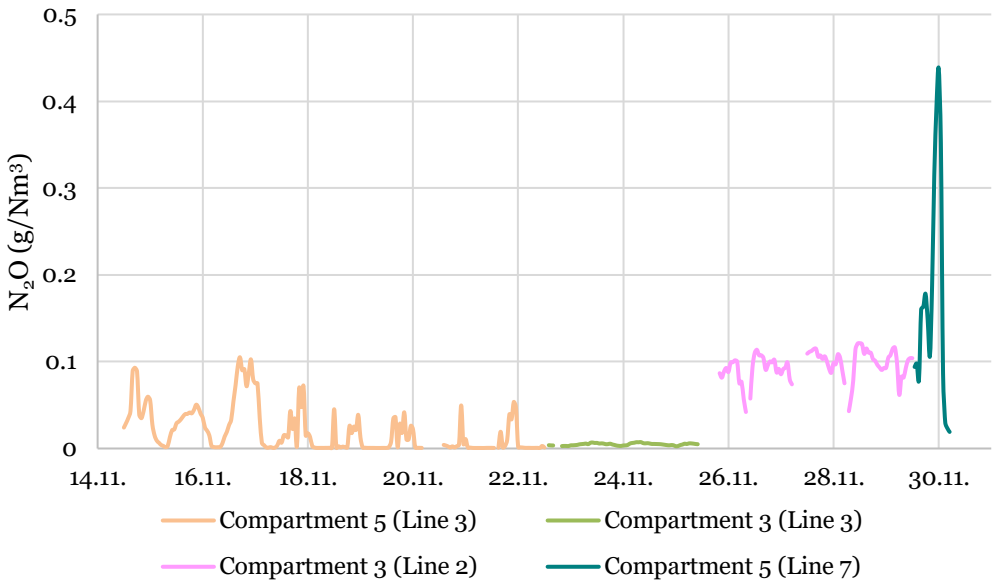

Figure 46 The measured N_2O concentrations at Viinikanlahti WWTP during the measurement campaign in November 2022.

The N_2O-N loads emitted from the aerobic compartments (compartments 3–5) in aeration line 3 are presented in figure 47 for the first week of the measurement campaign. The highest N_2O-N load seemed to originate from compartment 5 at a maximum hourly load around 35 gN/h. On average, the loads from compartments 4 and 5 were on a similar level, as the average load from compartment 5 (6.9 gN/h) was only slightly higher than that of compartment 4 (5.3 gN/h). On the contrary, the loads from compartment 3 were clearly the lowest. The loads varied between 0.9 and 1.9 gN/h, and thus showed little variation.

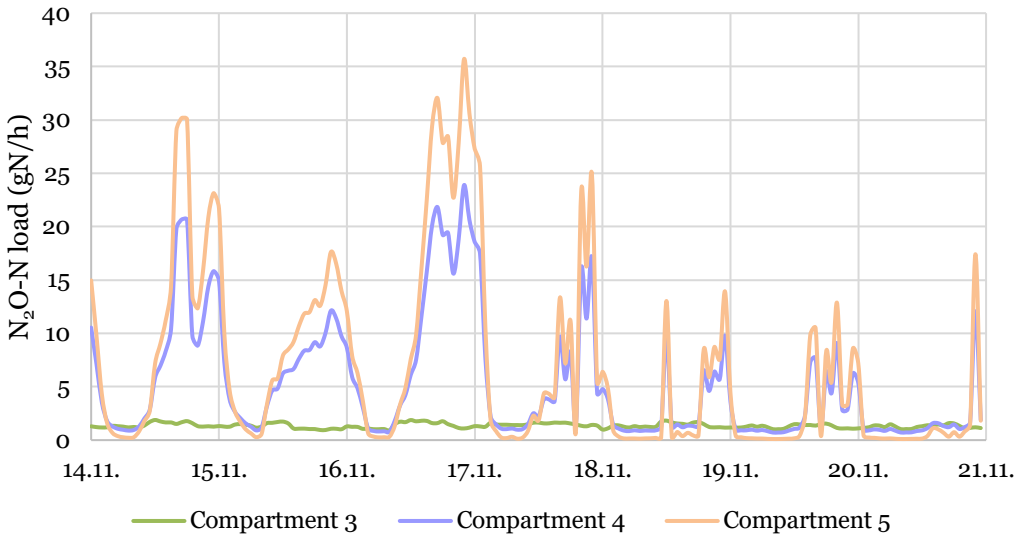

Figure 47 The estimated N_2O-N loads from each aerobic compartment in aeration line 3 during the first week of the measurement campaign at Viinikanlahti WWTP in November 2022.

The average hourly N_2O-N loads from the whole plant during the measurement campaign are presented in figure 48 for each weekday. The average load was 120 gN/h. Each day, the minimum loads (around 20 gN/h) occurred approximately from 4 AM to 8 AM. Outside that time period, there were no clear trends in the emitted N_2O-N loads between different weekdays. The highest N_2O-N load of 620 gN/h was emitted on Wednesday, while the average loads throughout the day were the lowest on Saturday and Sunday.

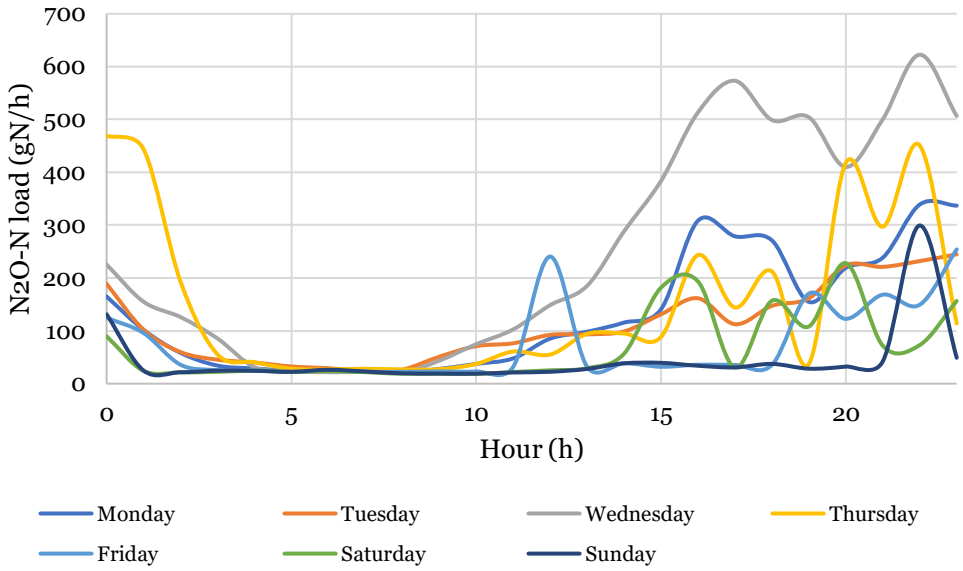

Figure 48 The average hourly plantwide N_2O-N loads emitted during the measurement campaign at Viinikanlahti WWTP in November 2022.

The emission factors were 0.08% relative to the influent total nitrogen load and 0.2% relative to the removed total nitrogen load. The average total nitrogen concentration in the influent was 56 mg/l and in the effluent 34.5 mg/l, both analyzed biweekly from 24-hour composite samples.

Between the measured N_2O concentrations and inflow rate to the plant, a moderate positive correlation (r = 0.5) was detected in compartment 5 of aeration line 3 with a 1-hour time lag. Visualization is included in figure 49. Similar correlation was not found between the parameters in compartment 3. The greatest share of the N_2O emissions originated from compartment 5 (figure 47), and thus the correlation with the inflow rate gives an indication that the highest emissions occurred when the loading in the treatment process was at its highest. The variability in the inflow rate is a good measure of the variability in the loading especially under dry-weather conditions, as the concentration of, e.g., total nitrogen in the influent is typically stable.

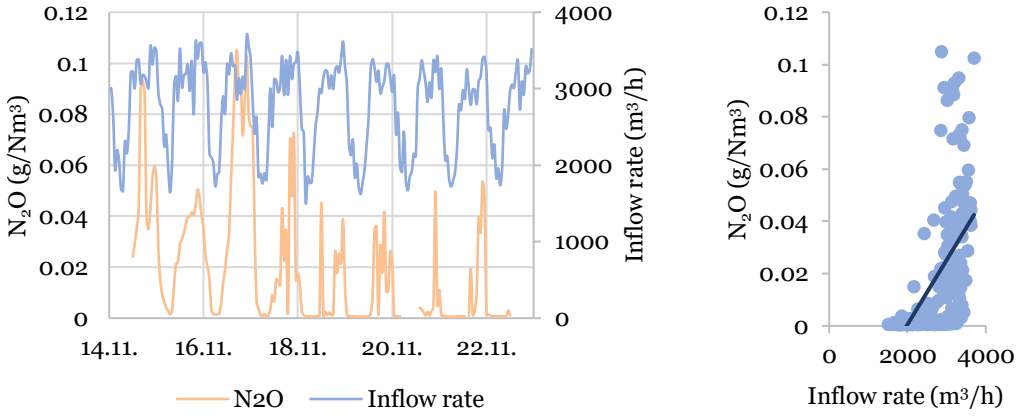

(a) (b)

Figure 49 The relationship between the N_2O concentrations measured in compartment 5 (aeration line 3) and inflow rate with a time lag of 1 hour.

The N_2O measurement data collected from compartments 3 and 5 in aeration line 3 was studied along with the online data from the DO probes and the NO_2^- samples analyzed during the measurement campaign. The N_2O emissions showed no correlation with DO in either of the compartments. The Pearson correlation was analyzed between DO and the N_2O concentrations measured in compartments 3 and 5, and the correlation coefficient was 0 in both analyses.

The measurement campaign in November included measurements in compartment 5 in two lines (aeration lines 3 and 7) with similar configuration, as described in section 3.3.3. Figure 50(a) compares the average, minimum and maximum N_2O concentrations measured from compartment 5 in line 3 and

line 7. The variation in the emissions was greater in line 7 than in line 3. For example, the average measured N_2O concentration was approximately ten times higher in line 7 than in line 3. In addition, the maximum N_2O concentration in line 7 was 4-fold compared to the maximum in line 3. The difference in the measured N_2O concentrations could have been affected by, e.g., uneven distribution of the loading between the aeration lines, variability in the environmental factors or in the microbial population of the activated sludge. For example, Gruber et al. (2021b) has linked the microbial population dynamics to different N_2O emission patterns in SBRs.

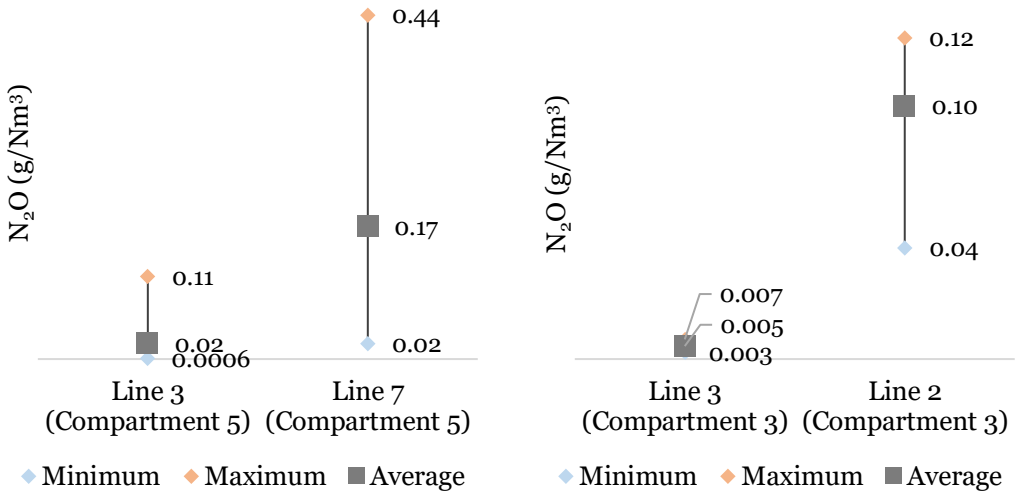

(a) (b)

Figure 50 Comparison between the N_2O emissions measured from the same compartment of two aeration lines. Emissions from compartment 5 in lines 3 and 7 are compared in (a) and compartment 3 in lines 2 and 3 in (b).

Another comparison between the emission levels was conducted between the measurement data from compartment 3 in aeration lines 2 and 3. As detailed in section 3.3.3, compartment 3 was the third aerobic compartment in line 2 and the first aerobic compartment in line 3. Figure 50(b) reveals that the emissions were significantly different between the lines. In line 3, the variation in the emissions was low, as the average, minimum and maximum N_2O concentrations fell between 0.003 and 0.007 g/Nm^3. Contradictorily, the emissions in line 2 exhibited greater variation with the average, minimum and maximum concentrations being 0.10, 0.04 and 0.12 g/Nm^3. The average N_2O concentration in line 2 was 20-fold compared to the average concentration measured in line 3. The different emission levels are likely explained by the different stage of nitrification in the compartments. Nitrification had proceeded further in compartment 3 in line 2 than in line 3, as compartment 3 was already the third aerobic compartment in line 2, while the compartment

was the first aerobic one in line 3. Thus, the production of N_2O seemed to proceed along with nitrification.

4.2.3 Comparison between the measurement campaigns

The average, minimum and maximum N_2O concentrations in aeration line 3 during the two measurement campaigns at Viinikanlahti WWTP are compared in figure 51. The measured off-gas N_2O concentrations in compartment 5 in November decreased from those measured in September, as the measured average concentration decreased from 0.09 g/Nm^3 to 0.02 g/Nm^3 and the maximum concentration from 0.56 g/Nm^3 to 0.11 g/Nm^3. In compartment 3, similar N_2O concentrations were measured during both measurement campaigns.

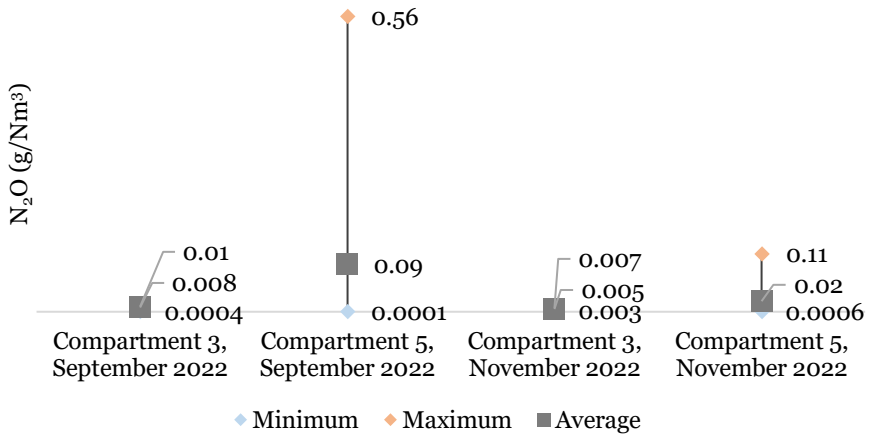

Figure 51 The average, minimum and maximum N_2O concentrations in aeration line 3 during the two measurement campaigns at Viinikanlahti WWTP.

The emission factors are collected to table 13 which is also complemented with other parameters describing the conditions during the measurement campaigns. The emission factor of 0.4% relative to the influent total nitrogen measured in September decreased to 0.08% in November. Similarly, a decrease from 1.1% to 0.2% was detected in the emission factor relative to the removed total nitrogen. The emission factors relative to the removed total nitrogen load are significantly higher than those related to the influent total nitrogen, indicating that the total nitrogen removal is not very efficient at Viinikanlahti WWTP. Indeed, the plant is not obliged to total nitrogen removal by the environmental permit, which likely decreases the amount of total nitrogen removed in the treatment process.

Table 13 The emission factors measured at Viinikanlahti WWTP and loading in the treatment process during the two measurement campaigns.

Parameter	September 2022	November 2022
Emission factor relative to influent total nitrogen (%)	0.4	0.08
Emission factor relative to removed total nitrogen (%)	1.1	0.2
Influent total nitrogen load (kgN/d)	3 600	3 700
Influent BOD_7 load (kg/d)	19 000	21 000
Influent COD load (kg/d)	45 000	36 000
BOD_7/N ratio after primary clarification	1.3	1.1
COD/N ratio after primary clarification	9.3	6.8
Temperature in the biological treatment (°C)	14–20	11–17

The average total nitrogen and BOD_7 loads (table 13) were relatively unchanged between the measurement campaigns. In contrast, a significant difference was detected in the COD load, as the average load was approximately 10 000 kg/d higher in September than in November. However, it should be noted that COD was analyzed once during both measurement campaigns, while biweekly composite samples were collected to analyze total nitrogen and BOD_7. Thus, the average loads were not necessarily representative of the loading during the measurement campaigns. On the other hand, the industrial wastewater conducted to Viinikanlahti WWTP could have affected the COD loading, similarly as it was detected to significantly affect the temperature of the wastewater, as detailed in section 3.3.2.

The COD/N and BOD_7/N ratios are also provided in table 13. They were calculated for the water after primary clarification to describe the ratios in the water conducted to the biological treatment. A COD/N ratio around 7–9 is well above the suggestion of 4–6 to promote the completion of heterotrophic denitrification (Henze et al., 2002; Pan et al., 2013b). However, the BOD_7/N ratio was close to 1 during both measurement campaigns, which indicates that a low share of the COD load was readily available for biodegradation during heterotrophic denitrification. For comparison, at Akaa and Kirkonkylä WWTPs, the BOD_7/N ratio was around 3. Interestingly, the measurement results suggest that heterotrophic denitrification did not contribute to the N_2O emissions, indicating that the relatively low BOD_7/N ratio was

sufficient to not promote N_2O production during heterotrophic denitrification. Low off-gas N_2O concentrations were measured in compartment 3 in aeration line 3 during both measurement campaigns, as visualized by figure 51. Thus, there seemed to be no dissolved N_2O in the water after the denitrifying anoxic compartments (compartments 1–2) that would have been stripped to gaseous N_2O at the start of aeration in compartment 3. Furthermore, the measured average and maximum off-gas N_2O concentrations in compartment 5 were 4 to 60-fold compared to the concentrations in compartment 3, indicating an increase in the emission of N_2O along with nitrification. This finding was also supported by the measurements in other aeration lines with one or no anoxic compartments instead of the two anoxic compartments in aeration line 3. Generally, higher emissions occurred in compartment 3 in lines where the number of anoxic compartments prior to compartment 3 dropped from two to 0–1. Visualizations and more detailed interpretations are provided in sections 4.2.1 (figure 45) and 4.2.2 (figure 50(b)). Furthermore, the high COD/N but low BOD_7/N ratio could indicate that there was a large COD load that could not be utilized during heterotrophic denitrification and was oxidized in the aerobic compartments. This oxidation process would compete with nitrification and could therefore enhance nitrification related N_2O production especially when the overall loading in the treatment process is at its highest.

The average temperature in the biological treatment was 18 °C in September and 15 °C in November. Thus, both measurement campaigns were conducted under warm-period conditions, even though the fluctuation in the temperature was high (14–20 °C in September and 11–17 °C in November). A temperature of 20 °C has been suggested to be ideal to support complete nitrification and denitrification (Massara et al., 2017). Thus, the relatively warm temperatures in the biological treatment likely benefit the nitrogen conversion processes and possibly also mitigate N_2O emission. However, measurements under cold-period conditions with the temperature remaining below, e.g., 12 °C were not conducted to study the seasonality of the N_2O emissions from the temperature perspective.

The DO levels in the aerobic compartments were more stable in November than in September. In compartment 5 in aeration line 3, where the highest emissions were measured, the DO level varied between 0.9 and 3.2 mg/l in September and between 1.7 and 2.4 mg/l in November. Thus, the drops in DO detected in September were avoided in November, which could have supported the lower N_2O emission level in November. For example, Peng et al. (2015) found that a DO level below 1.5 mg/l enhanced nitrifier denitrification in a nitrifying culture, which would support the results from Viinikanlahti WWTP in September, as the N_2O emission peaks occurred under a DO level of 0.9–1.5 mg/l, as visualized by figure 43 in section 4.2.1. Thus, the unstable

DO levels in September could be one of the most significant factors causing the different emission levels measured during the two measurement campaigns. However, also the available estimate of the influent COD load was higher in September than in November, which might have affected the N_2O emission level in September due to the increased loading in the treatment system. The COD load requires a significant air supply for its oxidation, which could have contributed to the DO dropping to an undesirable level. The diurnal variability in the N_2O emission level seemed to vary according to the loading in the treatment system. Moderate Pearson correlation (r = 0.5–0.6) was found between the inflow rate and N_2O with a 1–2-hour time lag in compartment 5 (aeration line 3) during both measurement campaigns, which can be assumed to also express correlation to the variability in the loading.

4.3 Akaa WWTP, Akaa

4.3.1 Measurement campaign in December 2022

The N_2O concentrations measured from four measurement locations at Akaa WWTP are presented in figure 52. In both measured lines, the emissions at the end of the aerobic compartment were higher than in the beginning of the compartment. The average N_2O concentrations in line 1 were 0.002 g/Nm^3 in the beginning of the compartment and 0.007 g/Nm^3 at the end of the compartment, resulting in over 3-fold difference. A slightly greater, 5-fold difference was detected from the measured concentrations in line 3, as the respective average concentrations were 0.006 and 0.03 g/Nm^3. The maximum concentration (0.23 g/Nm^3) was measured at the end of the aerobic compartment in line 3. Respectively, the minimum concentration (0.0002 g/Nm^3) was measured at the end of the aerobic compartment in line 1.

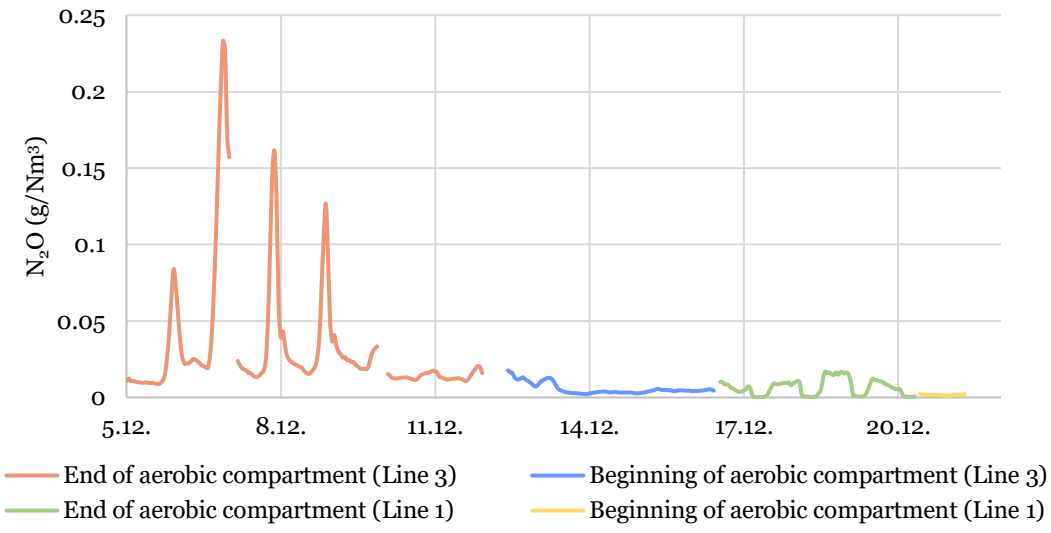

Figure 52 The N_2O concentrations measured at Akaa WWTP.

Furthermore, line 3 produced generally more N_2O emissions than line 1. However, this was assumed to be largely affected by the low pH in the process between 5 and 13 December, as specified in section 3.4.2. Line 3 was monitored from 5 to 16 December, and thus the decreased pH (5.4–6.4) could have significantly affected the measured N_2O concentrations. Line 1 was monitored between 16 and 21 December under normal pH conditions (6.5–7.0) and similar emission peaks to line 3 were not detected. Figure 53 visualizes the correlation between pH and N_2O. A negative Pearson correlation factor of -0.6 was calculated based on the measured N_2O data and online pH measurements in the aerobic compartments.

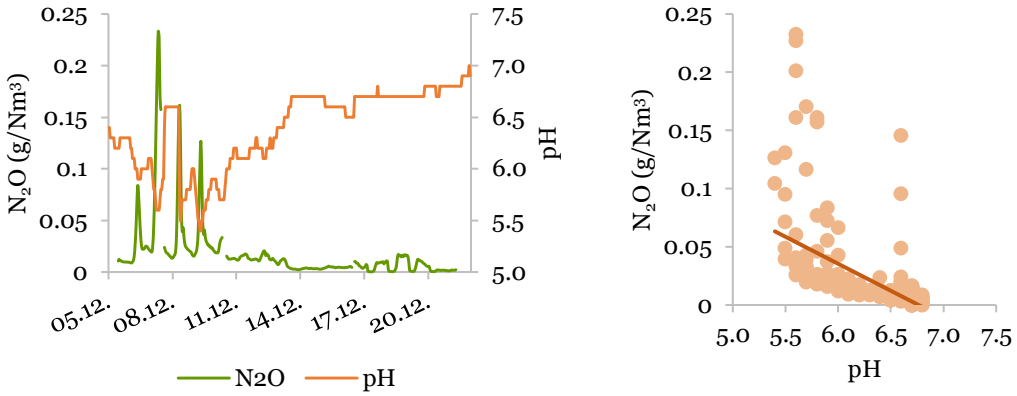

(a) (b)

Figure 53 The relationship between N_2O emissions and pH during the measurement campaign at Akaa WWTP.

A further comparison between the emission levels in lines 1 and 3 was performed by estimating the N_2O-N loads for the aerobic compartment of the lines. As the aerobic compartment is not divided into smaller compartments at Akaa WWTP, the off-gas N_2O concentration for the compartment was calculated as the average of the measured concentrations in the beginning and end of the compartment (figure 52). The loads are presented for the first week of the measurements in figure 54. There was a significant difference between the emissions from the two lines. The average N_2O-N load in line 1 was 1.7 gN/h and 6.8 gN/h in line 3, indicating a 4-fold difference between the average loads. Between the maximum N_2O-N loads, there was a 10-fold difference, as the maximum load from the aerobic compartment in line 1 was 4.4 gN/h and respectively 38 gN/h in line 3. A similar difference in magnitude was found between the minimum loads. In line 1, the minimum N_2O-N load was 0.2 gN/h, whereas the minimum load was 2.4 gN/h in line 3.

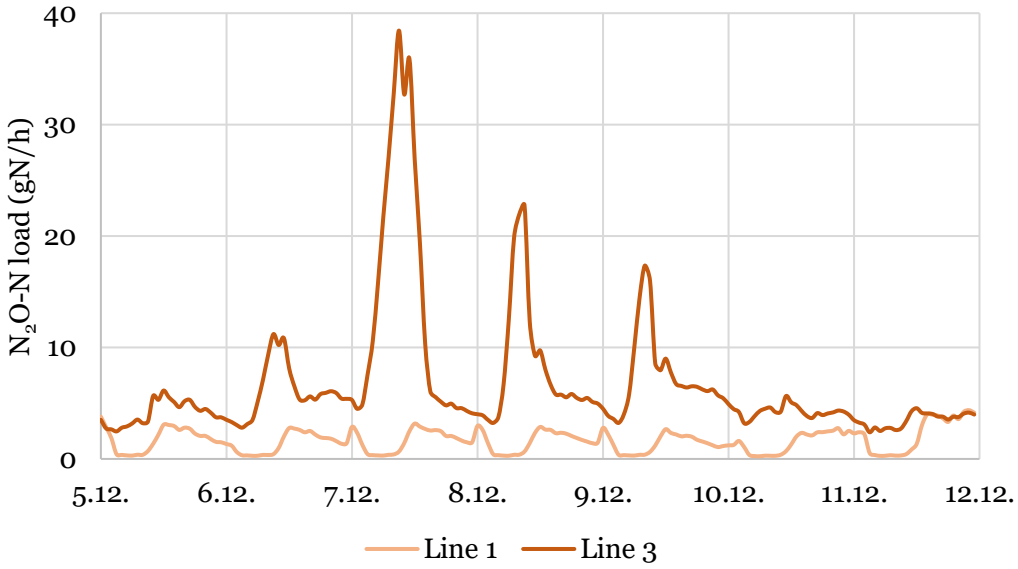

Figure 54 Comparison between the estimated N_2O-N loads emitted in the aerobic compartment in lines 1 and 3 from 5 to 12 December.

The estimated N_2O-N load from the whole plant, i.e., aeration lines 1–4, is presented for each weekday in figure 55. The hourly load varied between 6 and 78 gN/h, with the average being 17 gN/h. The most significant hourly variation was detected on Wednesday. The N_2O-N loads on Thursday and Friday exhibit more mediate variation in comparison to Wednesday, while little variation was detected in the loads from Saturday to Tuesday. Generally, the highest emission loads occurred between 6 AM and 12 AM and the lowest in the evening and nighttime between 4 PM and 4 AM.

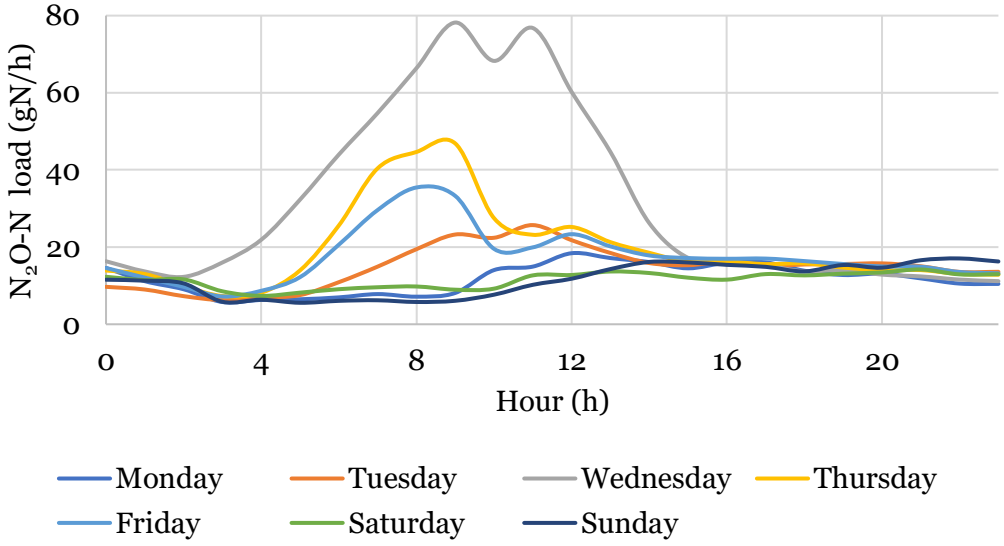

Figure 55 The estimated N_2O-N load for the whole plant, averaged for each weekday.

The emission factors relative to the influent total nitrogen and removed total nitrogen were 0.2% and 0.3%, respectively. The factors were based on the total N_2O-N load and the influent and effluent total nitrogen concentrations analyzed from a 24-hour composite sample during the measurement campaign. The concentrations were 86 and 37 mg/l, respectively.

Pearson correlation was studied between the inflow rate and the measured N_2O concentrations. A strong positive correlation ($r = 0.7$) with a 2-hour time lag was found between the two parameters at the end of the aerobic compartment in line 1. Visualization is provided in figure 56. A similar study for the other measurement locations revealed only low positive correlation ($r < 0.3$).

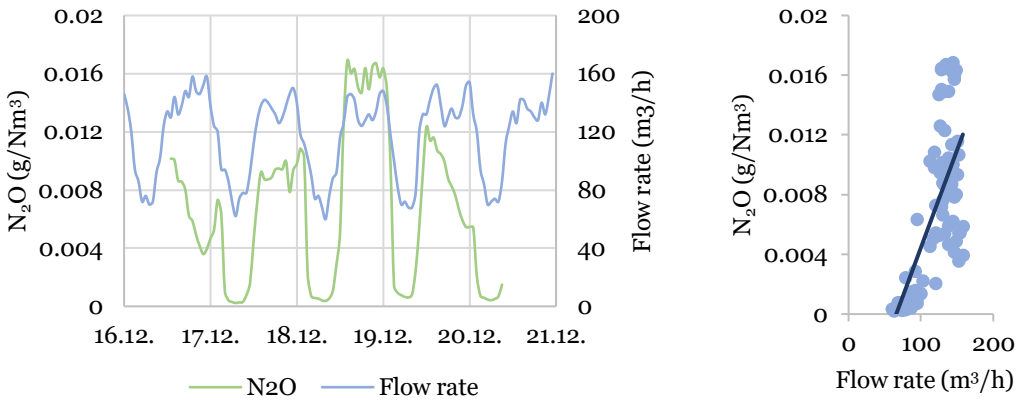

(a) (b)

Figure 56 The relationship between the N_2O concentrations and flow rate with a 2-hour time lag at the end of the aerobic compartment in line 1.

Correlation was also studied between the measured N_2O concentrations and DO levels based on the N_2O measurement data and online measurement data from the DO analyzers located at the end of the aerobic compartment in lines 1 and 3. A strong negative correlation was found between the N_2O emissions and DO in line 1, as the Pearson correlation coefficient was -0.8. Figure 57 visualizes the relationship between the N_2O and DO concentrations at the end of the aerobic compartment in line 1. Even though a low DO level around 0.5–1 mg/l caused an increase in the measured N_2O concentrations, the emission level was still well below 0.02 g/Nm^3.

A similar study for the collected data from line 3 exposed only low negative correlation between N_2O and DO, with the Pearson correlation coefficient being -0.3. Contrary to the drops in DO in line 1 to around 1 mg/l, the DO level in line 3 remained at a high level (3–5 mg/l) during the measurement campaign.

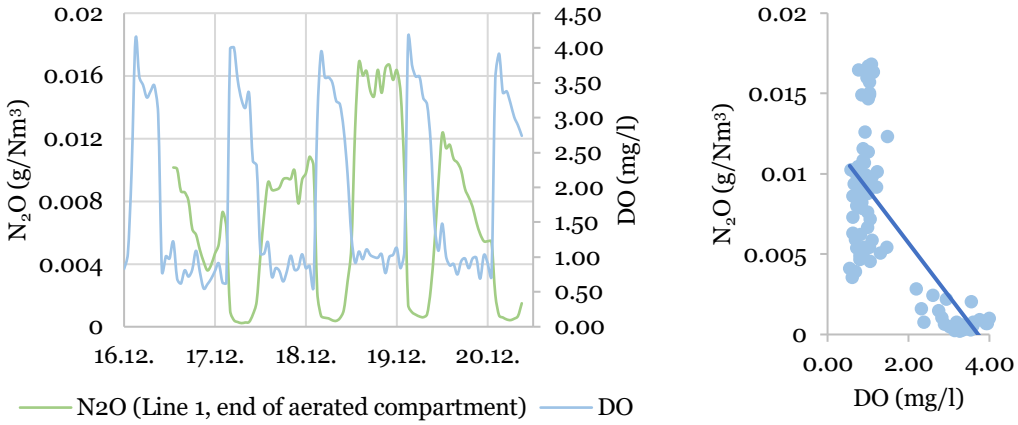

(a) (b)

Figure 57 The relationship between N_2O emissions and DO at the end of the aerobic compartment in line 1.

The NO_2^- samples (N = 23) analyzed during the measurement campaign were all below 0.1 mg/l, indicating no accumulation of NO_2^- that could have enhanced N_2O production. The NO_2^- samples also included samples from the end of the aerobic compartment in line 3 during the low pH and the NO_2^- concentrations in those samples were also below 0.1 mg/l.

4.3.2 Discussion of the results at Akaa WWTP

Emission factors of 0.2% relative to influent total nitrogen and 0.3% relative to removed total nitrogen were measured at Akaa WWTP. Table 14 contains the emission factors together with other parameters describing the measurement campaign.

Table 14 The emission factors measured at Akaa WWTP and other paramters describing the conditions during the measurement campaign.

Parameter	December 2022
Emission factor relative to influent total nitrogen (%)	0.2
Emission factor relative to removed total nitrogen (%)	0.3
BOD_7/N ratio after primary clarification	2.8
COD/N ratio after primary clarification	6.6
Temperature in the biological treatment (°C)	8–11

The temperature in the biological treatment (8–11 °C) indicated cold-period conditions. The low temperature did not cause a high emission level, as the

emission level was generally very low and high emissions were measured only during the low pH in the treatment process. The majority of the measured N_2O-N load was emitted in the first days of the measurement campaign during the low pH. A pH around 7 has been suggested to be ideal for N_2O emission mitigation (Massara et al., 2017), while the pH dropped to 5.4–6.4 at Akaa WWTP after a fault in $CaCO_3$ dosage appeared. Assumably, the emissions would have been lower, if the pH remained at the typical level of 6.5–7.0 also in the beginning of the campaign. The mechanism behind N_2O production during the low pH requires further studying, but for example Su et al. (2019) found that acidic pH promoted abiotic N_2O production, while its contribution to N_2O emissions under near-neutral pH was insignificant in comparison to the biological emission pathways considered in this thesis.

Furthermore, the DO levels below 1 mg/l detected at the end of the aerobic compartment in line 1 could be linked to increases in the measured N_2O concentrations. The drops in the DO level were likely a result of the increased flow rate causing an additional loading to the treatment process. Both DO and inflow rate had a strong correlation to the measured N_2O concentrations, as the Pearson correlation factor was -0.8 between N_2O and DO and 0.7 between N_2O and flow rate (with a 2-hour time lag). Similar correlation was not detected in the other measurement locations.

Regarding the contribution of nitrification and heterotrophic denitrification to the N_2O emissions, it can be concluded that heterotrophic denitrification did not significantly contribute to the emissions. In both measured lines, the measured N_2O concentrations were consistently lower in the beginning of the aerobic compartment after the anoxic phase than in the end of the aerobic compartment. The COD/N ratio around 7 was above the suggested ratio (4–6) to promote complete heterotrophic denitrification (Henze et al., 2002; Pan et al., 2013b). Furthermore, the BOD_7/N ratio around 3 suggested that there was likely a sufficient share of readily biodegradable matter for heterotrophic denitrification. As the emission level was also relatively low at the end of the aerobic compartment especially under normal pH, nitrification did not either produce high quantities of N_2O.

4.4 Modelling results

The Sumo4N model of the treatment process at Viinikanlahti WWTP was built according to the background detailed in section 3.6. The model simulation results were studied within a period from 12 to 28 September 2022. The calibration of the model was conducted according to the guidelines in table 9 (section 3.6). The model required calibration of the settling parameters of the secondary clarifier unit to fix the effluent TSS and COD concentrations closer to the calibration guidelines. The parameters named maximum Vesilind

settling velocity and coefficient for flocculent settling were increased to decrease the effluent TSS and COD. The fraction of non-settleable solids and the concentration of non-settleable solids were decreased to further fit the simulated effluent TSS and COD to the calibration guidelines. The calibration results for TSS and COD are visualized in figures 58 and 59, respectively.

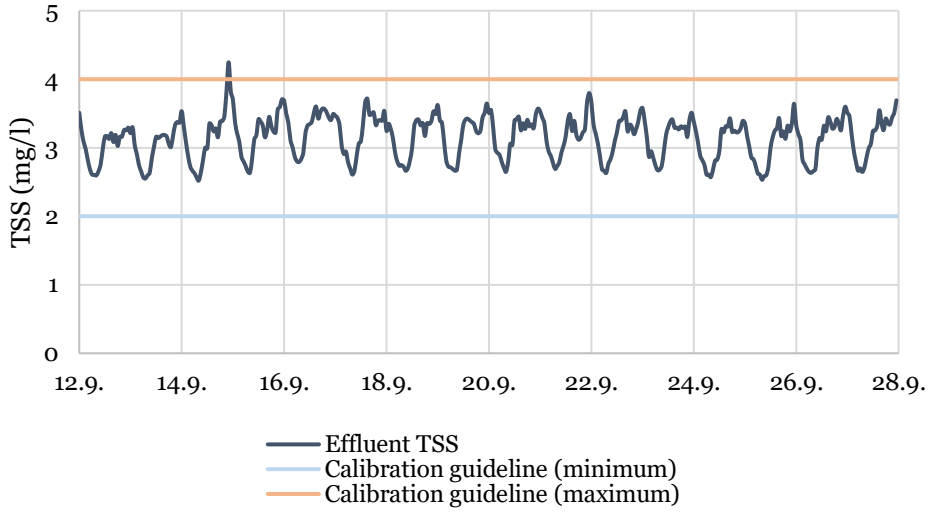

Figure 58 Calibration result of the effluent TSS concentration.

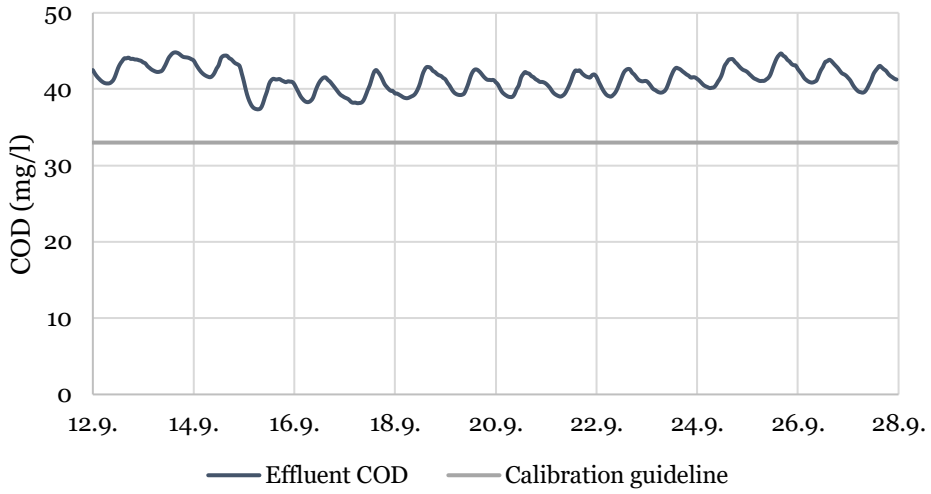

Figure 59 Calibration result of the effluent COD concentration.

The simulated effluent TSS concentration was well within the calibration guidelines. On the contrary, the COD concentration (around 40 mg/l) consistently exceeded the guideline (33 mg/l). However, the guideline was based on one 24-hour composite sample which gave little information regarding the variability in COD. Furthermore, the simulated effluent COD is mainly dependent on the fraction of unbiodegradable COD in the COD fractionation, and the data used for the fractionation was relatively old (over 15 years).

Thus, the simulated effluent COD was deemed to be sufficiently close to the guideline.

The other parameters in the focus of the calibration did not require further adjustment to fit the calibration guidelines. As visualized by figures 60 and 61, the effluent total nitrogen and the MLSS concentration in compartment 5 were within the guidelines. The other nitrogen compounds in the effluent, i.e., NH_4^+, NO_3^- and NO_2^-, were checked individually to confirm that their fractions of the total nitrogen concentration were in the correct level.

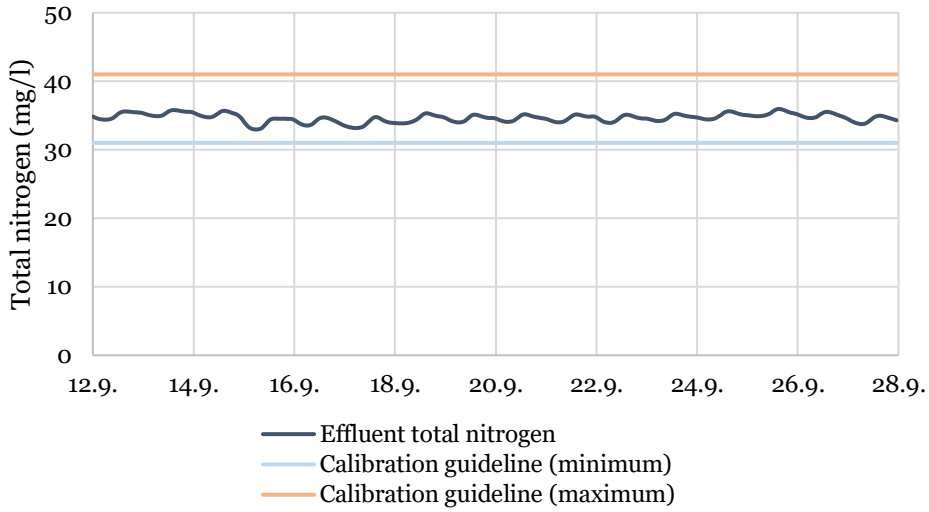

Figure 60 The simulated effluent total nitrogen concentrations.

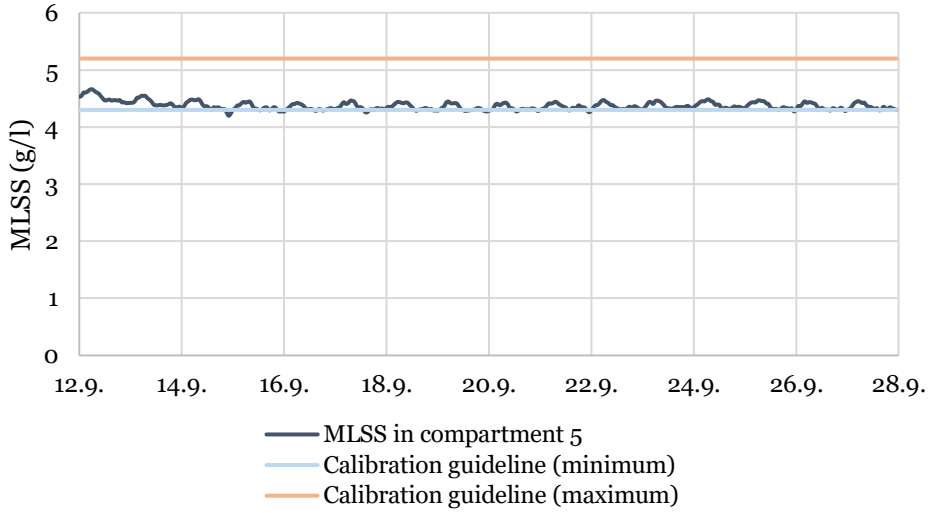

Figure 61 The simulated MLSS concentration in compartment 5.

After calibrating the model according to the general guidelines, the simulation results regarding N_2O were studied. Sumo4N had different default parameters than those proposed by Pocquet et al. (2016) and Hiatt and Grady

(2008a) related to nitrification, denitrification and N_2O production. The dissolved N_2O concentrations from all compartments are presented in figure 62 with the default parameters and in figure 63 with the parameters from Pocquet et al. (2016) and Hiatt and Grady (2008a). With both parameter sets, the model predicted the highest N_2O concentrations in the liquid phase to compartments 1, 2 and 3 of which compartments 1 and 2 were anoxic. Thus, the model seemed to predict the majority of the N_2O production to heterotrophic denitrification, contradicting the conclusion from the measurement campaign that N_2O was mainly produced during nitrification (section 4.2.3). The rest of the simulations were performed with the Sumo4N default parameters which gave slightly lower dissolved N_2O concentrations in the anoxic compartments than the other set of parameters.

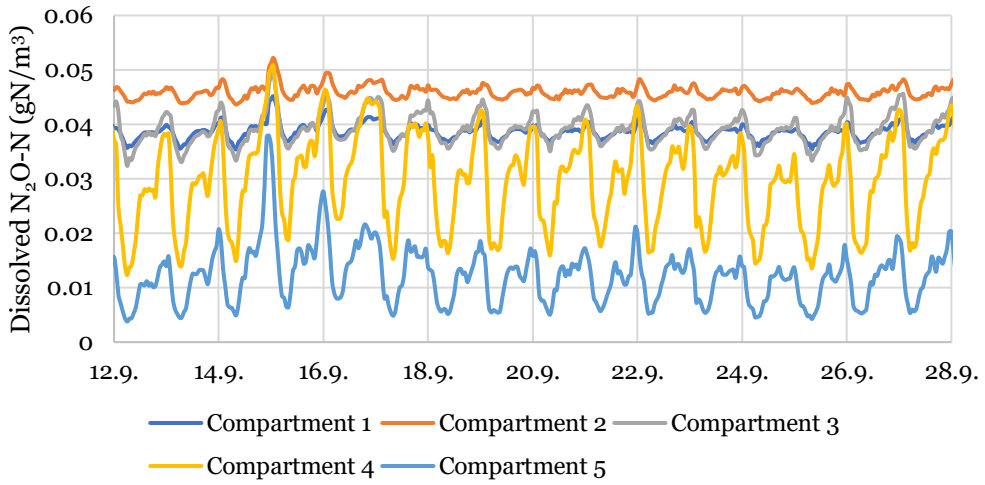

Figure 62 The dissolved N_2O-N concentrations in compartments 1–5 with Sumo4N default parameters.

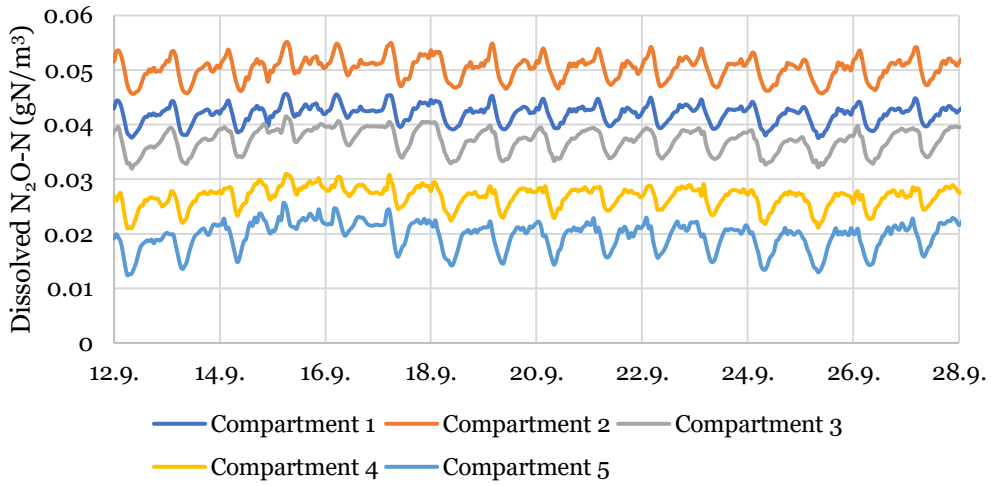

Figure 63 The dissolved N_2O-N concentrations in compartments 1–5 with parameters proposed by Pocquet et al. (2016) and Hiatt and Grady (2008a).

Figure 64 presents the simulated and measured N_2O concentrations from compartment 3 and 5 with the Sumo4N default parameters. The overprediction of the N_2O concentrations in compartment 3 could be partly due to the N_2O produced in the anoxic compartments being stripped to gaseous form at the start of the aerobic phase. In compartment 5, the diurnal variation was simulated correctly but the simulated maximum N_2O peaks (10–25 ppmv) were significantly lower than the measured peaks (50–300 ppmv).

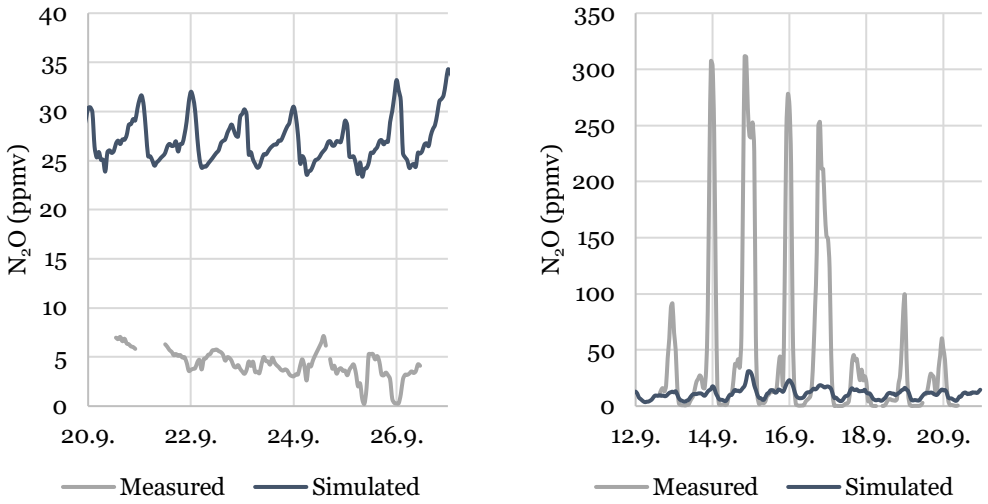

(a) (b)

Figure 64 The measured and simulated N_2O concentrations in the off-gas in compartment 3 (a) and in compartment 5 (b) after the calibration according to the general guidelines.

To reduce the share of heterotrophic denitrification in N_2O production, the growth of HDN was reduced by adjusting the maximum specific growth rate of HDN. Furthermore, the maximum specific growth rate of AOB was reduced to decrease the nitrification rate at the beginning of the aerobic phase. The growth rates were adjusted without causing unrealistic deviation from the calibration guidelines regarding the effluent quality and MLSS in compartment 5. A further calibration attempt was made to improve the simulated N_2O concentrations by adjusting the reduction factors specific for the two nitrification related emission pathways, i.e., NH_2OH oxidation and nitrifier denitrification. The factors affect the N_2O production predicted by the model.

The general conclusion was that the model predicted similar N_2O concentrations to the aerobic compartments. As visualized by the calibration result (scenario 1) in figure 65, the simulated N_2O emissions in both compartments were close to 20–25 ppmv. While the simulated and measured concentrations were relatively similar in compartment 3, the peaks measured in the N_2O concentrations in compartment 5 were not reproduced by the model. It

was also noted that reducing the growth rate of HDN could not significantly decrease the N_2O production in the anoxic compartments before it started to deteriorate the overall nitrogen removal predicted by the model.

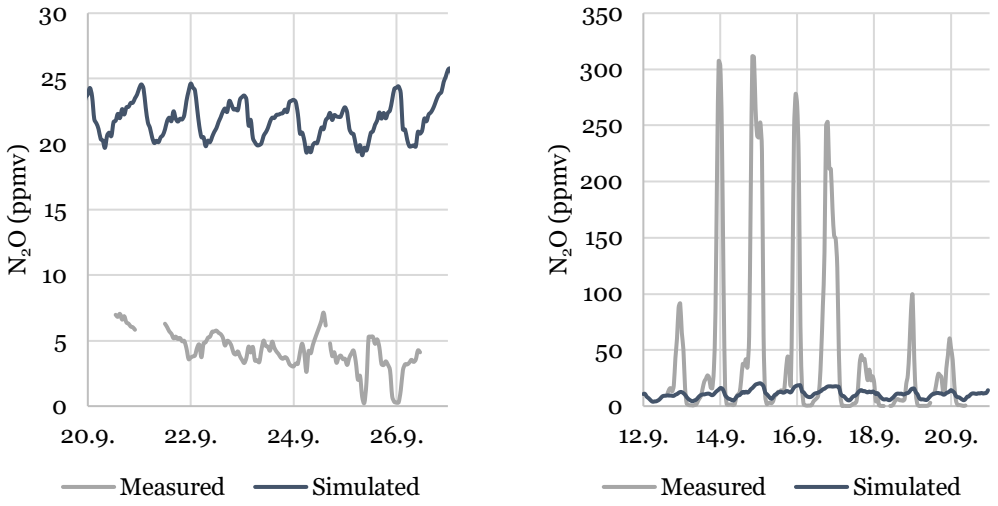

(a) (b)

Figure 65 A calibration result (scenario 1) underestimating the N_2O concentrations in compartment 5 (b). The result for compartment 3 (a) was better.

Another calibration effort (scenario 2) resulted in better prediction of the N_2O peaks in compartment 5 but caused significant overestimation to the concentrations in compartment 3. This scenario is visualized in figure 66.

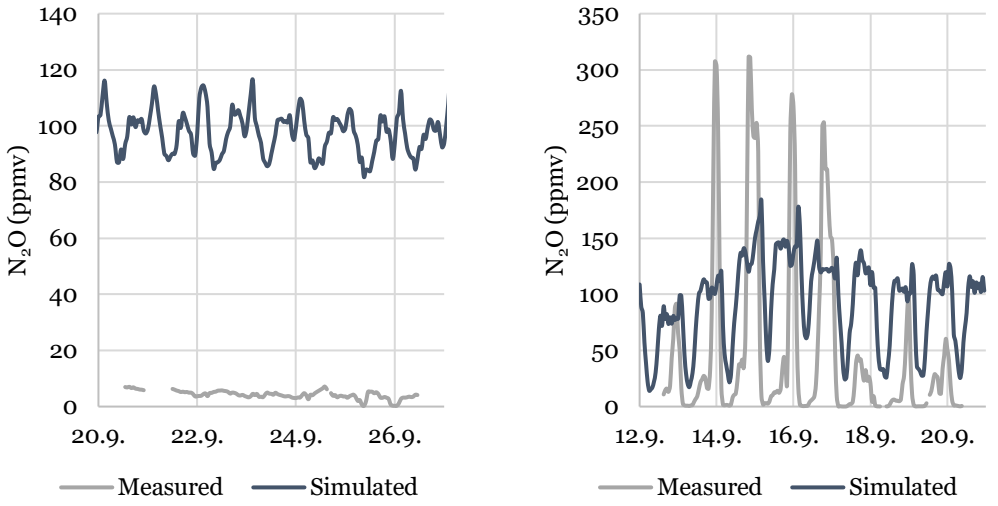

(a) (b)

Figure 66 A calibration result (scenario 2) overestimating the off-gas N_2O concentrations in compartment 3 (a). The result for compartment 5 (b) was better.

All calibrated parameters are listed to table 15. The settling related parameters are the calibrated parameters of the secondary clarifier. The other four parameters were calibrated to improve the simulation results regarding N_2O emissions.

Table 15 The calibrated Sumo4N parameters in the modelling experiment.

Parameter	**Value after calibration**	**Default value in SUMO**
Maximum Vesilind settling velocity (m/d)	500	300
Coefficient for flocculent settling (L/g)	7.0	2.5
Fraction of non-settleable solids (%)	0.05	0.1
Non-settleable TSS (g/m^3)	15	20
Maximum specific growth rate of AOB (1/d)	0.7	0.9
Maximum specific growth rate of OHOs/HDN (1/d)	2	4
Reduction factor for NO reduction to N_2O by AOB	Scenario 1: 0.009 Scenario 2: 0.25	0.0015
Reduction factor for HNO_2 reduction to N_2O by AOB	Scenario 1: 0.065 Scenario 2: 0.05	0.25

As a conclusion from the modelling experiment, the Sumo4N model accurately modelled the diurnal variation in the N_2O concentrations that was especially distinct in compartment 5. However, the measured and simulated N_2O concentrations in the two compartments could not be matched after a relatively light calibration effort targeted to adjust the N_2O production. Thus, a deeper understanding of the model should be acquired to assess the potential of the model to simulate N_2O emissions. Further calibration is needed to determine if the model can reproduce the measurement results or if it is too limited to accurately model the dynamic N_2O emission patterns.

5 Discussion

Section 5 is divided into three parts to discuss the results of this thesis. The results from the N_2O measurement campaigns are compared to each other and to previous studies in section 5.1. Section 5.2 is targeted to discuss the reliability of the data used in the study and the feasibility of the assumptions that were made to produce the results. The relevance of the results, both from the measurement campaigns and the modelling experiment, is discussed in section 5.3.

5.1 Comparison of the results to previous studies

The emission factors measured at the three treatment plants are compiled in table 16, categorized according to the temperature in the biological treatment unit during the measurements. The considered emission factors are only the factors relating the N_2O-N load to the influent total nitrogen load and a threshold of 12 °C is applied to differentiate cold-period conditions from warm-period conditions. The COD/N and BOD_7/N ratios are also provided to describe the availability of organic matter in the water conducted to the biological treatment. The table is complemented with the emission factors measured by Hilander (2022) at Kakolanmäki WWTP in Turku and Nenäinniemi WWTP in Jyväskylä in Finland.

Table 16 Emission factors measured at five Finnish WWTPs in 2022–2023.

Treatment plant	**EF (% of the influent total nitrogen emitted as N_2O-N)**		**COD/N ratio**	**BOD_7/N ratio**	**Reference**
	T < 12 °C	**T > 12 °C**			
Akaa WWTP	0.2	-	7	3	
Kirkonkylä WWTP	1.8	0.04	7–8	3	
Viinikanlahti WWTP	-	0.08–0.4	7–9	1	
Kakolanmäki WWTP	1.7	0.09	-	-	Hilander (2022)
Nenäinniemi WWTP	1.3	1.0	-	-	Hilander (2022)

Generally, the emission factors were well above 1% during the cold-period conditions and below 1% under the warm-period conditions. The emission factor of 0.2% measured at Akaa WWTP was lower than the emission factors varying from 1.3% to 1.8% at the other WWTPs under the cold-period conditions. At three treatment plants (Kirkonkylä, Viinikanlahti and Kakolanmäki

WWTPs), low emissions were measured under the warm-period conditions, as the measured emission factors were below 0.1%. Especially distinct seasonal variation was detected at Kirkonkylä WWTP and Kakolanmäki WWTP, where the emission factors were 0.04–0.09% during the warm period and 1.7–1.8% during the cold period. This suggests strong seasonal variability in the N_2O emissions, which has also been confirmed by several previous studies (Daelman et al., 2015; Gruber et al., 2020). A wide range of emission factors (0.02–2.6 % of the influent total nitrogen) measured under cold-period and warm-period conditions has also been reported by Mikola et al. (2014) from four Finnish WWTPs. Thus, the categorization of the emission factors according to temperature indicates that lower temperatures (e.g., below 12 °C) in biological nitrogen removal during the cold period can promote a higher N_2O emission level than the generally lower emission level measured during the warm period. Temperatures below 12 °C are also significantly lower than the temperature of 20 °C that has been suggested to be optimal for N_2O emission mitigation (Massara et al., 2017).

The COD/N ratio was above 7 during all measurement campaigns, while the BOD_7/N ratio was 1 at Viinikanlahti WWTP and 3 at Akaa and Kirkonkylä WWTPs. A COD/N ratio of 7 complies with the recommendation that the ratio should be above 4–6 to promote complete heterotrophic denitrification (Henze et al. 2002; Pan et al. 2013a). This supports the finding that heterotrophic denitrification did not contribute to the N_2O emissions, as N_2O production seemed to proceed along with nitrification. The role of denitrification in N_2O production could be studied during the measurement campaigns at Akaa WWTP and Viinikanlahti WWTP where there seemed to be no dissolved N_2O originating from the anoxic compartments that would be stripped to gaseous N_2O emission at the start of aeration. However, the BOD_7/N ratio of 1 at Viinikanlahti indicates that the share of readily biodegradable organic matter in the total COD load was relatively low. In comparison, the BOD_7/N ratio of 3 at Akaa WWTP suggests a higher share of readily biodegradable matter. The readily biodegradable organic matter is the fraction of the total COD load that can be consumed in heterotrophic denitrification. Even though the BOD_7/N ratio was low at Viinikanlahti WWTP, it seemingly did not result in heterotrophic denitrification related N_2O production during the measurement campaigns.

The emission factors in table 16 can also be compared to those measured at Viikinmäki WWTP in Helsinki which is currently the only Finnish treatment plant with long-term N_2O measurement data. The continuous online off-gas measurement unit was installed in 2012 (Kosonen, 2013). Figure 67 presents the monthly average emission factors relative to influent total nitrogen measured at Viikinmäki WWTP between January 2021 and May 2022, adapted

from Hilander (2022). The emission factors vary from 0.6% to 1.6%, indicating significant seasonality in the emission levels also at Viikinmäki WWTP. Emission factors below 1% were measured between April and August, while the monthly average factors increased above 1% from September to March. The daily emission factors in figure 68 exhibit even greater variation, ranging from 0.5% to 2.6%. The daily emission factors below 0.5% in March–April 2022 are explained by poor nitrification during the time, and they are therefore not representative of the emission level under normal conditions.

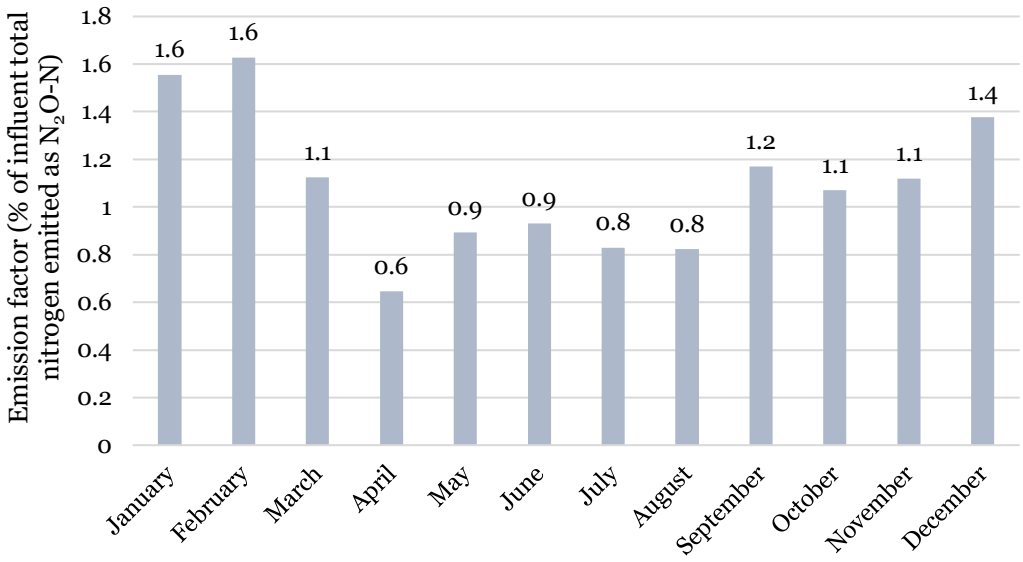

Figure 67 The monthly average N_2O emission factors at Viikinmäki WWTP between January 2021 and May 2022, adapted from Hilander (2022).

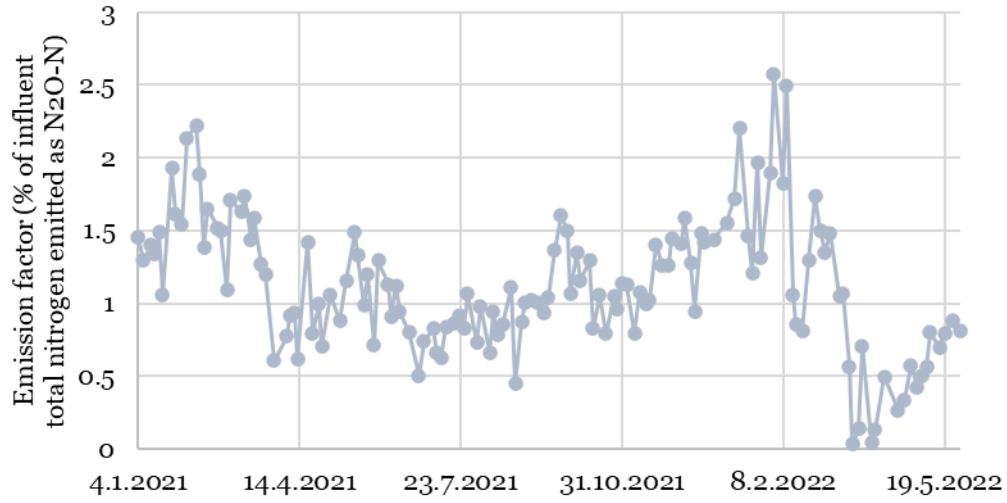

Figure 68 The daily average N_2O emission factors at Viikinmäki WWTP between January 2021 and May 2022, adapted from Hilander (2022).

The emission factors measured at the five Finnish treatment plants (table 16) comply with the varying emission levels measured at Viikinmäki WWTP. The emission factors of 1.3–1.8% measured at Kirkonkylä, Kakolanmäki and Nenäinniemi WWTPs during the cold period correspond well to the highest emission factors of 1.4–1.6% at Viikinmäki WWTP. In contrast, the emission factors below 0.1% measured at Kirkonkylä, Viinikanlahti and Kakolanmäki WWTPs under the warm-period conditions are significantly lower than the typical emission level at Viikinmäki WWTP which does not seem to fall below 0.5%. However, the variability in the emission level captured during two measurement campaigns at the same WWTP can be expected to portray similar seasonality of the emissions that is typical to Viikinmäki WWTP based on the long-term N_2O emission data.

A comparison to reported emission factors from other studies revealed that the N_2O emission level measured at Finnish WWTPs is in the same order of magnitude than in full-scale WWTPs abroad. Long-term N_2O measurements (more than a year) have been conducted by Daelman et al. (2015) at Kralingseveer WWTP in the Netherlands and by Gruber et al. (2020) at three WWTPs in Switzerland. The reported emission factors ranged between 1–2.8% of influent total nitrogen emitted as N_2O-N. Furthermore, Ahn et al. (2010a) reported emission factors varying from 0.01% to 1.8% during short-term measurement campaigns (24 hours) at 12 full-scale WWTPs in the United States. In conclusion, the emission factors varying around 0.04–2% at Finnish WWTPs is well in line with the reported international N_2O emission level. The emission factors vary both below and over the fixed emission factor of 1.6% suggested by IPCC (2019).

5.2 Sources of error

During the measurement campaigns, each aerobic compartment and aeration line could not be measured, which affected the accuracy of the spatial variation that was detected during the measurement campaigns. However, the temporal variation in the emissions could be accurately captured due to the high-resolution measurement data collected with the gas analyzer.

Regarding the data analysis to produce the results, assumptions and estimations were made related to the N_2O measurement data and aeration data. The N_2O concentrations were estimated for the missing compartments with linear regression from the measurement data and all aeration lines were assumed identical. If only one compartment was measured during the campaign, all compartments were assumed to have the same N_2O concentration, even though significant spatial variation was detected when more than one compartment was monitored. Furthermore, a 10-fold difference was measured in the average N_2O concentrations between two lines of similar

configuration at Viinikanlahti WWTP in November 2022, which contrasted the assumption of identical aeration lines.

At Viinikanlahti WWTP and Kirkonkylä WWTP, there were aeration lines with varying number of aerobic compartments, or the number changed during the measurements. In the data analysis, a uniform configuration was assumed for all lines for the duration of the measurement campaign. This was mainly due to the limited resources to estimate the compartment-specific aeration flow rates. However, the increased N_2O emissions from lines with additional aerobic compartments were accounted for in the total load calculation by distributing a higher air flow rate to the aerobic compartments that were considered in the data analysis. Simultaneously, this caused an overestimation to the emission loads from the compartments that were considered.

Additionally, changes in other operational or environmental conditions can directly affect the reliability of the measurement data. For example, the temporary drop in pH at Akaa WWTP in December 2023 resulted in a higher emission level than was detected under the normal pH level. At Kirkonkylä WWTP, the operation of the treatment process was changed during the measurement campaign in January 2023, which complicated the comparability of the spatial variation measured between the measurement locations. Thus, the measurement data from these campaigns was not entirely representative of the stable conditions at the plants.

The aeration data from each WWTP required processing to estimate the air flow to each aerobic compartment. At Akaa WWTP and Kirkonkylä WWTP, the total air flow rate had to be estimated first. The estimation was based on the data from the frequency converter controlling the air compressor. The total air flow was equally divided between the aeration lines, and the data from Kirkonkylä WWTP was further divided to estimate the compartment-specific air flow rates. For example, the DO levels at Akaa WWTP varied significantly between the aeration lines, which could indicate uneven distribution of the total air flow between the aeration lines. At Kirkonkylä WWTP, a part of the frequency data was not recorded during the measurement campaign in January, which required additional estimations. The air flow rates (m^3/h) were also normalized to Nm^3/h, which required the assumption that ideal gas law could be applied.

At Viinikanlahti WWTP, the air flow rate per aeration line was measured as a normalized volumetric flow, but the distribution between the aerobic compartments was unknown. To distribute the total air flow, the SUMO process model constructed based on the treatment process was utilized. The model calculated the air flow rates to the compartments relying on the DO concentrations that were input to the model. The simulated air flow rates were

utilized to determine an average share for each compartment of the total air flow rate.

To calculate the emission factors, the N_2O-N load was related to influent and removed total nitrogen loads which were calculated based on the influent and effluent total nitrogen concentrations. Typically, these concentrations were available from a 24-hour composite sample analyzed once during the measurement campaigns. The concentrations directly affected the loads to which the N_2O-N loads were related to and thus the magnitude of the emission factors. The composite samples were not necessarily entirely representative of the influent and effluent quality during the whole measurement campaign, which would have required additional samples for confirmation. Furthermore, the influent samples at Akaa WWTP contain reject waters from the treatment process mixed to the influent water, which likely increased the calculated influent total nitrogen load to which the N_2O-N load was related to.

The SUMO process model constructed for the treatment process of Viinikanlahti WWTP included estimations for the quality of the primary settled water. A half the $Fe_2(SO_4)_3$ dosed prior to the primary settler was assumed to be removed in the settled sludge. Laboratory results from influent total nitrogen and COD were used to estimate dynamic data series of the total nitrogen and COD concentrations in the influent. To estimate the same concentrations for the pre-treated water, the laboratory results from the permanganate-based COD of the influent and pre-treated water had to be utilized to obtain an estimate of the dichromate-based COD reduction in the primary settler. No nitrogen removal was assumed for the primary settler, even though some of the total nitrogen is removed in the settled sludge. In addition, the reference COD fractionation was reported in 2008 which might not be completely representative of the current influent characteristics of Viinikanlahti WWTP. For example, the COD fractions may have changed due to population growth in the area and the resulting increase in inflow or changes in the industrial wastewater quality conducted to the plant. Furthermore, the COD fractions required modifications to be input to the model.

5.3 Relevance of the results

The measured emission factors, compiled in table 16 (section 5.1), describe the plant-specific N_2O emission level at the WWTPs during the measurement campaigns. Therefore, the emission factors can be assumed to better estimate the emission level at the time of the measurements than the fixed emission factor of 1.6% proposed by IPCC (2019). However, as the measurement campaigns were relatively short (4–19 days), the measured emission factors are not able to explicitly describe the N_2O emission level at the studied plants nor at Finnish WWTPs in general. Therefore, more longer-term measurements

are needed before reliable alternatives to the fixed emission factor by IPCC (2019) can be suggested. As was concluded from the long-term monitoring data from Viikinmäki WWTP, it seemed that the short-term variability in the emission level, i.e., daily emission factors, was higher than the monthly emission level. Thus, the short-term measurement campaigns conducted during this thesis may have underestimated or overestimated the emission level which longer-term measurements could even out more effectively. Vasilaki et al. (2019) drew a similar conclusion by comparing studies of N_2O measurement campaigns conducted at full-scale WWTPs. They found that short-term and medium-term measurements with a duration less than a year resulted in a wider range of reported emission factors (0–4% of influent total nitrogen emitted as N_2O-N, average below 1%) than long-term measurements with a minimum duration of one year (0.5–3%, average 1.5%). Therefore, long-term N_2O emission data is required to reliably estimate the emission level. Moreover, it is important that the measurements are conducted in several measurement locations, as significant spatial variation was detected between two compartments of the same aeration line and between two identically operated aeration lines.

The N_2O modelling experiment with one Finnish full-scale WWTP (Viinikanlahti WWTP) suggests that the mechanistic Sumo4N model has potential in supporting the quantification of N_2O emissions from wastewater treatment. However, a deeper understanding of the model and more calibration are needed before final conclusions can be made, as currently the model can only simulate the diurnal variation in the N_2O emissions but not the spatial variation that is also significant based on the results from the on-site measurements. The quality of the input data should also be improved with up-to-date COD characterization data and online measurement data instead of laboratory analysis data that had to be relied on in the modelling experiment. Long-term N_2O measurement data would also benefit further N_2O modelling studies, as the potential of modelling in simulating the emission seasonality could be assessed. For example, the effect of temperature on the N_2O emission level should be studied, as the variability in temperature is very pronounced at Finnish WWTPs. Furthermore, the applicability of the data-driven and hybrid modelling approaches should be considered alongside mechanistic models. Relatively little of such modelling studies exist, even though they could be equally potential alternatives to mechanistic models.

6 Conclusions

The objectives of this thesis were to 1) provide additional information of the N_2O emission level at Finnish WWTPs and 2) assess the potential of N_2O modelling in emission quantification. The first objective was primarily achieved by N_2O measurement campaigns conducted at three Finnish WWTPs (Akaa, Kirkonkylä and Viinikanlahti WWTPs). The related data analysis resulted in emission factors as an indication of the N_2O emission level. Additionally, correlation was studied between the emissions and available data from other process variables to determine the extent to which they can explain the measured N_2O emission level and its variability.

The focus for the second objective was to conduct a literature review focusing on N_2O modelling approaches and a modelling experiment with SUMO wastewater treatment process modelling software. In the literature review, the knowledge gaps in N_2O modelling were studied, as they limit the applicability of modelling in reliable emission quantification. The modelling experiment was conducted with Sumo4N process model which includes all three N_2O emission pathways and data obtained from Viinikanlahti WWTP in September 2022. The model was utilized to simulate N_2O emissions and compare them to the N_2O measurement data collected at the plant. Light calibration of the model was performed. The modelling results formed the basis to study the potential of N_2O modelling in the Finnish context by identifying needs related to data and further studies.

The N_2O emissions were measured at the treatment plants by conducting 1–2 measurement campaigns at each plant with a duration of 4–19 days. N_2O was measured continuously from the off-gas released from the aerobic compartments of the biological treatment units with a gas-collecting hood and an FTIR-based gas analyzer. Furthermore, two measurement campaigns were conducted at Kirkonkylä WWTP and Viinikanlahti WWTP to capture the seasonality in the emissions. Additionally, dissolved NO_2^- concentrations were analyzed from wastewater samples collected near the measurement locations to study the correlation between N_2O and NO_2^- that has been suggested by literature. Additional data from online monitoring and laboratory analyses was provided by the plant operators to produce the results.

The emission factors that were calculated based on the measurement data from each measurement campaign relate the emitted N_2O-N load to the influent total nitrogen load and to the removed total nitrogen load. The emission factors at Kirkonkylä WWTP were 0.04% relative to influent total nitrogen and 0.05% relative to removed total nitrogen, respectively, in June–July 2022. In January 2023, the respective emission factors were 1.8% and 3.0%. At Viinikanlahti WWTP, emission factors of 0.4% and 1.1% were measured in

September 2022 and 0.08% and 0.2% in November, relative to the influent total nitrogen and removed total nitrogen loads, respectively. Emission factors of 0.2% relative to influent total nitrogen and 0.3% relative to removed total nitrogen were measured at Akaa WWTP in December 2022.

Correlations were found between the off-gas N_2O concentration and other parameters but none of the studied parameters could explicitly explain the variation in the emissions. At Akaa and Viinikanlahti WWTPs, moderate to strong Pearson correlation ($r = 0.5–0.7$) was found between the N_2O concentrations and inflow rate, while the correlation was low ($r < 0.4$) at Kirkonkylä WWTP. Inflow rate can be used to express the variation in the loading in the treatment process. At Akaa WWTP, possible factors affecting the N_2O emissions were low pH and low DO, as both parameters had a negative Pearson correlation factor of -0.6–-0.8 to the measured N_2O concentrations. A similar correlation was found between N_2O and DO in the last aerobic compartment at Viinikanlahti WWTP in September 2022. The strongest correlation ($r = 0.9$) between N_2O and NO_2^- was also detected at Viinikanlahti WWTP during the same measurement campaign. At Kirkonkylä WWTP, the bypass of the primary clarification targeted to support heterotrophic denitrification with readily biodegradable matter could undesirably enhance N_2O production during nitrification by increasing the load of organic matter oxidized in the aerobic compartments.

Overall, there was significant variability in the emissions between the plants and between two measurement campaigns conducted at the same plant, as suggested by the varying emission factors. The measured N_2O concentrations had differences of 2 to 6000-fold when comparing the minimum and maximum concentrations measured in one compartment or the average concentrations of two compartments, indicating both diurnal and spatial variation in the emissions.

The N_2O measurement data collected from Akaa WWTP and Viinikanlahti WWTP enabled the study of the contribution of heterotrophic denitrification to the N_2O emissions. It was concluded that heterotrophic denitrification did not contribute to N_2O production while nitrification was the major contributor to the emissions. At both WWTPs, low emission levels were detected at the beginning of the aerobic phase, indicating that there were no large quantities of dissolved N_2O from the anoxic phase that would be stripped to gaseous form at the start of aeration. Thus, it seems apparent that denitrifying anoxic compartments in the biological treatment can decrease the total N_2O emissions. The COD/N and BOD_7/N ratios were 7–9 and 1–3, respectively, in the water conducted to biological treatment during all measurement campaigns, suggesting that the ratios were sufficient to ensure the availability of the readily biodegradable organic matter for denitrification.

Based on the literature review, several mechanistic models have been proposed to model one or more of the N_2O emission pathways. The applicability of the models is limited by the operational and environmental conditions in which they are valid. In addition, the uncertainty of the mechanisms behind the N_2O emission pathways has resulted in the large selection of the models. The mechanistic models typically struggle with overparameterization, which results in heavy calibration effort. The potential of the more novel modelling approaches, including data-driven and hybrid models, has been acknowledged, but relatively little application of such models exists. Therefore, these modelling approaches should be studied further. For example, hybrid models can significantly decrease the calibration effort that the purely mechanistic models require. On the other hand, data-driven and hybrid models require larger amounts of data than the mechanistic models, and process data to such an extent is typically not collected at WWTPs.

The Sumo4N model predicted the diurnal variability in the N_2O emissions well but the spatial variation in the emissions was not simulated correctly. The conclusion was drawn after a light calibration effort. Thus, the calibration of the model would need more focus to obtain improved simulation results. Furthermore, the application of data-driven and hybrid models could be considered as alternatives to the mechanistic model, especially if mechanistic modelling appears to be too limited in simulating the dynamic N_2O emissions. In addition, the quality of the input data should be improved with online measurement data and up-to-date COD characterization data.

A comparison to reported emission factors from N_2O measurements at other WWTPs in Finland and abroad revealed that the emission factors measured during this thesis were in line with other full-scale WWTPs. Generally, higher emission factors seem to be measured under cold-period conditions, even though categorization according to temperature could not explicitly explain the variation in the N_2O emissions. The varying emission factors measured during this thesis and in other studies suggest that a fixed emission factor recommended by IPCC is likely to oversimplify the dynamic N_2O emission patterns. However, the emission factors from short-term measurement campaigns are not reliable enough to be proposed as an alternative to the fixed emission factor. Therefore, it is recommended that short-term measurements are replaced with long-term measurements, preferably with a duration over one year, to accurately capture the seasonality of the N_2O emissions and study the key mechanisms and process parameters affecting N_2O production. Long-term measurement data would also support the development of N_2O modelling as a tool to quantify N_2O emissions and plan mitigation strategies.

References

Ahn, J. H., Kim, S., Park, H., Rahm, B., Pagilla, K. & Chandran, K. (2010a). N_2O Emissions from Activated Sludge Processes, 2008–2009: Results of a National Monitoring Survey in the United States. *Environmental Science and Technology*, 44(12): 4505–4511. DOI: 10.1021/es903845y

Ahn, J. H., Kim, S., Park, H., Katehis, D., Pagilla, K. & Chandran, K. (2010b). Spatial and Temporal Variability in Atmospheric Nitrous Oxide Generation and Emission from Full-Scale Biological Nitrogen Removal and Non-BNR Processes. *Water Environment Research*, 82(12): 2362–2372. DOI: 10.2175/106143010X12681059116897

Alex, J., Benedetti, L., Copp, J., Gernaey, K. V., Jeppsson, U., Nopens, I., Pons, M.-N., Rosen, C., Steyer, J. P. & Vanrolleghem, P. (2018). Benchmark Simulation Model no. 2 (BSM2). Report by the IWA Taskgroup on Benchmarking of Control Strategies for WWTPs.

Amaral, A., Gillot, S., Garrido-Baserba, M., Filiali, A., Karpinska, A. M., Plósz, B. G., De Groot, C., Bellandi, G., Nopens, I., Takács, I., Lizarralde, I., Jimenez, J. A., Fiat, J., Rieger, L., Arnell, M., Andersen, M., Jeppsson, U., Rehman, U., Fayolle, Y., Amerlinck, Y. & Rosso, D. (2019). Modelling gas-liquid mass transfer in wastewater treatment: when current knowledge needs to encounter engineering practice and vice versa. *Water Science and Technology*, 80(4): 607–619. DOI: 10.2166/wst.2019.253

Awaitey, A. (2020). Carbon footprint of Finnish wastewater treatment plants (Master's thesis, Aalto University, Espoo, Finland). Retrieved 22 February 2023 from https://aaltodoc.aalto.fi/

Bellandi, G., De Mulder, C., Van Hoey, S., Rehman, U., Amerlinck, Y., Guo, L., Vanrolleghem, P. A., Weijers, S., Gori, R. & Nopens, I. (2018). Tanks in series versus compartmental model configuration: Considering hydrodynamics helps in parameter estimation for an N_2O model. Paper presented at 6th IWA/WEF Water Resource Recovery Modelling 2018: Quebec, Canada.

Chen, H., Zeng, L., Wang, D., Zhou, Y. & Yang, X. (2020). Recent advances in nitrous oxide production and mitigation in wastewater treatment. *Water Research*, 184: Article 116168. DOI: 10.1016/j.watres.2020.116168

Conthe, M., Lycus, P., Arntzen, M. Ø., Ramos da Silva, A., Frostergård, Å., Bakken, L. R., Kleerebezem, R. & van Loosdrecht, M. C. M. (2019). Denitrification as an N_2O sink. *Water Research*, 151: 381–387. DOI: 10.1016/j.watres.2018.11.087

Daelman, M. R. J., van Voorthuizen, E. M., van Dongen, U. G. J. M., Volcke, E. I. P. & van Loosdrecht, M. C. M. (2015). Seasonal and diurnal variability of N_2O emissions from a full-scale municipal wastewater treatment plant. *Science of the Total Environment*, 536: 1–11. DOI: 10.1016/j.scitotenv.2015.06.122

de Haas, D. & Andrews, J. (2022). Nitrous oxide emissions from wastewater treatment - Revisiting the IPCC 2019 refinement guidelines. *Environmental Challenges*, 8: Article 100557. DOI: 10.1016/j.envc.2022.100557

Domingo-Félez, C. & Smets, B. F. (2016). A consilience model to describe N_2O production during biological N removal. *Environmental Science: Water Research & Technology*, 2(6): 923–930. DOI: 10.1039/c6ew00179c

Domingo-Félez, C. & Smets, B. F. (2020). Modelling Denitrification as an Electric Circuit Accurately Captures Electron Competition between Individual Reductive Steps: The Activated Sludge Model-Electron Competition Model. *Environmental Science & Technology*, 54: 7330–7338. DOI: 10.1021/acs.est.0c01095

Duan, H., Ye, L., Erler, D., Ni, B.-J. & Yuan, Z. (2017). Quantifying nitrous oxide production pathways in wastewater treatment systems using isotope technology - A critical review. *Water Research*, 122: 96–113. DOI: 10.1016/j.watres.2017.05.054

Foley, J., de Haas, D., Yuan, Z. & Lant, P. (2010). Nitrous oxide generation in full-scale biological nutrient removal wastewater treatment plants. *Water Research*, 44(3): 831–844. DOI: 10.1016/j.watres.2009.10.033

Gasmet Technologies. (n.d.). GT5000 Terra Technical Datasheet. Retrieved 17 November 2022 from https://www.gasmet.com/products/category/portable-gas-analyzers/gt5000-terra/#GT5000Terracontact

Gasmet Technologies. (2018). FTIR Gas Analysis. Vantaa, Finland: Gasmet Technologies. Retrieved 17 November 2022 from https://www.gasmet.com/products/technology/ftir-fourier-transform-infrared/

Gruber, W., Villez, K., Kipf, M., Wunderlin, P., Siegrist, H., Vogt, L. & Joss, A. (2020). N_2O emission in full-scale wastewater treatment: Proposing a refined monitoring strategy. *Science of the Total Environment*, 699: Article 134157. DOI: 10.1016/j.scitotenv.2019.134157

Gruber, W., von Känel, L., Vogt, L., Luck, M., Biolley, L., Feller, K., Moosmann, A., Krähenbühl, N., Kipf, M., Loosli, R., Vogel, M., Morgenroth, E., Braun, D. & Joss, A. (2021a). Estimation of countrywide N2O emissions from wastewater treatment in Switzerland using long-term monitoring data. *Water Research X*, 13: Article 100122. DOI: 10.1016/j.wroa.2021.100122

Gruber, W., Niederdorfer, R., Ringwald, J., Morgenroth, E., Bürgmann, H. & Joss, A. (2021b). Linking seasonal N_2O emissions and nitrification failures to microbial dynamics in a SBR wastewater treatment plant. *Water Research X*, 11: Article 100098. DOI: 10.1016/j.wroa.2021.100098

Guo, L. & Vanrolleghem, P. A. (2014). Calibration and validation of an activated sludge model for greenhouse gases no. 1. (ASMG1): prediction of temperature-dependent N_2O emission dynamics. *Bioprocess and Biosystems Engineering*, 37: 151–163. DOI: 10.1007/s00449-013-0978-3

Haimi, H., Mäkelä, A. & Antikainen, J. (2022). Mäntsälän jätevedenpuhdistamon ilmastusprosessin ajotapatarkastelu. Helsinki: FCG Finnish Consulting Group.

Henze, M., Gujer, W., Mino, T. & van Loosdrecht, M. (2000). Activated sludge models ASM1, ASM2, ASM2d and ASM3. London, UK: IWA Publishing. ISBN: 1 900222 24 8

Henze, M., Harremoës, P., Jansen, J. L. C. & Arvin, E. (2002). Wastewater treatment: Biological and Chemical Processes. Berlin, Germany: Springer. ISBN: 978-3-642-07590-2

Hiatt, W. C. & Grady, C. P. L. (2008a). An Updated Process Model for Carbon Oxidation, Nitrification, and Denitrification. *Water Environment Research*, 80(11): 2145–2156. DOI: 10.2175/106143008X304776

Hiatt, W. C. & Grady, C. P. L. (2008b). Application of the Activated Sludge Model for Nitrogen to Elevated Nitrogen Conditions. *Water Environment Research*, 80(11): 2134–2144. DOI: 10.2175/106143008X304767

Hilander, H. (2022). Nitrous oxide emission dynamics and emission factors of two Finnish wastewater treatment plants (Master's thesis, Aalto University, Espoo, Finland). Retrieved 22 February 2023 from https://aaltodoc.aalto.fi/

Hwangbo, S., Al, R., Chen, X. & Sin, G. (2021). Integrated Model for Understanding N_2O Emissions from Wastewater Treatment Plants: A Deep Learning Approach. *Environmental Science and Technology*, 55(3): 2143–2151. DOI: 10.1021/acs.est.0c05231

IPCC. (2019). Wastewater treatment and discharge. In E. Calvo Buendia, K. Tanabe, A. Kranjc, B. Jamsranjav, M. Fukuda, S. Ngarize, A. Osako, Y. Pyrozhenko, P. Shermanau & S. Federici, *2019 Refinement to the 2006 IPCC Guidelines for National Greenhouse Gas Inventories* (Volume 5). Switzerland: IPCC. ISBN: 978-4-88788-232-4

Itokawa, H., Hanaki, K. & Matsuo, T. (2001). Nitrous oxide production in high-loading biological nitrogen removal process under low cod/n ratio condition. *Water Research*, 35(3): 657–664. DOI: 10.1016/S0043-1354(00)00309-2

Kampschreur, M. J., Temmink, H., Kleerebezem, R., Jetten, M. S. M. & van Loosdrecht, M. C. M. (2009). Nitrous oxide emission during wastewater treatment. *Water Research*, 43(17): 4093–4103. DOI: 10.1016/j.watres.2009.03.001

Klotz, M. G. & Stein, L. Y. (2011). Genomics of Ammonia-Oxidizing Bacteria and Insights into Their Evolution. In B. B. Ward, D. J. Arp & M. G. Klotz (Eds.), *Nitrification* (pp. 57–93). Washington, D. C.: American Society of Microbiology. DOI: 10.1128/9781555817145.ch4

Kosonen, H. (2013). Nitrous oxide emissions at the Viikinmäki wastewater treatment plant - results and process correlations found in a long-term online monitoring campaign (Master's thesis, Aalto University, Espoo, Finland). Retrieved 22 February 2023 from https://aaltodoc.aalto.fi/

Kosse, P., Blomberg, K., Mikola, A., Heinonen, M., Kuokkanen, A., Lange, R.-L., Lübken, M. & Wichern, M. (2016). Climate change and greenhouse gas emissions within the context of urban wastewater management. *Water Solutions*: 89–94. Retrieved 6 September 2022 from https://www.researchgate.net/publication/306119690

Law, Y., Ni, B-J., Lant, P. & Yuan, Z. (2012a). N_2O production rate of an enriched ammonia-oxidising bacteria culture exponentially correlates to its ammonia oxidation rate. *Water Research*, 46: 3409–3419. DOI: 10.1016/j.watres.2012.03.043

Law, Y., Ye, L., Pan, Y. & Yuan, Z. (2012b). Nitrous oxide emissions from wastewater treatment processes. *Philosophical Transactions of the Royal Society*, 367: 1265–1277. DOI: 10.1098/rstb.2011.0317

Li, K., Duan, H., Liu, L., Qiu, R., van den Akker, B., Ni, B.-J., Chen, T., Yin, H., Yuan, Z. & Ye, L. (2022). An Integrated First Principal and Deep Learning Approach for Modeling Nitrous Oxide Emissions from Wastewater Treatment Plants. *Environmental Science and Technology*, 56: 2816–2826. DOI: 10.1021/acs.est.1c05020

Loosli, R., Joss, A., von Känel, L., Braun, D., Vogt, L., Bührer, T., Morgenroth, E. & Gruber, W. (2021). Guideline for the evaluation of nitrous oxide monitoring at WWTPs. ETH, Zürich, Switzerland & Eawag, Dübendorf, Switzerland.

Maktabifard, M., Awaitey, A., Merta, E., Haimi, H., Zaborowska, E., Mikola, A. & Mąkinia, J. (2022). Comprehensive evaluation of the carbon footprint components of wastewater treatment plants located in the Baltic Sea region. *Science of the Total Environment*, 806: Article 150436. DOI: 10.1016/j.scitotenv.2021.150436

Mampaey, K. E., Beuckels, B., Kampschreur, M. J., Kleerebezem, R., van Loosdrecht, M. C.M. & Volcke, E. I.P. (2013). Modelling nitrous and nitric oxide emissions by autotrophic ammonia-oxidizing bacteria. *Environmental Technology*, 34(12): 1555–1566. DOI: 10.1080/09593330.2012.758666

Mannina, G., Ekama, G., Caniani, D., Cosenza, A., Esposito, G., Gori, R., Garrido-Baserba, M., Rosso, D. & Olsson, G. (2016). Greenhouse gases from wastewater treatment - A review of modelling tools. *Science of the Total Environment*, 551–552: 254–270. DOI: 10.1016/j.scitotenv.2016.01.163

Mannina, G., Rebouças, T. F., Cosenza, A. & Chandran, K. (2019). A plant-wide wastewater treatment plant model for carbon and energy footprint: Model application and scenario analysis. *Journal of Cleaner Production*, 217: 244–256. DOI: 10.1016/j.clepro.2019.01.255

Marques, R., Rodriguez-Caballero, A., Oehmen, A. & Pijuan, M. (2016). Assessment of online monitoring strategies for measuring N_2O emissions from full-scale wastewater treatment systems. *Water Research*, 99: 171–179. DOI: 10.1016/j.watres.2016.04.052

Massara, T. M., Malamis, S., Guisasola, A., Baeza, J. A., Noutsopoulos, C. & Katsou, E. (2017). A review on nitrous oxide (N_2O) emissions during biological nutrient removal from municipal wastewater and sludge reject water. *Science of the Total Environment*, 596–597: 106–123. DOI: 10.1016/j.scitotenv.2017.03.191

Mikola, A., Heinonen, M., Kosonen, H., Leppänen, M., Rantanen, P. & Vahala, R. (2014). N_2O emissions from secondary clarifiers and their contribution to the total emissions of the WWTP. *Water Science and Technology*, 70(4): 720–728. DOI: 10.2166/wst.2014.281

Mäki, R. (2022). Lähtötiedot N2O mittauksille, Viinikanlahti. Unpublished.

Ni, B-J., Ruscalleda, M., Pellicer-Nàcher, C. & Smets, B. F. (2011). Modelling Nitrous Oxide Production during Biological Nitrogen Removal via Nitrification and Denitrification: Extensions to the General ASM Models. *Environmental Science and Technology*, 45: 7768–7776. DOI: 10.1021/es201489n

Ni, B-J., Yuan, Z., Chandran, K., Vanrolleghem, P. A. & Murthy, S. (2013a). Evaluating Four Mathematical Models for Nitrous Oxide Production by Autotrophic Ammonia-Oxidizing Bacteria. *Biotechnology and Bioengineering*, 110(1): 153–163. DOI: 10.1002/bit.24620

Ni, B-J., Ye, L., Law, Y., Byers, C. & Yuan, Z. (2013b). Mathematical Modeling of Nitrous Oxide (N_2O) Emissions from Full-Scale Wastewater Treatment Plants. *Environmental Science and Technology*, 47: 7795–7803. DOI: 10.1021/es4005398

Ni, B.-J., Peng, L., Law, Y., Guo, J. & Yuan, Z. (2014). Modeling of Nitrous Oxide Production by Autotrophic Ammonia-Oxidizing Bacteria with Multiple Production Pathways. *Environmental Science and Technology*, 48: 3916–3924. DOI: 10.1021/es405592h

Okabe, S., Aoi, Y., Satoh, H. & Suwa, Y. (2011). Nitrification In Wastewater Treatment. In B. B. Ward, D. J. Arp & M. G. Klotz (Eds.). *Nitrification* (pp. 405–433). Washington, D. C.: American Society of Microbiology. DOI: 10.1128/9781555817145.ch16

Pan, Y., Ye, L., Ni, B.-J. & Yuan, Z. (2011). Effect of pH on N_2O reduction and accumulation during denitrification by methanol utilizing denitrifiers. *Water Research*, 46: 4832–4840. DOI: 10.1016/j.watres.2012.06.003

Pan, Y., Ni, B.-J., Bond, P. L., Ye, L. & Yuan, Z. (2013a). Electron competition among nitrogen oxides reduction during methanol-utilizing denitrification in wastewater treatment. *Water Research*, 47(10): 3273–3281. DOI: 10.1016/j.watres.2013.02.054

Pan, Y., Ni, B.-J. & Yuan, Z. (2013b). Modeling Electron Competition among Nitrogen Oxides Reduction and N2O Accumulation in Denitrification. *Environmental Science & Technology*, 47: 11083–11091. DOI: 10.1021/es402348n

Peng, L., Ni, B.-J., Ye, L. & Yuan, Z. (2015). The combined effect of dissolved oxygen and nitrite on N_2O production by ammonia oxidizing bacteria in an enriched nitrifying sludge. *Water Research*, 73: 29–36. DOI: 10.1016/j.watres.2015.01.021

Peng, L., Ni, B.-J., Law, Y. & Yuan, Z. (2016). Modeling N_2O production by ammonia oxidizing bacteria at varying inorganic carbon concentrations by coupling the catabolic and anabolic processes. *Chemical Engineering Science*, 11: 386–394. DOI: 10.1016/j.ces.2016.01.033

Pijuan, M. & Zhao, Y. (2022). Full-scale source, mechanisms and factors affecting nitrous oxide emissions. In L. Ye, J. Porro & I. Nopens (Eds.), *Quantification and Modelling of Fugitive Greenhouse Gas Emissions from Urban Water Systems* (pp. 11–41). Scientific and Technical Report Series No. 26. London, UK: IWA Publishing. ISBN: 9781789060461

Pocquet, M., Queinnec, I., & Spérandio, M. (2013). Adaptation and identification of models for nitrous oxide (N2O) production by autotrophic nitrite reduction. Paper presented at 11th IWA Conference on Instrumentation, Control and Automation (ICA2013) 2013: Narbonne, France.

Pocquet, M., Wu, Z., Queinnec, I. & Spérandio, M. (2016). A two pathway model for N_2O emissions by ammonium oxidizing bacteria supported by the NO/N_2O variation. *Water Research*, 88: 948–959. DOI: 10.1016/j.watres.2015.11.029

Poh, L. S., Jiang, X., Zhang, Z., Liu, Y., Ng, W. J. & Zhou, Y. (2015). N_2O accumulation from denitrification under different temperatures. *Applied Microbiology and Biotechnology*, 99(21): 9215–9226. DOI: 10.1007/s00253-015-6742-7

Pöyry Environment Ltd. (2008). Tampereen Vesi - Viinikanlahden jätevedenpuhdistamo: Puhdistamon mallinnus ja simulointi.

Ren, Y., Ngo, H. H., Guo, W., Ni, B.-J. & Liu, Y. (2019). Linking the nitrous oxide production and mitigation with the microbial community in wastewater treatment: A review. *Biosource Technology Reports*, 7: Article 100191. DOI: 10.1016/j.biteb.2019.100191

Richardson, D., Felgate, H., Watmough, N., Thomson, A. & Baggs, E. (2009). Mitigating release of the potent greenhouse gas N2O from the nitrogen cycle - could enzymic regulation hold the key? *Trends in Biotechnology*, 27(7): 388–397. DOI: 10.1016/j.tibtech.2009.03.2009

Rieger, L., Gillot, S., Langergraber, G., Ohtsuki, T., Shaw, A., Takács, I. & Winkler, S. (2012). Guidelines for Using Activated Sludge Models. London, United Kingdom: IWA Publishing. ISBN: 9781780401164

Schulthess, R. V., Kühni, M. & Gujer, W. (1995). Release of nitric and nitrous oxides from denitrifying activated sludge. *Water Research*, 29(1): 215–226. DOI: 10.1016/0043-1354(94)E0108-I

Snip, L. J. P., Boiocchi, R., Flores-Alsina, X., Jeppsson, U. & Gernaey, K. V. (2014). Challenges encountered when expanding activated sludge models: a case study based on N_2O production. *Water Science and Technology*, 70(7): 1251–1260. DOI: 10.2166/wst.2014.347

Spérandio, M., Pocquet, M., Guo, L., Ni, B.-J., Vanrolleghem, P. A. & Yuan, Z. (2016). Evaluation of different nitrous oxide production models with four continuous long-term wastewater treatment process data series. *Bioprocess and Biosystems Engineering*, 39(3): 493–510. DOI: 10.1007/s00449-015-1532-2

Spérandio, M., Lang, L., Sabba, F., Nerenberg, R., Vanrolleghem, P., Domingo-Félez, C., Smets, B. F., Duan, H., Ni, B.-J. & Yuan, Z. (2022). Modelling N_2O production and emissions. In L. Ye, J. Porro & I. Nopens (Eds.), *Quantification and Modelling of Fugitive Greenhouse Gas Emissions from Urban Water Systems* (pp. 167–196). Scientific and Technical Report Series No. 26. London, UK: IWA Publishing. ISBN: 9781789060461

Stein, L. Y. (2011). Heterotrophic Nitrification and Nitrifier Denitrification. In B. B. Ward, D. J. Arp & M. G. Klotz (Eds.). *Nitrification* (pp. 95–114). Washington, D. C.: American Society of Microbiology. DOI: 10.1128/9781555817145.ch5

Stein, L. Y. & Yung, Y. L. (2003). Production, Isotopic Composition, and Atmospheric Fate of Biologically Produced Nitrous Oxide. *Annual Review of Earth and Planetary Sciences*, 31: 329–356. DOI: 10.1146/annurev.earth.31.110502.080901

Su, Q., Domingo-Félez, C., Jensen, M. M. & Smets, B. F. (2019). Abiotic Nitrous Oxide (N_2O) Production Is Strongly pH Dependent, but Contributes Little to Overall N_2O Emissions in Biological Nitrogen Removal Systems. *Environmental Science & Technology*, 53: 3508–3516. DOI: 10.1021/acs.est.8b06193

Takács, I. (2022). Sumo Technical Reference. Sigale, France: Dynamita.

Tallec, G., Garnier, J., Billen, G. & Gousailles, M. (2008). Nitrous oxide emissions from denitrifying activated sludge of urban wastewater treatment plants, under anoxia and low oxygenation. *Bioresource Technology*, 99(7): 2200–2209. DOI: 10.1016/j.biortech.2007.05.025

Tchobanoglous, G., Burton, F. L. & Stensel, H. D. (2003). Wastewater Engineering: Treatment and Reuse (4th ed.). Metcalf & Eddy, Inc. New York, USA: McGraw-Hill.

Tumendelger, A., Toyoda, S. & Yoshida, N. (2014). Isotopic analysis of N2O produced in a conventional wastewater treatment system operated under different aeration conditions. *Rapid Communications in Mass Spectrometry*, 28: 1883–1892. DOI: 10.1002/rcm.6973

Vasilaki, V., Volcke, E. I. P, Nandi, A. K., van Loosdrecht, M. C. M. & Katsou, E. (2018). Relating N_2O emissions during biological nitrogen removal with operating conditions using multivariate statistical techniques. *Water Research*, 140: 387–402. DOI: 10.1016/j.watres.2018.04.052

Vasilaki, V., Massara, T. M., Stanchev, P., Fatone, F. & Katsou, E. (2019). A decade of nitrous oxide (N_2O) monitoring in full-scale wastewater treatment processes: A critical review. *Water Research*, 161: 392–412. DOI: 10.1016/j.watres.2019.04.022

Vasilaki, V., Conca, V., Frison, N., Eusebi, A. L., Fatone, F. & Katsou, E. (2020). A knowledge discovery framework to predict the N_2O emissions in the wastewater sector. *Water Research*, 178: Article 115799. DOI: 10.1016/j.watres.2020.115799

Wunderlin, P., Mohn, J., Joss, A., Emmenegger, L. & Siegrist, H. (2012). Mechanisms of N_2O production in biological wastewater treatment under nitrifying and denitrifying conditions. *Water Research*, 46(4): 1027–1037. DOI: 10.1016/j.watres.2011.11.080

Zhang, M., Lawlor, P. G., Li, J. & Zhan, X. (2012). Characteristics of Nitrous Oxide (N_2O) Emissions from Intermittently-Aerated Sequencing Batch Reactors Treating the Separated Liquid Fraction of Anaerobically Digested Pig Manure. *Water, Air, & Soil Pollution*, 223(5): 1973–1981. DOI: 10.1007/s11270-011-0998-z

Zhu-Barker, X., Cavazos, A. R., Ostrom, N. E., Horwath, W. R. & Glass, J. B. (2015). The importance of abiotic reactions for nitrous oxide production. *Biogeochemistry*, 126: 251–267. DOI: 10.1007/s10533-015-0166-4